CHANGES IN NEURONAL FIRING AND SYNCHRONY PRECEDE RECRUITMENT OF MESIAL TEMPORAL NETWORKS INTO GENERALIZING SEIZURES

By

Amrit Misra

June 2014

A Dissertation Presented to the Faculty of
Drexel University College of Medicine
in partial fulfillment of the Requirements for the Degree of
Doctor of Philosophy

____

Karen Moxon PhD
Professor
School of Biomedical Engineering
Science and Healthcare Systems
Drexel University

____

Michael Sperling MD
Baldwin Keyes Professor of
Neurology
Thomas Jefferson University

____

Wen-Jun Gao PhD
Associate Professor
Neurobiology & Anatomy

____

Joshua Jacobs PhD
Assistant Professor
School of Biomedical Engineering
Science and Healthcare Systems
Drexel University

____

Banu Onaral PhD
H H Sun Professor of Biomedical
Engineering and Electrical Engineering
Drexel University

____

Ahmet Sacan PhD
Assistant Professor
School of Biomedical Engineering
Science and Healthcare Systems
Drexel University

CHANGES IN NEURONAL FIRING AND SYNCHRONY PRECEDE RECRUITMENT OF MESIAL TEMPORAL NETWORKS INTO GENERALIZING SEIZURES

A Thesis

Submitted to the Faculty

of

Drexel University

by

Amrit Misra

in partial fulfillment of the

requirements for the degree

of

Doctor of Philosophy

June 2014

DEDICATION

The following body of work is dedicated to my ever supporting parents Bijay and Janaki, my inspirational baby sister Nyati, and my loving fiancée Jessica without whom, none of this would be possible.

ACKNOWLEDGEMENTS

I would like to acknowledge the efforts of the following individuals for their contributions to this body work. First and foremost, the participants of this study who selflessly volunteered their time and their comfort for the sake of this work. Secondly, my advisor Karen Moxon and the member of my committee Michael Sperling, Banu Onaral, Wen-Jun Gao, Joshua Jacobs, and Ahmet Sacan, whose guidance directed the course of this research. Thirdly, my colleagues at the University of Pennsylvania, John Fred Burke, Ryan Williams and Ashwin Ramayya for their efforts in developing a successful human recording protocol. Fourth the neurosurgeons Ashwini Sharan and James Evans who implanted all of our electrodes and the EMU technicians Dale and Ted Wyeth who always made themselves available for our work. Fifth, my friends and colleagues Suganya Karunakaran and Xianda Long whose insight and expertise may be found in in every aspect of this work, and lastly the exemplary contributions of my mentor Dane Grasse whose work formed the foundation of this project. This work was supported financially through grants from the Coulter Foundation and NIH (MH55687, MH61975, & MH081248-02).

TABLE OF CONTENTS

LIST OF TABLES

LIST OF ILLUSTRATIONS

ABSTRACT

CHANGES IN NEURONAL FIRING AND SYNCHRONY PRECEDE RECRUITMENT OF MESIAL TEMPORAL NETWORKS INTO GENERALIZING SEIZURES

Amrit Misra
Advisor: Karen Moxon PhD

Despite extensive study, the mechanisms underlying seizure generation and propagation are poorly understood. One approach is to study changes in the neuronal activity (of inhibitory and excitatory subpopulations) that occur during the recruitment of networks into a propagating seizure, to gain insight into mechanisms by which seizures spread across the brain. Recent work, comparing intra- and extracelluar recordings in ex-vivo preparations of human neocortex has implicated a failure in feed-forward inhibition underlying the spread of seizure. However, direct in-vivo study of inhibitory and excitatory population dynamics in the neocortex is difficult, due to an inability to separate single neuron activity into excitatory and inhibitory subpopulations. In the mesial temporal lobe (MTL) it is considerably easier to isolate these subpopulations, and several studies in the rodent MTL have, indeed, demonstrated an intricate spatiotemporal interplay between inhibitory and excitatory neuron firing and their corresponding synchrony to local field potentials during the transition to seizure. While this work suggests potential mechanisms for network recruitment into seizure, no direct observations have been made in the MTL of epileptic patients. This report provides methods to prolong the longevity of single neuron recordings in the human MTL. Using these recordings, evidence is presented that supports the hypothesis that recruitment of MTL networks into seizures of neocortical origin is preceded by specific spatiotemporal increases in synchrony. In detail, within the MTL there is a decrease in inhibitory interneuron firing that coincides with the inhibitory population becoming more coherent to their local field potentials. This increased synchrony between neurons and the local field occurs at frequencies similar to those of regional synchrony between MTL networks and the seizure focus. These results suggest a mechanism by which downstream networks are prepared for recruitment into generalizing seizures. Interestingly, these spatiotemporal changes occur prior to the first electrographic manifestation of seizure in the brain, implying that in addition to their role in seizure propagation, changes in interneuron firing and interneuron-field synchrony in the MTL may be reflective of early seizure activity in other brain structures as well, and may thus be a useful tool in developing improved early detection algorithms.

CHAPTER 1: Introduction

1.1 Overview

With over 2 million cases in the US alone and annual expenditures topping 15 billion dollars,[1] epilepsy represents a tangible threat to our nation's heath. Epilepsy is clinically defined as a neurological disorder consisting of repeated seizures. Seizures are, in turn, defined as a paroxysmal events characterized by abnormally excessive or synchronous neuronal activity[2]. In general, seizures are attributed to an imbalance between inhibitory and excitatory mechanisms of the brain but the underlying pathophysiology that leads to this is still not well understood. Individual seizures are typified by the development of large amplitude rhythmic oscillations, often time several orders of magnitude larger than normal background activity. The clinical presentation varies with the brain structures that are involved and can range from violent convulsions (involving basal ganglia or motor cortex) to lapses of awareness (involving specific thalamo-cortical circuits). No, one, underlying cause can be attributed to seizure generation, however in the case of focal epilepsy, seizures initiate from a distinct pathologic zone of onset. This zone can sometimes be associated with overt pathologies, such as mass lesions or traumatic injuries, but these are not requisite for seizure generation. From this onset zone, rhythmic ictal (seizure-related) oscillations spread across the brain and subsume normal function. Understanding the mechanism by which this occurs is of paramount importance in order to develop more effective treatment strategies.

In epilepsy, while the imbalance between excitation and inhibition appears to favor excitation, multiple studies have demonstrated that, in humans, inhibition is actually enhanced in epileptic tissue. Deep brain electrical stimulation studies suggest that epileptic MTL exhibits an increase in protective inhibition, perhaps developing as a control mechanism for the uncontrolled excitation that occurs during seizure. In epileptic tissue, stimulation thresholds for developing after-discharges are higher than in non-epileptic tissue[3]; paired electrical pulses show enhanced suppression in epileptogenic tissue compared to contralateral controls[4]; and single pulse stimulation showed prolonged inhibition of synchronously firing neurons in epileptic tissue[5]. Given this evidence, the question arises, how then can seizures generate in a network that appears to have enhanced inhibition? A hypothesis that is gaining increasing attention in the scientific community is that, during interictal periods, basal inhibition is elevated in epileptic tissue, but immediately prior to seizure, this protective inhibition breaks down allowing seizures to recruit the local networks.

1.2 Changes in interneuron firing

Several recent studies in both ex-vivo slices and in-vivo preparations support the theory of inhibitory failure facilitating transition to seizure. Ziburkis et al. used extracellular recordings of rodent hippocampal slices to identify an interplay between putative inhibitory interneurons and excitatory pyramidal cells during induced seizure like events[6]. Specifically, interneuron firing abruptly stopped prior to pyramidal cell activity and ictal discharges, suggesting that when local inhibition was temporarily arrested, seizure activity was allowed to develop. Similarly Gnatkovsky et al. used intra- and extracellular recordings in an ex-vivo whole rodent brain preparation to demonstrate that, in entorhinal cortex, inhibitory firing sharply decreases before ictal activity develops in seizure like events[7]. Most recently, in an in-vivo rodent model of spontaneous seizure, Grasse et al. used extracellular recordings to demonstrate similar patterns of a decrease in inhibitory firing followed by an increase in excitatory pyramidal cell firing as ictal activity developed in CA3 hippocampus[8]. Despite using different models, in different regions of the MTL, all of these studies identify a distinct pattern of reduction in firing rate for the inhibitory population prior to the development of rhythmic ictal activity in the LFP, suggesting that failure of inhibition does occur prior to network recruitment into seizure. Despite the preponderance of animal work, this has not yet been demonstrated in-vivo in humans, and thus will be a primary focus of this thesis.

1.3 Interneuron synchrony

To identify possible motivators for the changes in interneuron firing rate that have been described during the transition to seizure, we look to the various inputs that these neurons receive. In this case, these inputs are the accumulated post-synaptic potentials that arrive from adjacent neurons. The local field potential (LFP) is effectively a summation of this cumulative activity and, so, to understand changes that occur in firing rate (neuronal output) we must relate it to the local field potential (neuronal input). To measure this neuronal synchrony between firing rates and local field potentials, we can employ a measure called the unit-field coherence[9]. By breaking down the local field potential into its various frequency components and assessing how synchronized output-firing is to each of these signals, we gain insight into which frequency components are most influential to the observed changes in firing rate. By then identifying generators of this this oscillatory frequency, we can infer which regions of the brain may be motivating the changes in firing rate that are observed. In the case of the interneurons of the MTL, this population is known to both modulate and be modulated by theta oscillations. Grasse et al. also demonstrated an increase in theta band coherence for inhibitory interneurons in the MTL of spontaneously seizing rats prior to the electrographic onset of seizure, making this oscillation of particular interest. Again, pre-ictal interneuron synchrony has not yet been investigated in-vivo in humans and thus will be a second focus of this thesis work.

1.4 Field-field synchrony

It is clear that the concept of synchronized neural activity is central to our present understanding of epilepsy, however synchrony can occur on varying temporal and spatial scales. At the cellular level, synchrony may occur between individual neurons as measured by cross-correlation or between individual neurons and the local field potential as measured by unit-field coherence, (mentioned above.) These measures occur within small volumes (<1 mm^3) of tissue and when studying seizure recruitment within these volumes, these measures are made on a scale on the order of hundreds of milliseconds. As mentioned previously, in focal epilepsy, seizures often start in a distinct focus and propagate to numerous downstream regions, so restricting an analysis to one region (such as the MTL) only provides a local view into changes associated with recruitment into seizure. To get a more comprehensive look at how seizures are spreading, it is necessary to look across brain structures, which changes the type of synchrony that must be analyzed. When looking across larger distances, i.e. between different brain regions, synchrony is generally discussed between the local field potentials at each region, and is usually measured in terms of field-field coherence or directed field-field coherence. As expected, the time scale of field-field coherence is correspondingly larger (on the order of seconds) since propagation lasts longer over greater distances. Importantly, whereas unit-field coherence provides a rough measure of which frequencies of the LFP most influence the firing of a neuronal population, directed field-field coherence is reflective of which frequencies are being used to convey information between brain structures. For the present work, to avoid confounding changes in neuronal activity associated with seizure generation with those associated with recruitment into seizure, only seizures with neocortical foci that spread to the MTL were studied. To this end, both unit-field coherence within the MTL and field-field coherence between the seizure focus and the MTL are used to complement one another and connect changes at the distant seizure focus with those in downstream MTL networks.

1.5 Aims of this thesis

To address the gap in knowledge regarding seizure propagation in mesial temporal networks, this thesis separately studies changes in the activity of putative excitatory (pyramidal) and inhibitory (interneuron) cell populations, to identify specific patterns in neuronal activity and synchrony during the transition to seizure within the human MTL. **It is the central hypothesis of this thesis that pre-ictal patterns of neuronal activity in the putative interneuron and pyramidal cell populations of the mesial temporal lobe are sensitive and specific to seizure propagation and may be used for clinically relevant early detection of seizure onset.** This hypothesis was tested through the pursuit of 3 specific aims.

Aim 1: Design a suitable chronic recording platform for human recordings in MTL

> A) Test candidate electrode coating for improving short-term chronic single unit recording in MTL
>
> *Hypothesis: The use of Poloxamer P-188, an amphiphilic copolymer that can self-insert into cellular membranes that are damaged during electrode placement, will reduce the magnitude of initial cell death, and thereby attenuate the immune response and resultant glial scarring, thereby improving recording longevity.*

> B) Develop a protocol for chronic, multiple, single-unit recording from the mesial temporal lobe of patients undergoing inpatient diagnostic testing.
>
> *Hypothesis: Mechanical failure is a primary cause of poor neuron yield and poor recording quality.*

Aim 2: Identify pre-ictal neuronal activity in MTL that is sensitive to seizure onset

A) Identify neuronal firing patterns of MTL neurons prior to and during seizure propagation to MTL

Hypothesis: Prior to generalization to MTL, inhibitory neurons will exhibit changes in synchrony to ongoing oscillations and decrease in firing rate that are consistent with attenuation of protective inhibition.

B) Identify patterns of synchrony (field-field coherence) between the presumptive seizure focus and the MTL prior to and during seizure propagation to MTL

Hypothesis: Single neuron activity patterns in MTL are influenced by changes in upstream networks that facilitate seizure propagation and recruitment of MTL.

Aim 3: Incorporate information about pre-ictal interneuron firing patterns to improve seizure prediction/early detection

A) Develop a seizure prediction/early detection algorithm that identifies ictal activity from the changes in neuronal firing patterns before ictal spiking onset (current industry standard).

Hypothesis: By isolating changes in interneuron activity from overall changes in neuronal activity, the pre-ictal patterns identified in Aim 2 may be used to improve early seizure detection algorithms.

Through the accomplishment of these 3 aims, this thesis presents evidence that the inhibitory subpopulation of the MTL is selectively modulated prior to recruitment into seizure at frequencies that are known to 1) influence interneurons and 2) to simultaneously convey specific information from upstream seizing networks. By disrupting oscillations at these frequencies, we may be able to interrupt this process and promote more robust protective inhibition to limit the extent of seizure propagation. Moreover, the downstream counterparts of seizure-associated changes in neuronal activity at the focus can provide information about impending seizure prior to the first electrographic manifestation, and improve existing efforts at early seizure detection.

1.6 Contributions of this thesis

The following work encompasses investigations in biomaterials, experimental methodology, and human electrophysiology. Elements have been reported to the general scientific community in the form of peer reviewed publications and presentations at national scientific conferences. The investigation of the use of Poloxamer in intracranial implantations as described in chapter 2 has been published in the Journal of Neural Engineering[10]. Similarly, the investigation of methodological improvements to existing human microwire recordings as described in chapter 3 has also been published in the Journal of Neural Engineering[11]. At the time of publication of this document, the investigation of interneuron firing and coherence dynamics during seizure propagation (Chapter 4) has been documented in an article submission to the journal Nature Communications and is under peer review. This material has also been presented at the 2013 Society for Neuroscience national conference (San Diego, CA) and at the 2014 American Academy of Neurology national conference (Philadelphia, PA). Lastly, the investigation of automated seizure detection using single neurons based variables (Chapter 5) has been prepared as a manuscript for submission to the journal Epilepsia, but at its current state is considered preliminary data. Further patients are required to validate these results for the seizure population at large before submitting for peer review.

CHAPTER 2: Preventing neuronal damage and inflammation in-vivo during cortical microelectrode implantation through the use of poloxamer P-188

2.1 Introduction

Diagnostic intracranial recordings have been the standard of care for patient with multi-drug resistant epilepsy for several decades. While such recordings do provide insight into the average activity of several hundred thousand neurons at a time, the activity of individual neurons becomes lost in the average. Histological studies in the mesial temporal lobe (MTL) have demonstrated that within the recording region of a given electrode lies an amalgam of inhibitory and excitatory neurons. Thus in a simple spatial average, intracranial recordings cannot hope to distinguish the different activities of these two distinct populations. In contrast, microwire recordings provide the spatial resolution to record from individual inhibitory and excitatory cells, but, as a consequence, are limited to a small volume from which activity is recorded. Over the course of several weeks of recording, this limitation in recording volume eventually motivates a loss in signal to noise ratio terminating in the failure of the recording.

Early hypotheses concerning the reason for such failure focused on the development of a glial scar[12,13] that pushes nearby neurons out of recording range; however, more recent studies have suggested that failure is due, at least in part, to loss of neurons within the recording zone immediately adjacent to the microelectrode (<200µm)[14]. While neuronal cell death and loss of neurites continues for at least 16 weeks post-implantation[15], the majority of the loss occurs within the first two weeks[15,16]. During insertion, microelectrodes mechanically damage the membranes of neurons and glial cells alike. Intracellular proteins are released into the extracellular environment and trigger an acute inflammatory response around the microelectrode. Microglia, oligodendrocyte precursors and astrocytes release signaling proteins into the local environment initiating a cascade of events that leads to glial cell proliferation[17], and this inflammation is accompanied by neurodegeneration[15,17]. To mitigate this biological response, researchers have either focused on biomaterials efforts (changing the size, shape, or material properties of the implant[12,18,19] or the use of pharmacologic anti-inflammatory agents[20–23]. To date, however, no studies have examined strategies that directly repair the initial damage due to the microelectrode insertion in-vivo. Recent in-vitro work has shown that the tri-block copolymer Poloxamer (P-188) promotes cell viability and cell recovery by sealing ruptured cell membranes in mechanically injured neurons[24,25] thereby preventing post-injury axonal bead formation[18,26] and enhancing overall neuroprotection. To test whether Poloxamer can mitigate in-vivo cellular damage and inflammation from electrode insertion, this study quantifies glial activation and changes in neuronal cell density due to the chronic implantation of electrodes coated with Poloxamer and uncoated controls at two, four and six weeks post implantation in adult male Long-Evans rats. Unlike other chronic implant biocompatibility studies, we have affixed the implants to the skull for the purposes of making periodic extracellular recordings to verify electrode function.

2.2 Methods and Materials

2.2.1 Microelectrodes

As part of ongoing work, microelectrodes were manufactured from porous silicon substrates with ceramic insulation. The porous substrate was chosen both to ease the initial loading of Poloxamer onto the surface and because of previous findings that indicate a reduction in glial activation in porous over smooth electrodes[26]. These ceramic based multi-site electrode arrays (CBMSE) were fabricated according to methods previously described by Moxon et al.[18]. The width of the electrode at the tip was 66.4µm and tapered to 113µm at the most proximal recording site (Figure 2.1d). Electrode fabrication was performed in clean room facilities and additional handling was kept to a minimum to reduce contamination. As a result, no special measures were taken to sterilize electrodes against endotoxin. All electrodes were sterilized prior to implantation by sonication for 5 minutes in DI water followed by 5 minutes in 70% isopropyl alcohol.

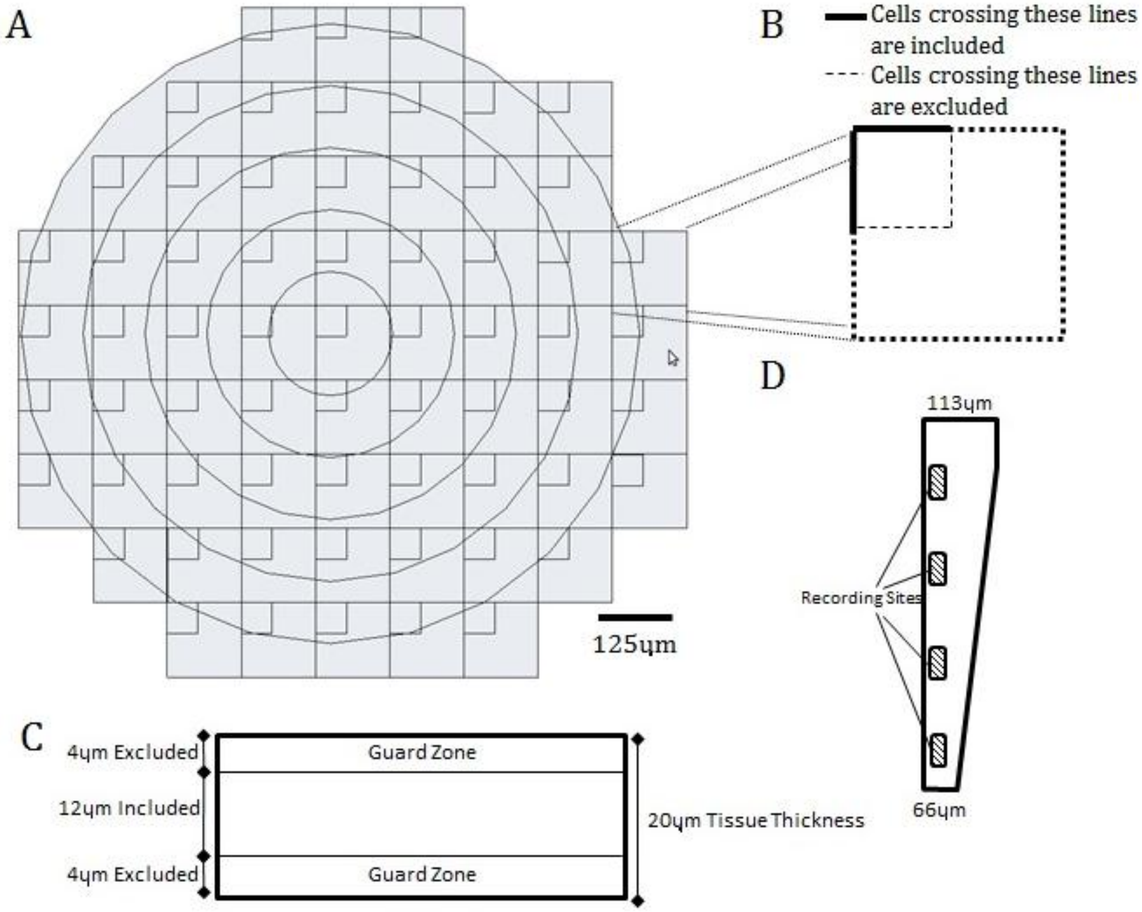

Figure 2. 1 Schematic representation of stereoinvestigator and elctrode A) Schematic representation of the array of counting frames that was superimposed onto tissue slices using the Stereoinvestigator software package. B) Blowup of a single counting frame. Cells crossing the solid boundary lines were included in the count while cells crossing the dashed boundary lines were not, thereby serving to prevent double counting cells. C) A schematic cross section of the tissue slice illustrating the 4um guard zones that were not sampled to reduce influence from non uniform tissue slices. D) Schematic of the tip of the CBMSE electrode shaft that was implanted in rat cortex.

2.2.2 Implantation of Microelectrodes

All animal procedures were performed utilizing sterile techniques approved by the Drexel University Institutional Animal Care and Use Committee (IACUC) and adhered to National Institute of Health (NIH) guidelines. Adult male Long-Evans rats between 275-299g were used in this study. Animals were intubated and anesthetized using 4.5 % isoflourane in oxygen at 2 L / min. The rat's head was shaved and the area of interest was disinfected with isopropyl alcohol followed by a Betadine swab. Ophthalmic ointment (Altaire Pharmaceuticals, Aquebogue NY) was applied to the animal's eyes to prevent corneal damage. Each animal was placed on a stereotactic frame (Cartesian Research Inc, Portland OR), and anesthesia was maintained in oxygen in 0.5 L/min for the duration of the surgery. A midline incision was made in the skin, and the skull was centered to bregma on the stereotactic frame. A 3mm x 5mm craniotomy was drilled for each of two electrodes at 2.5 mm bilaterally and 0 mm anterior to bregma. In order to support the electrode cap, a series of smaller anchoring points were drilled in the skull for placement of four metal screws. The bone plug of the craniotomy was carefully removed and the dura was gently pierced with fine micro-forceps. Immediately prior to insertion, one of two electrodes was loaded with Poloxamer by two 5 minute immersions in 100µm Poloxamer (Sigma) dissolved in saline separated by 10 minutes of air drying. The remaining control electrode was dipped in sterile saline with the same procedure. After a final 10 minutes of air drying, the microelectrodes were inserted into the cortex at a rate of 50µm/min until the most ventral recording site reached the deep layers of the cortex and at least one neuron was observed on all four sites (approximately 1.8 mm). During the electrode insertion, saline was applied to the open craniotomies to reduce brain exposure and to minimize iatrogenic damage. During insertion, neural activity was monitored using a high speed data acquisition system using a unity gain headstage connected to an external preamplifier (Plexon, Dallas TX) in a manner similar to our previously published work [26], to ensure that Poloxamer was not interfering with electrode recording ability. After insertion, the craniotomies were covered with dental acrylic, paying particular attention to leaving the electrode interface connectors exposed. The skin incision was then closed with surgical staples and the animal was allowed to recover from anesthesia on a heating pad at 25° C until it regained normal gait and grooming behavior.

Neuronal activity was recorded during electrode implantation and at weeks 1, 2, 4 and 6 post implantation. For each recording session, single neurons were discriminated from broadband recordings as described in previous publications [18]. In brief, animals were anesthetized and a tethered headstage amplifier (100x) was connected to the exposed Omnetics connector that affixes the electrode to the animal's skull. Signals were further amplified by a 1000x preamplifier and sampled at 40 kHz. Broadband signals were bandpass filtered from 600Hz – 10kHz, displayed on a computer screen and played over audio speakers. Neuronal activity was examined as the cutaneous surface of the skin and body hairs were stimulated with a wooden probe. A threshold above the mean and equal to 5 times the variance of the signal was set and a recording site with at least one discriminable single unit that exceeded the threshold was identified as active.

2.2.3 Tissue Processing for Immunohistochemistry

To measure the effects of neural repair using Poloxamer, animals were euthanized at two weeks (n = 5), four weeks (n = 5), and six weeks (n = 5) post implantation. The animals were sacrificed with an overdose of Euthasol (Virbac, Fort Worth, TX) and then perfused transcardially with 0.5 L of ice cold PBS (Sigma) followed by 0.5 L of ice cold 4% paraformaldehyde (Fisher). Brains were removed such that the implanted neural probes remained intact. After fixation of the brain in paraformaldehyde for 48 hours, the brains were dissected and the electrodes were retrieved from the tissue. The brains were placed into 30% sucrose in PBS solution (4° C) to equilibrate for three to five days. After the equilibration period, the tissue was frozen and sections of 20 µm thickness were cut using a Leica CM3500 cryotome in the horizontal plane through the depth of the cortex (1 mm). The sections were collected using a low-distortion tape system, serially sorted into four sets and mounted onto slides[27]. There were approximately 20 slices per brain per set.

2.2.4 Immunohistochemistry

Sections from cortex were stained to measure the size of the hole left by the microelectrode and to observe brain tissue response. After mounting onto slides, cortical sections were washed in PBS and blocked in goat serum for an hour at room temperature. Sections were then incubated overnight with one of 3 primary antibodies or nissl myelin stained. Group one received mouse monoclonal Anti-CD68 (ED1, Serotek, 1:1000) to stain for reactive macrophages and microglia. The second group received mouse monoclonal anti-Neuronal Nuclei (NeuN, Millipore, 1:1000) to stain for neuron cell nuclei. Group three received rabbit polyclonal anti-glial fibrillary acidic protein (GFAP, Sigma, 1:1000) to identify astrocytes, and group four was stained with nissl myelin staining. After the incubation in primary antibodies, sections were washed in PBS and incubated in appropriate secondary antibodies labeled with a fluorescent marker (Jackson Immuno Research) for two hours at a 1:100 dilution. All fluorescently stained sections received a DAPI counter stain (Thermo Scientific).

2.2.5 Hole size analysis

The functional recording radius for microelectrodes is approximately 140µm from the recording site[28]. For our electrodes, these sites are located at the surface of a silicon shank or ~30-60µm from the center of the electrode. Thus we expect that neurons found in the 0-100µm and the 100-200µm bins will be within the functional range for extracellular recordings. During explantation, some degree of tissue loss within these regions was unavoidable[12,14]. To ensure that cell counts were not being biased by such loss of tissue, the explant hole size was characterized for each sample. Fluorescent images were taken at 2.5x magnification around the implant site and then converted into grayscale. Hole areas were determined from these images (ImageJ, NIH).

2.2.6 Qualitative analysis stereological techniques for cell counts

Design-based stereology was used to characterize the cellular presence in the histological sections because it allows for three-dimensional interpretation of structures from each section and is an assumption free method that can be used to study objects of different shapes[29]. A further advantage of this method is that it estimates the total number of objects in any three dimensional volume regardless of that volume's shape or size. Cell counts were made directly from the tissue slices, rather than static images processed by a camera, allowing for the verification of cell presence through multiple focal planes. For the photomicrographs in Figures 2.5, 2.6 and 2.8, the contrast and brightness were adjusted to highlight cell presence and explant site, but such post-processing steps were not utilized during data collection. Cell counts were performed using a Firefly Microfire camera (Olympus America, Inc) attached to a Zeiss Axioplan, which in turn was connected to a Dell workstation using Steroinvestigator Software (Microbrightfield, Inc, Williston VT). A motorized stage was controlled by the software suite to allow for precise tracking along the X and Y and Z axes. Sectioned tissue samples were cursorily observed at a magnification of 2.5X. The center of each electrode hole was located and served as a reference for the coordinate system used for subsequent analysis. Using a contour tool the electrode hole was traced and a circle of 500µm radius was automatically generated about the center of the delineated hole. A standard optical fractionator probe was then used for quantitative analysis of each fluorescent antibody for astrocytes (GFAP), neurons (NeuN), and microglia (ED1) at a higher magnification of 100X oil objective. To do so, a sampling grid was generated within the traced contour and an unbiased counting probe was placed within each grid box (Figure 2.1a). The sampling grid and counting frame dimension were chosen to create a 17.3% sampling percentage within the selected contour. At each sampling site, the tissue was scanned in the Z axis, and cell presence was acknowledged when a nucleus came into focus. The counting frame area was selected to be 2500µm^2 (in X, 50µm; in Y, 50µm) and the grid size of 120µm x 120µm. The thickness of interest (optical dissector height) was set at 12µm leaving a 4µm top and bottom guard zone. To avoid estimation errors, cells were not counted within the guard zone areas. Cell counts were then normalized as described in the following section.

2.2.7 Cell density profile across distance

During cell counting, the coordinates of each cell were recorded with respect to the center of the electrode hole (origin) and the radial distance from the origin to the cell was determined in microns. The cells were binned in 5 annular domains based on distance from the origin: < 100 µm, 100-200µm, 200-300µm, 300-400µm, and 400-500µm. Because the width of the recording electrode varied from 66µm to 115µm, the inner most domain (<100µm) was mostly occupied by the electrode itself. For each slice and each cell type, the total number of cells within each annular domain ware reported as densities by dividing the cell counts by the volume sampled. Because we were interested in changes in cell density around the microelectrode, cell densities for each annular domain were normalized to a baseline cell density defined in the 400-500µm annular domain of the control electrode (i.e. the cell density of control in the 400-500 □m annular domain equals 100%). For the <100µm domain, the amount of tissue remaining after explant was variable both due to the shape of the microelectrode and the fact that some tissue remained on the electrode as has been observed in similar studies [12,14]. Therefore, approximately two-thirds of the counting frames were not completely filled with tissue and those frames were discarded. The remaining frames were analyzed separately.

2.2.8 Intensity analysis

In addition to determining cellular densities, protein expression is of particular interest as a marker of cellular activation. To be consistent with earlier work [14], an intensity based method was used to assess the extent to which GFAP expression differed in the tissue surrounding Poloxamer coated and control microelectrodes. Using the same microscope setup, 10X fluorescent images were acquired, for the GFAP marker, around the implant site. Image analysis was then performed using a custom program developed in MATLAB in a manner similar to He et al., 2006[30]. To account for variations in staining intensity between subjects, the intensity of staining in tissue more than 1 mm from injury site was subtracted from the intensity around the electrode hole. Then, for each slice, a set of ten equidistant lines that spanned the full diameter of the electrode hole was superimposed on the image. The orientation of the lines with respect to the hole was random. Using a consistent intensity scale, the intensity of staining was quantified across the ten lines to create an intensity profile. For each line, the edge of the hole was identified visually. The average magnitude of the intensity was reported in four intervals from the tissue edge: 0-50µm, 50-100µm, 100-150µm and 150-200µm.

2.2.9 Statistical analysis

To assess whether Poloxamer interfered with the ability to record single units, the number of active recording sites (maximum = 4) at weeks 1, 2, 4 and 6 on coated microelectrodes was compared to those on noncoated microelectrodes using paired t-tests, separately for each time point. Differences were considered significant at $p < 0.05$.

To verify that no bias was introduced due to tissue loss across treatments and implantation duration, differences in the hole size around the microelectrodes were compared using a two-way analysis of variance (ANOVA) with fixed factors of duration and treatment with $p < 0.05$ considered significant.

To assess difference in immunoreactivity in the annular domain closest to the microelectrode (< 100µm) normalized density of ED1, GFAP and NeuN positive cells around Poloxamer treated microelectrodes were separately compared to the density of cells around control electrodes using paired t-tests. Due to the fact that this domain was largely filled by the microelectrode, the number of usable sampling frames was limited and, so, this annular domain was tested separately from the other domains. (see section 2.2.6). A Bonferroni corrected significance threshold of $p < 0.016$ was used to determine significance.

To assess difference in immunoreactivity at greater distances from the microelectrode (100µm-500µm), normalized density of ED1, GFAP and NeuN positive cells around Poloxamer treated microelectrodes were separately compared to densities of cells around control electrodes using a repeated measures ANOVA with three within subject factors (distance, treatment, depth) and one between subject factor (duration) using $p < 0.05$ for significance. Finally, planned comparisons using Student's t-test with Bonferroni correction ($p < 0.004$) were used to identify differences between experimental groups at specific time points when warranted.

2.3 Results

2.3.1 Characterization of tissue loss and immunoreactivity adjacent to microelectrode

To determine if Poloxamer interfered with our ability to record single neurons, the number of active recording sites on Poloxamer coated microelectrodes was compared to those on control electrodes. During implantation, more than 90% of the recording sites for both Poloxamer coated and control microelectrodes had at least one discriminable neuron. After implantation, the number of active sites remained stable at approximately 50% throughout the 6 weeks of the study (Figure 2.2). There were no differences between the number of active recording sites seen in Poloxamer coated vs. control microelectrodes electrodes ($p > 0.05$; paired t-test), indicating that Poloxamer did not compromise the ability to detect single neuron activity.

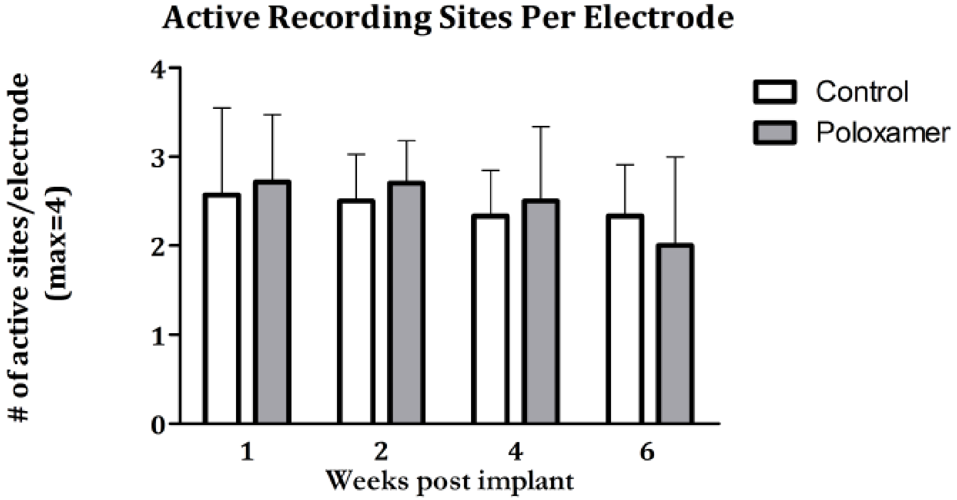

Figure 2. 2 Average number of active recording sites (sites where at least one neuron could be recorded) in control and Poloxamer coated implants over the 6 week study period. No significant differences exist between coatings conditions or time points.

Because the effects of implantation are likely to be greatest near the electrode surface, variations in the amount of tissue removed during explanation[12,14] would affect the variability of the measurements and potentially bias the observations. No significant differences were found in hole size across treatments (F(1) = 0.418, $p > 0.5$), duration (F(2) = 0.74, $p > 0.5$) or the duration treatment interaction (F(2)=0.558, $p > 0.5$) Thus, any tissue that was removed during explants of the microelectrode was similar across groups.

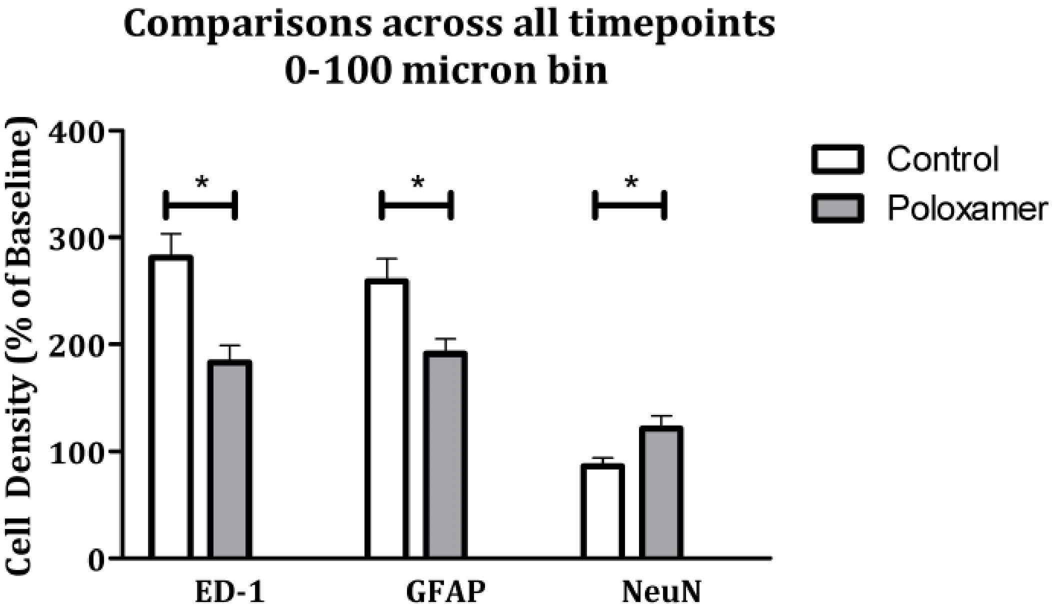

Figure 2. 3 Comparisons of cellular density in tissue found less than 100 microns away from the center of the implant across all time points. There is a pattern of significantly decreased immune reactivity (ED-1 & GFAP) and increased neuronal survival (NeuN) that is consistent across stains. Significance is set at the Bonferroni corrected p value of $p < 0.016$.

Finally, to assess the impact of Poloxamer in the remaining tissue closest to the microelectrode, the cell density within 100 µm of the electrode was compared between groups (Figure 2.3). Control electrodes showed significantly more ED1 and GFAP immunoreactivity around the microelectrodes compared to Poloxamer coated microelectrodes (t(84) = -3.54 p < 0.016, t(83) = -2.68, p < 0.016). Moreover, there were fewer NeuN positive cells identified around control electrodes compared to the Poloxamer coated microelectrodes (t(75) = 2.526, p < 0.016). These data suggest that Poloxamer reduces the inflammatory response around the microelectrode, increasing the density of neurons immediately adjacent to the microelectrode.

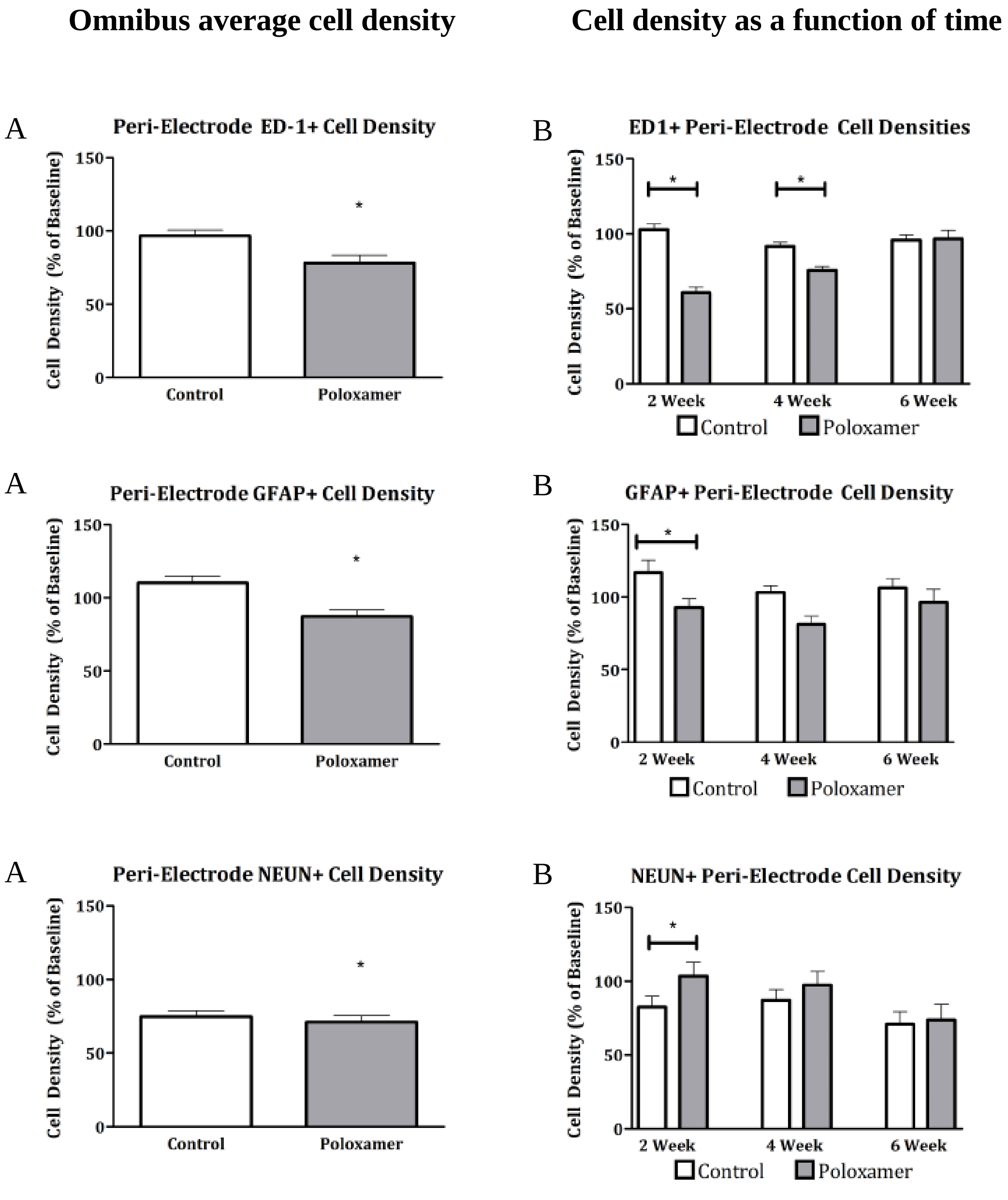

Figure 2. 4 A) Omnibus average cell density of microglia (TOP), glia (MIDDLE), and neurons (BOTTOM) for control and Poloxamer groups. Significance is set at $p < 0.05$. B) Planned comparisons between Poloxamer coated and control implants at 2, 4 and 6 weeks for microglia (TOP), glia (MIDDLE), and neurons (BOTTOM) Significance is set at the Bonferroni corrected value $p < 0.016$

2.3.2 Peri-electrode cellular response

2.3.2.1 Microglial response (ED1)

Across 15 animals, 5174 ED1+ cells were counted. For ED1 immunoreactivity, the omnibus test showed significant main effects for distance ($F(1.043,12.515) = 22.428$, $p < 0.0001$) and treatment ($F(1,12) = 71.534$, $p < 0.0001$) but not duration or depth. The main effect of treatment demonstrated a significant decrease in microglial cell density in Poloxamer coated electrodes over control (Figure 2.4, top left). Because the main effect of duration failed to provide insight into the time course of action of Poloxamer in vivo, planned comparisons with Bonferroni correction were made between coated and control electrodes at 2, 4 and 6 week durations. ED1 immunoreactivity for the coated group was significantly less than for the control group at two weeks ($t(131.865) = 3.926$, $p < 0.001$) and four weeks ($t(133.736) = 3.099$, $p < 0.01$) but not at six weeks post implantation (Figure 2.4, top right).

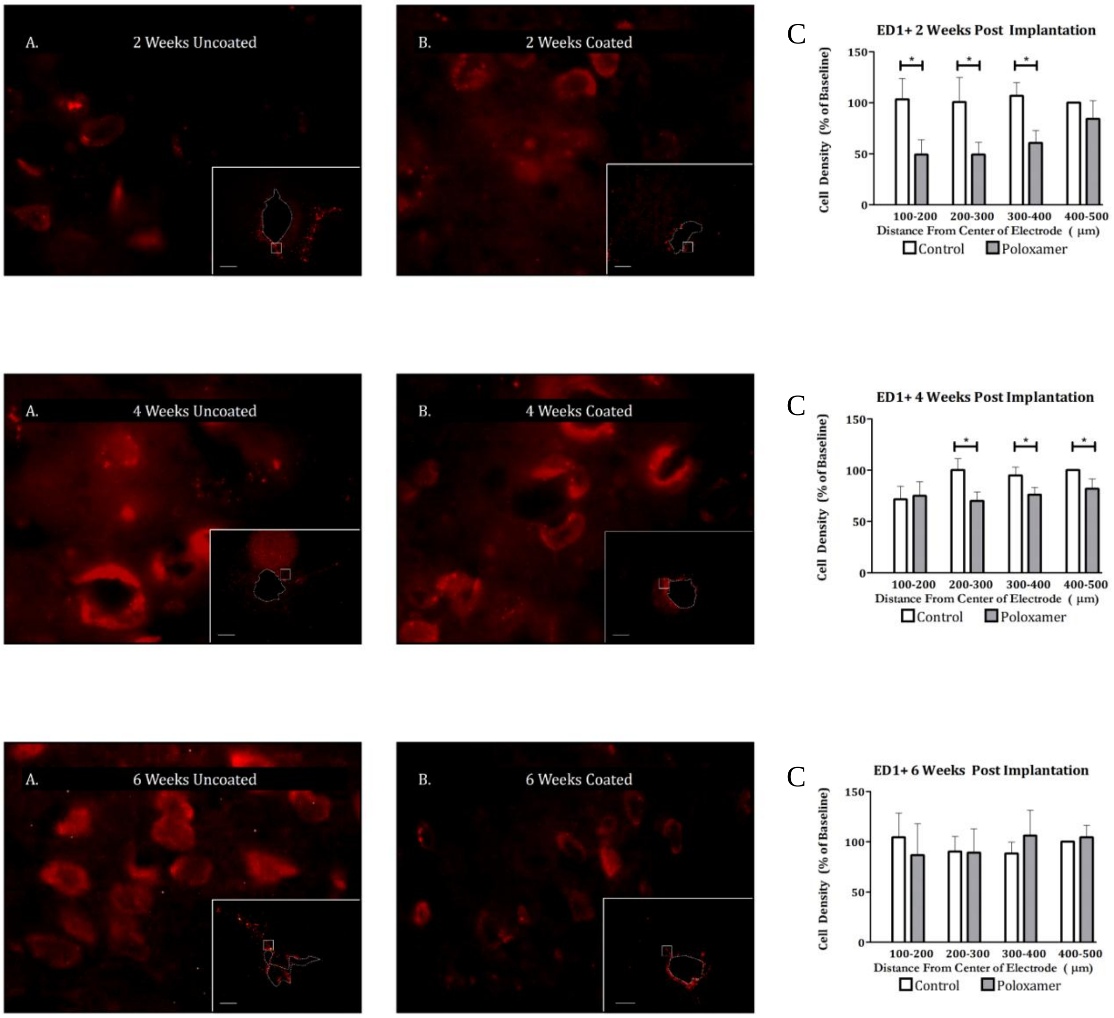

Figure 2. 5 Planned comparisons between peri-electrode ED1 positive cell count in Poloxamer coated and control implants at 2 weeks (TOP), 4 weeks (MIDDLE), and 6 weeks (BOTTOM) post implantation. Significance is set at the Bonferroni corrected $p < 0.004$. Right) 100x Photomicrographs of exemplar peri-electrode tissue surrounding uncoated (A) versus Poloxamer coated (B) controls. Insets are 5x images of the entire implant site. The white dotted line represents the border of the explant site. Scale bar = 100um. Post processing adjustments for brightness and contrast are for publication purposes only. Data collection was done on the tissue directly.

In a similar manner, the effect of distance was examined independently for each time point post-implant (Figure 2.5). At two and four weeks, Poloxamer coated microelectrodes had fewer ED1 positive cells compared to control at a majority of distances tested. And, in agreement with planned comparisons reported above, there were no difference at 6 weeks.

2.3.2.2 Astrocyte cell density

Astrocyte cell presence was characterized by GFAP staining of slides from 15 animals containing a total of 4873 GFAP+ cells. Similar to the ED1 staining condition, the omnibus test showed significant main effects for both treatment and distance but not for duration or depth. ($F(1,12) = 15.997$, $p < 0.005$) In addition, there were no significant interactions between any of the main effects. Electrodes coated with Poloxamer recruited fewer astrocytes than control electrodes (Figure 2.4, middle left). To evaluate the effects of Poloxamer treatment on the astrocytic response over time, planned comparisons were made between Poloxamer and control electrodes at two, four, and six week implant durations (Figure 2.4, middle right). At two weeks, astrocyte cell density surrounding Poloxamer treated microelectrodes was significantly lower than that around controls ($t(196.768) = 4.467$, $p < 0.0001$), but not at four or six weeks, further supporting robust effects of Poloxamer at shorter time periods. This difference at two weeks was mainly due to an elevated number of GFAP positive cells around control electrodes with little difference in the number of GFAP positive cells within the 500 micron annulus for Poloxamer treated microelectrodes (Figure 2.6).

2.3.2.3 Astrocyte protein expression

To provide a view that is consistent with earlier work [14], line intensity profiles were taken as a function of distance away from the edge of scar in GFAP stained samples. ANOVA showed significant main effects for treatment (F(1,380) = 13.443, $p < 0.001$), distance (F (1,380) = 17.843, $p < 0.001$) and duration (F(1,380) = 119.858, $p < 0.001$). As was the case for the GFAP cell counts, there was a significant decrease in the measured fluorescent intensity of GFAP stained tissue surrounding coated electrodes as compared to untreated controls. Planned comparisons revealed that at 2 weeks after implantation, GFAP intensity was significantly decreased compared to control (t(15) = 3.0304, $p < 0.01$) Consistent with cell density analysis, above, at 4 and 6 weeks, there were no differences in intensity of GFAP staining (Figure 2.7).

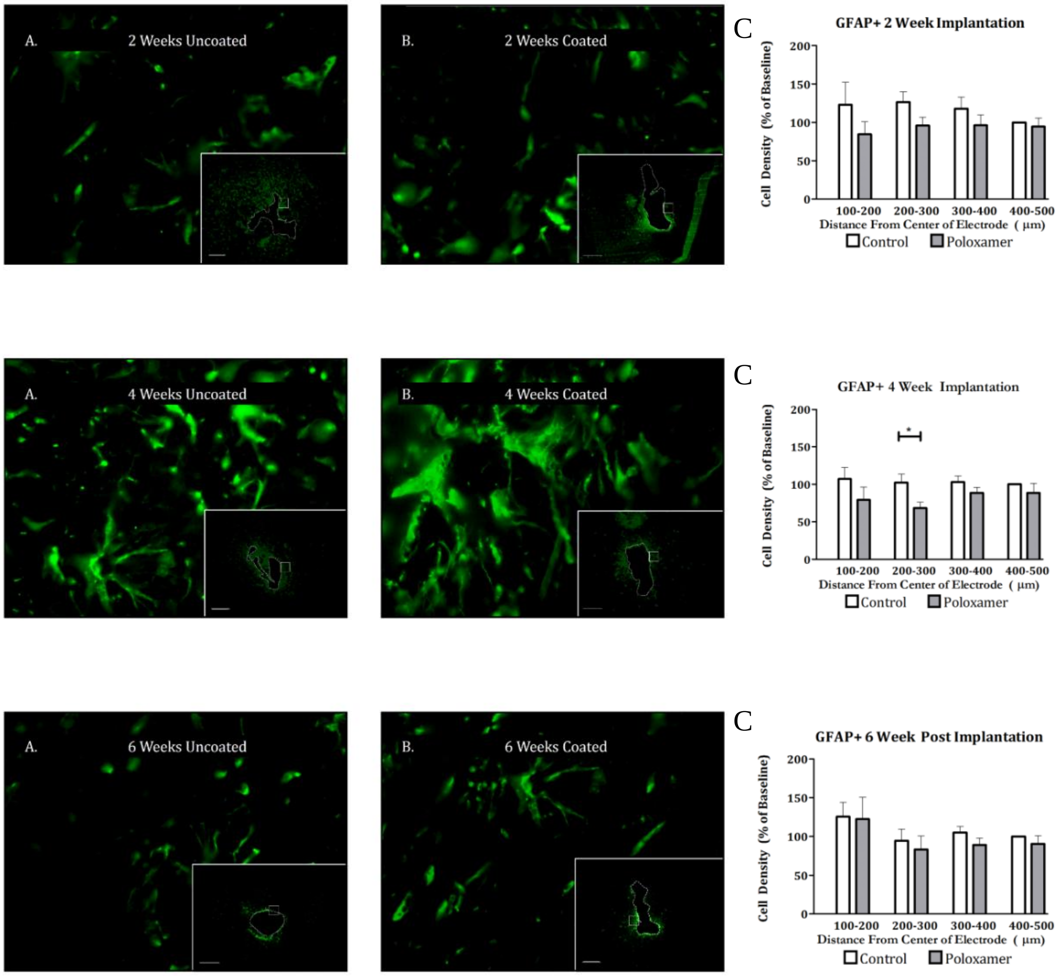

Figure 2. 6 Planned comparisons between peri-electrode GFAP positive cell count in Poloxamer coated and control implants at 2 weeks (TOP), 4 weeks (MIDDLE), and 6 weeks (BOTTOM) post implantation. Significance is set at the Bonferroni corrected $p < 0.004$. Right) 100x Photomicrographs of exemplar peri-electrode tissue surrounding uncoated (A) versus Poloxamer coated (B) controls. Insets are 5x images of the entire implant site. The white dotted line represents the border of the explant site. Scale bar = 100um. Post processing adjustments for brightness and contrast are for publication purposes only. Data collection was done on the tissue directly.

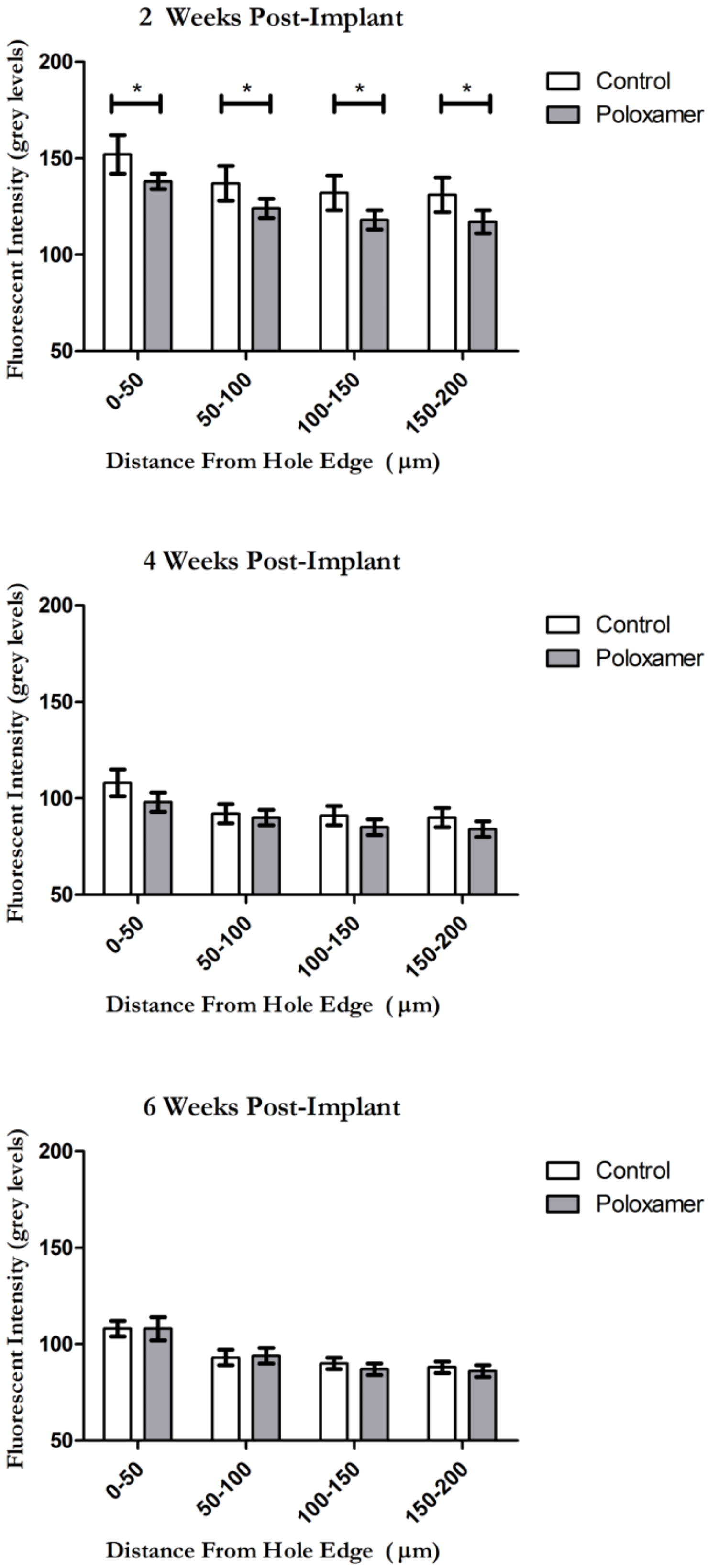

Figure 2. 7 GFAP fluorescent intensity profiles as measured from the edge of the explant site (Note that 0 is no longer the center of the hole as it was in the cell count analysis) at 2 weeks (TOP), 4 weeks (MIDDLE) and 6 weeks (BOTTOM). The y axis scale is reported in grey levels where 0 represents the grey level of normal tissue found far from the implant site. Significance is set at the Bonferroni corrected $p < 0.004$. Note that at 2 weeks, fluorescence intensity is markedly elevated compared to 4 and 6 weeks because the glial scar has not yet contracted by this time point, and the astrocytes are still diffusely occupying the peri-electrode space.

2.3.2.4 Neuronal survival (NeuN)

Neuronal presence around the implanted electrode was characterized by using the NeuN stain for neuronal nuclei. Across 15 animals 10,499 neurons were observed. We found a significantly greater density of neurons around Poloxamer coated electrodes, as indicated by the significant omnibus for treatment (Figure 2.4 bottom left, $F(1,12) = 11.018$, $p < 0.01$). The omnibus also showed a significant main effect of distance ($F(1.676,20.115) = 10.150$, $p < 0.005$) but not for duration or depth, as was observed in the ED1 and GFAP staining condition. To assess the effect of implant duration on the response to treatment, planned comparisons (with Bonferroni correction) of peri-implant neuron density were made between control and Poloxamer coated electrodes at two, four and six weeks post implant (Figure 2.4, bottom right). These comparisons show that neuron density was higher surrounding Poloxamer electrodes at two weeks ($t(196.768) = 3.81$, $p < 0.0005$), but not at four or six weeks post implant. When examining the effect of distance, in a manner complimentary to the ED1 and GFAP staining, the loss of neurons was greatest closest to the microelectrode, within the 200µm relevant for neural recording (Figure 2.8).

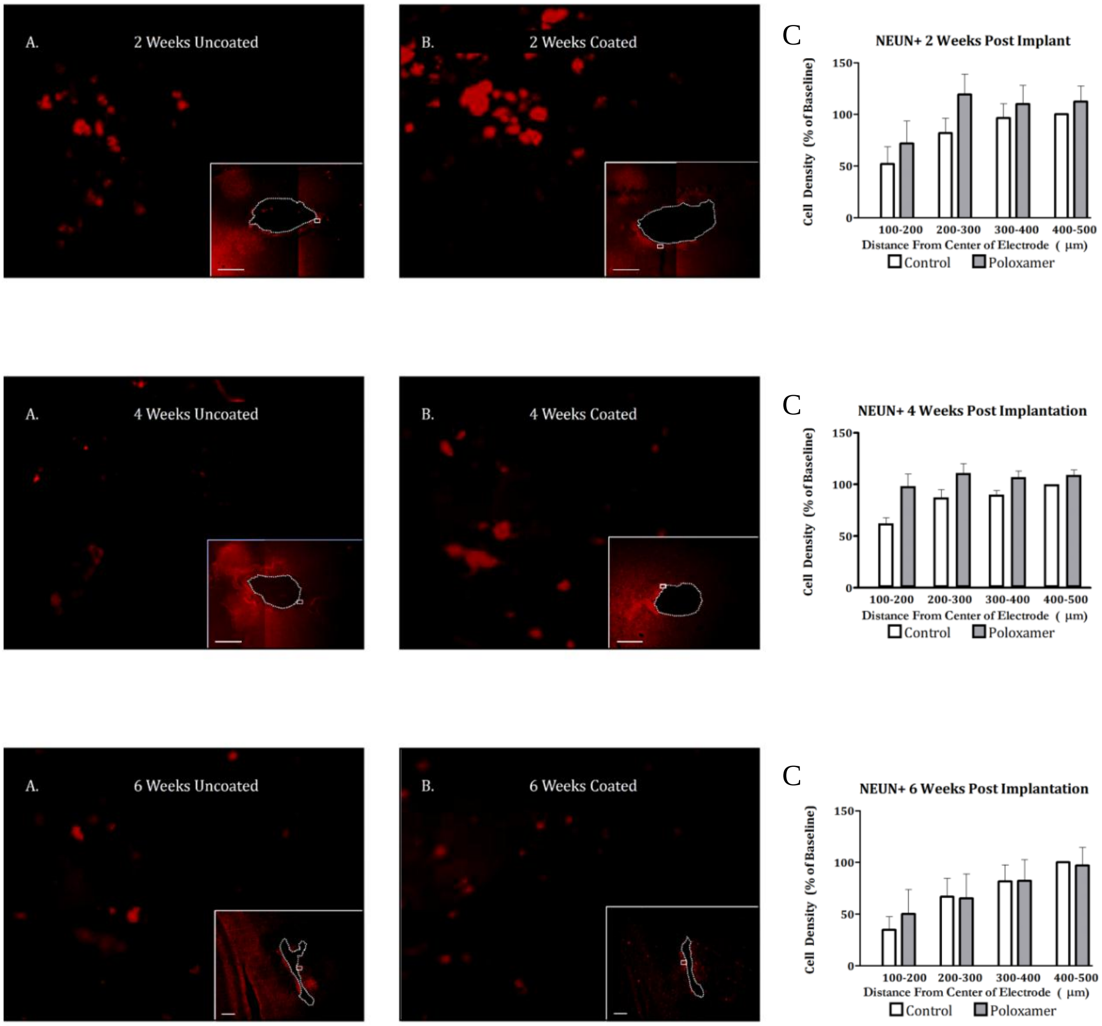

Figure 2. 8 Planned comparisons between peri-electrode neuron count in Poloxamer coated and control implants at 2 weeks (TOP), 4 weeks (MIDDLE), and 6 weeks (BOTTOM) post implantation. Significance is set at the Bonferroni corrected $p < 0.004$. Right) 100x Photomicrographs of exemplar peri-electrode tissue surrounding uncoated (A) versus Poloxamer coated (B) controls at 2 weeks (TOP), 4 weeks (MIDDLE), and 6 weeks (BOTTOM) post implantation. Insets are 5x images of the entire implant site. The white dotted line represents the border of the explant site. Scale bar = 100um. Post processing adjustments for brightness and contrast are for publication purposes only. Data collection was done on the tissue directly.

2.4 Discussion

The results of this study suggest that a surface coating of Poloxamer can reduce the acute inflammatory response to surgical implantation of microelectrodes into the CNS. Markers of significant neuroprotective effects (increased neuron survival or reduced gliosis) were present at 2 weeks post implantation (ED1, GFAP, & NeuN) and at 4 weeks (ED1). By 6 weeks, however, there was no significant difference between the Poloxamer coated electrodes and uncoated electrodes in all metrics. These results suggest that further testing with Poloxamer to reduce cell death and gliosis around the microelectrode is warranted, especially if controlled, long-term release can be achieved.

2.4.1 Assessing neuroprotection

Three staining conditions were used to assess the inflammatory response to chronic implantation. The rationale for choosing these stains is provided in brief. Surgical insertion of a microelectrode tears dendritic and axonal processes and will induce some degree of neuronal cell death [26,31] Beyond this initial mechanical trauma, neuron loss about implanted electrodes (characterized by NeuN stain) may be attributed to the release of cytotoxic mediators to the local environment, displacement from growing scar tissue, and damage caused by persistent micromotion[32]. Concomitant vascular damage and the release of inflammatory mediators and chemotactic factors from dying cells, attract and activate circulating monocytes/nearby microglia[33] and have been shown to significantly affect the degree of glial scaring and cell death around neuroprostheses[22]. The number of phagocytic cells and their state of activation, as characterized by ED1 staining, can therefore provide a gauge for assessing immune response[31,34,35].

In tandem, the recruitment of glial cells contributes to the formation of an astrocyte barrier separating the injury site from healthy tissue[12,31]. Astrocyte participation in glial scar formation includes changes in metabolic state and secretion of neural growth factor, which helps in repairing damaged neural tissue[36]. Reactive astrocytes exhibit phenotypic changes characterized by hypertrophy and increase in expression of glial fibrillary acidic protein (GFAP), which is critical to astrocyte function and their ability to support neighboring damaged neurons[17] and as such their presence and activity (characterized by GFAP staining) reflects the amount of injury sustained.

Long term success of implanted extracellular electrodes depends on electrodes maintaining their proximity to active neurons so that extracellular potentials may be recorded. There are two modes by which the electrode may fail to remain in proximity to the neuronal population of interest. First, the aforementioned glial response may form a physical barrier. A majority of neurons will fire with an amplitude that can be detected within a radius of 140μm of an implanted electrode[28], so a scar of sufficient size may attenuate the extracellular voltage changes beyond our ability to detect. Second, the local neuronal population may die off, due, in part, to mechanical trauma during implantation or subsequent micro-motion[32]. In either case, a neuron-specific marker such as NeuN will demonstrate the extent to which the local population is removed from the implanted electrode.

2.4.2 Time course of cellular response

For the six weeks studied here, the tissue closest to the electrode (<100μm from hole center) maintained significantly more neurons and fewer activated glia (ED1 and GFAP positive cells). Beyond this innermost domain, significant effects could still be observed in a time dependent manner with all effects lost by 6 weeks post implantation. Given Poloxamer's theorized mechanism of action, one would expect that the most pronounced differences between Poloxamer coated and control implants would be present immediately after implantation. In fact, we found a significant reduction in neuronal cell loss and reduced upregulation of cells associated with the inflammatory response normally associated with microelectrode insertion. Of course Poloxamer is not completely effective and in the 200μm adjacent to the electrode surface there is a reduction in the density neurons compared to baseline. This is in accord with other similarly coated single shank electrode implant studies that show a steep loss of neurons in the early immune response up to 150μm from the implant surface [14,21,22,37] with neuron loss extending further up to 300μm from the implant surface in the late immune response[37]. It is possible that higher loading doses, controlled, long-term release or parallel adjuvant therapy may take advantage of this recovery and delay the onset of chronic neuron loss or avoid it all together. The glial response shows a similar finding at 2 weeks, with significantly lower peri-electrode astrocyte and glial cell density. Astrocytes were observed to have long, thin, easily resolved cellular processes indicating newly migrated cells that have not yet undergone activation. Cell counts were fairly uniform within the 400µm of the implant surface with a slight trend towards decreasing in count at greater distances from the implant surface. Though not statistically significant at every distance, the counts were consistently lower in Poloxamer coated implants than in controls. Similarly ED1+ cell counts were also significantly depressed around Poloxamer coated electrodes. Therefore, the impact of Poloxamer in the early stages of glial scar formation was substantial.

By 4 weeks post implantation, the number of ED1 positive cells remains attenuated compared to control but any effect of Poloxamer on the number of neurons or the density of GFAP positive cells was lost in the annular domains beyond 100 microns from the hole center. Although significant differences between Poloxamer and control electrodes were lost, there was a trend toward fewer GFAP positive cells and more neurons around the Poloxamer treated microelectrodes. On possibilities is that by reducing the extent of the initial cellular damage, fewer pro-inflammatory cytokines and immunogenic intracellular moieties are available to recruit microglia and their response was correspondingly attenuated. This observed activation of astrocytes and the formation of an astrocytic sheath are in agreement with other studies of chronic implant response[12,15,20,31].

In the late immune response (6 weeks post implantation), the effects of Poloxamer appear to be lost as no differences between control and Poloxamer coated implants could be noted in any of the staining conditions. This may be due to several factors including the depletion of Poloxamer over time and a fundamental change in the type of damage that occurs as the immune response progresses. The compliance mismatch between the electrode and surrounding tissue and micro-motion inherent to tethered implants could cause persistent mechanical trauma and cellular necrosis[32] that could potentially be mitigated by Poloxamer if delivered chronically. However, prolonged microglial activation and the corresponding release of reactive oxide species[14] could also progressively damage and destroy remaining neurons (via an apoptotic rather than necrotic mechanism). While there is evidence to suggest that Poloxamer does prevent apoptotic cell death in-vitro in response to mechanical trauma[25], it is unknown whether its function is similar in-vivo under chronic inflammatory conditions, and further work is needed to better characterize the long term immune response to Poloxamer coated implants.

2.4.3 Summary

The purpose of this study was to explore the use of Poloxamer P-188 as a neurorepair agent during chronic extracellular recordings in-vivo. The biologic failure mode for chronic neural implants is associated with the development of a glial scar including the recruitment of astrocytes and microglia to the implant-tissue interface[31]. Concomitantly there is a diminishing of the local neuron population, either from cell death or displacement by the growing glial scar[14]. Thus, to ensure the ability to make chronic extracellular recordings of single neurons from such implants, it is necessary to mitigate the degree of glial scar formation and associated neuronal loss. Many groups have attempted to address this problem with the use of anti-inflammatory agents (delivered either locally or systemically) or through non-immunogenic electrode coatings that discourage the foreign body response[19,21,22,38]. However, these methods are limited in that they attempt to modulate the body's responses and not the underlying cause, namely mechanical trauma from a foreign body and subsequent necrotic cell death. Poloxamer has been demonstrated in numerous studies to repair/prevent further damage caused to cellular membranes in diverse cell types including: erythrocytes (ex-vivo), myocytes (in-vitro and in-vivo) neurons (in-vitro)[24,39,40]. The present study has demonstrated that Poloxamer also has a role to play in the in-vivo repair of implantation associated damage to neurons and glia. While the apparent neuroprotective effects of Poloxamer appear to be limited to the acute immune response, further optimization and combination therapies may prolong Poloxamer's neuroprotective effects. This use of Poloxamer potentially targets an as yet unexplored option for attenuating the immune response to chronic micro-electrode implantation.

In summary, this study demonstrates that a simple dip coating of Poloxamer P-188 significantly increases peri-electrode neuronal survival and decreases immune response in the one month following implantation, but the apparent neuroprotective effects are lost by 6 weeks. This window of time encompasses the majority of diagnostic inpatient intracranial implants where single neuron recording might be performed, and thus represents a potentially valuable tool for improving recording yield in this acute implantation scenario.

CHAPTER 3: Methods for implantation of microwire bundles and optimization of single/multiunit recordings from human mesial temporal lobe

3.1 Introduction

In addition to their importance in the study of seizure propagation, single neuron recordings from human subjects is becoming of increasing interest to neuroscientists and engineers alike as our understanding of the role of single neuron activity in cognition, motor control, and information processing becomes better understood. It is now well established that patterns of single neuron activity convey information about the state of neuronal networks, sensory input, and motor output[41–43]. Therefore, changes in these patterns of activity after neurological injury or disease can provide insight into the underlying mechanisms of the disorder and, potentially, insight into therapeutic interventions. While numerous studies have employed either multielectrode arrays (cortical recordings)[44] or microwire bundles (mesial structure recordings) [45–48] to record single neuron activity in humans, few provide specific methodological details about the required troubleshooting approaches for successful recordings, especially from mesial structures. As a result, adoption of single neuron recording protocols has been restricted to a few clinical sites worldwide[49–55] and, consequently the pool of single neuron data available to researchers has been limited. In an effort to improve recording quality and increase single neuron yield, we studied failure modes and developed protocols to reduce the failure rate and improve the probability of high yield single neuron recordings from mesial temporal structures in humans.

The most common method to obtain in-vivo neuronal activity is through extra-cellular recordings, in which a small microwire (<60 μm) is manually placed in the immediate vicinity of an intact neuron[56]. Using single tungsten electrodes, microwire arrays, and drivable tetrodes, extracellular neuronal recordings have long been a staple of animal electrophysiology studies. Indeed, if these electrodes are placed close enough to a neuron, activity from a single cell can be obtained (single-unit activity; SUA). Failing this, it remains possible to record multi-unit activity (MUA) from the collection of cells in a somewhat larger neighborhood around the recording site[28,57]. In animal studies, both SUA and MUA have been used to gain a mechanistic understanding of the neural origin of cognitive function as well as pathophysiology.

For a variety of technical reasons, extracellular SUA/MUA recordings are more difficult to obtain in humans. These technical considerations understandably dissuade clinicians from recording neuronal activity in the modern clinical setting, which places a premium on minimizing operative time and streamlining surgical protocol. Compounding this problem, SUA/MUA recordings do not have a well-defined role for clinical application in intracranial monitoring for epileptic foci localization[58]. Neuronal recordings are thus obtained almost exclusively for basic science research purposes, unrelated to the clinical problem of seizure localization. Indeed, there is limited opportunity to apply SUA/MUA recordings toward clinical and diagnostic use.

There is a growing gap between data that are clinically relevant and data that reflect the underlying pathophysiology of neurological diseases, such as epilepsy. The former is focused on the macroscopic level and the latter is caused by abnormal firing patterns of individual neurons. To bridge this gap, it is necessary to increase the availability of human single neuron data. With this goal in mind, we document the technical challenges that impede established methods for extracellular SUA/MUA recordings[59] in the clinical setting, and explore approaches to overcoming them. We have found that these methods can be implemented to reliably and efficiently record SUA/MUA in humans, as described in this report.

3.2 Materials and Methods

3.2.1 Patients

The presented methods for chronic SUA/MUA recording were developed in 11 patients who underwent implantation of intracranial depth electrode patients at Thomas Jefferson University's Epilepsy Monitoring Unit. This represented the entire population of consenting patients requiring (intracranial) electroencephalography (EEG) with depth electrodes during the study period. All research protocols were approved by the Thomas Jefferson University Institutional Review Board (Philadelphia, PA) and adhere to guidelines governing human subjects research as put forth by the Office for Human Research Protections of the US Department of Health and Human Services (45 CFR 46.100:505) of the Thomas Jefferson University Office of Human Research. All study candidates gave informed consent to participate in implantation of additional microwire and data collection.

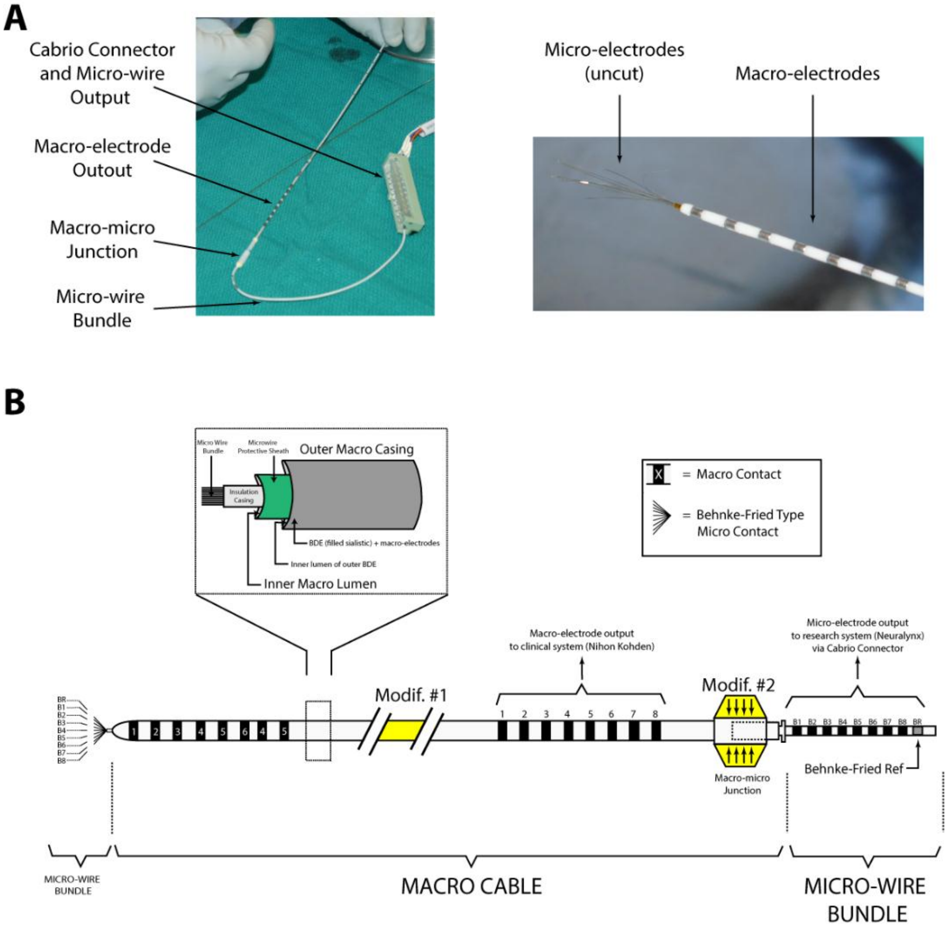

Figure 3. 1 The electrode. A: The AdTech macro-micro electrode consists of an outer piece that houses the macro electrodes (BFD) and an inner piece that houses the micro-electrodes (IWB). A Cabrio connector is used connect the output of the microwires to a downstream device (either ohmmeter or recording system). The macro- and micro-meet at their respective junctions. The right panel shows the projections of the microwires out of the end of the macro-electrode as received by the manufacturer. B: Schematic of the macro-micro electrode. Two modifications were implemented in our methods. First, (Modif #1), the electrode was lengthened by 2 inches to provide extra slack and minimize digital manipulation. Second, (Modif #2) the junction was minimized in width to fit through the large bore passing needle

3.2.2 Electrodes

Extracellular neuronal recordings were obtained from commercially available FDA approved combined macro-micro depth electrodes (Behnke-Fried depth electrode and inner-wire bundle; Ad-Tech Medical, Racine WI), based on the design initially developed at UCLA[59,60]. The electrode is manufactured as two separate components (Figure 3.1). The clinical component (henceforth referred to as the Behnke-Fried Depth; BFD), consists of 8 standard cylindrical, depth macro-electrodes (90-10 platinum iridium contacts, 1.3 mm in diameter, 0.8 mm in length) that are embedded on the surface of a silastic tube with a hollow lumen. The research component (henceforth referred to as the inner-wire bundle; IWB), runs through the lumen of the BFD and consists of 8 microwires (90-10 Platinum-Iridium; 40 micron diameter; Teflon insulation) and 1 reference wire (an additional microwire stripped of insulation). A protective sheath slides along the IWB to facilitate threading into the lumen of the corresponding clinical BFD (see Figure 3.1). The wires terminate in a pigtail-type configuration that connects to a 10 contact Cabrio® connector (AdTech Medical, Racine, WI). To create a connection between the unsterilized ohmmeter and the sterile surgical field, we mated the micro-electrodes with a sterilized Cabrio connector and a sterilized 5-ft customized extension ribbon cable. The extension cable was then mated to a non-sterilized custom breakout box, which was built to allow access to individual microwires and the un-insulated reference.

3.2.3 Implantation procedure

With experience gathered over 11 patients, we have developed a protocol to implant the BFD-IWB electrode. This protocol has been used to record neuronal activity reliably in each patient and consists of the following steps. First, we assemble the equipment needed to cut and implant the electrodes: the IWB and BFD pieces, a 15-blade scalpel, an open container of saline, a clean cutting surface, a sterilized Cabrio connector with a custom 5-ft extension cable, the ohmmeter with custom tip-jack breakout box, and a custom 1.5-mm inner diameter Large Bore Passing Needle (LBPN; AdTech Medical, Racine, WI). Next, we thread the IWB through the BFD and manually manipulate the microelectrodes until they hold a splayed pattern. (Figure 3.2c) This should be differentiated from the as-received state of the microwire bundle depicted in Figure 3.1a. With the IWB threaded through the BFD, we then check the impedances of the microwires (see section 3.2.5 Impedance Testing), cut the microwires, and re-check the impedances. Each microwire is cut individually, at different lengths (ranging from 1-5 mm) with a fresh 15-blade. Obtaining both pre- and post-cut impedances ensures that the surface of each microwire is properly exposed. Threading the IWB through the BFD before the microwires are cut (1) establishes that IWB-BFD is free of manufacturing errors that would otherwise prevent a successful implant and (2) allows us to visualize the final, desired splay pattern of the micro-electrodes before implantation. The IWB is then removed from the BFD and set aside until implantation.

In the following text, we outline our implantation method, which is illustrated with an example case of a left sided craniotomy for the placement of depth and subdural strip electrodes (see Figures 3.2-3.4). All implantations were performed by, or under the direct supervision of, the same neurosurgeon. Before incision, we used scalp fiducial markers to co-register the three-dimensional surgical field to pre-operative magnetic resonance imaging (MRI), to allow for precise positioning of the BFD in the targeted structures using an image guided, frameless stereotactic approach. For all patients the targeted structures were hippocampus or amygdala. After exposure of the implantation site, the pia arachnoid is cut to allow entry of the BFD through the cortex (Figure 3.2a). At this time, a flexible arm with adjustable rigidity was fixated to the headframe and the LBPN was tunneled 3-5 cm through subcutaneous tissue from the incision boundary to a convenient exit site (Figure 3.2b). Next, the image guidance tool (Stryker, Kalamazoo, MI) is attached to the flexible arm in order to locate the target structure on the pre-op MRI; once the target was accepted, the arm was locked into place (Figure 3.2d). Then, using the slotted electrode guide, the BFD was implanted to the appropriate depth in order to reach the target structure (Figure 3.2e). All BFD’s were placed using a transverse temporal approach. With the BFD in place, the IWB was threaded through the lumen of the implanted BFD. The IWB was slowly advanced by hand to engage the tissue beyond the distal tip of the BFD, and the IWB was coupled to the BFD at the proximal end (Figure 3.2f). The coupled BFD-IWB complex was then passed subcutaneously through the LBPN to the exit site (Figure 3.2g). Finally, the BFD-IWB was affixed to the skull via a rigid surgical fixation plate adjacent to the edge of burr hole/craniotomy (not shown). The number of implanted depth electrodes was determined by the number of mesial sites required for each patient’s diagnostic study. Once all electrodes were implanted and tunneled (Figure 3.2h), the exposure was closed in routine manner.

3.2.4 Post-implant monitoring

After implantation, the electrodes (BFD-IWB) were carefully wrapped in a bandage to create a “headwrap.” The microwires were made accessible within the headwrap to measure post-op impedances. Patients recovered in the intensive care unit overnight. After recovery, patients were moved to the epilepsy monitoring unit (EMU). Clinical electrodes were connected to an EEG monitoring system (Nihon Kohden, Tokyo, Japan) using standardized cable interconnects (Integra, Plainsboro NJ). Under the supervision of the research team, technicians then connected the microwires of the IWB to custom Cabrio adapters and a headstage pre-amplifier (HS-36h, Neuralynx, Bozeman MT). The headstage preamplifier and all excess wire were securely wrapped to the patient's skull for the duration of the patient’s stay. Amplified microwire signals were sent to a high-speed data acquisition system (Digitalynx S, Neuralynx, Bozeman MT) using shielded 25-ft tethers, which were less restrictive than the analogous clinical tethers. Recordings began immediately after the initial hook-up. Signal quality optimization will be discussed in the results section.

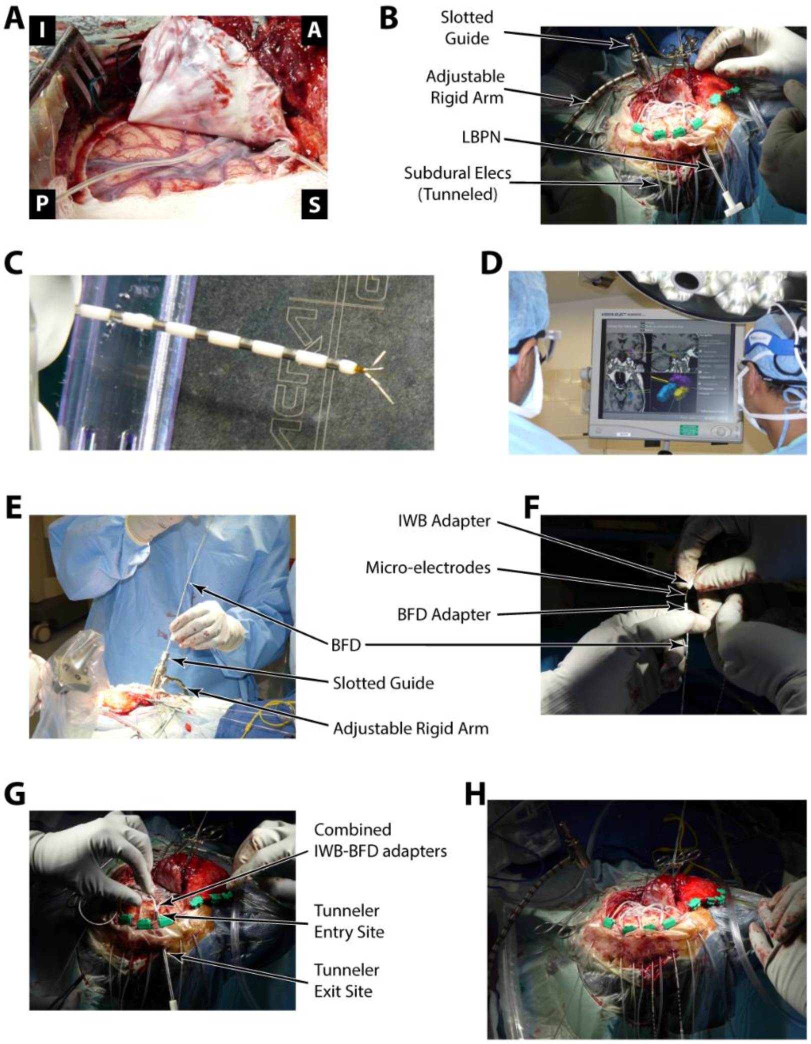

Figure 3. 2 Illustration of implantation procedure. See methods (section 3.2.3) for a full description of each panel in the Figure in relation to electrode implantation.

3.2.5 Impedance testing

We isolated micro-electrode breaks by performing routine impedance testing. Using a clinically approved impedance meter (model IMP-1; Bak Electronics, Sanford FL), electrode impedance was measured at the following time points: 1) post sterilization (ex-vivo), 2) post final-cut (ex-vivo), 3) post implantation, 4) postoperatively, 5) when the patient arrived on the neurological intensive care unit (NICU), 6) when the patient arrived on the long-term epilepsy monitoring unit (EMU), and 7) periodically over the course of the recording. All impedances measurements were made between individual microwires and the internal reference wire whenever possible. In cases where the reference wire was broken, an intact microwire was used in its stead. Ex-vivo impedances were performed in sterile saline. Typical impedances of intact electrodes ranged between 50 and 500 kΩ. Measurements greater than 1MOhm were considered open. Post-implant measurements were consistently 20-30 kΩ higher in-vivo versus the saline bath. An example of impedance measurements for the entirety of an example patient's hospital stay is given in Figure 3.3b. We note that Figure 3.3b displays a different patient than Figures 3.2, 3.4, and 3.5. This is done to show an example of how micro-electrode impedance changed as a function of time, which we only recorded in the first 4 patients. After the first 4 patients, we began wrapping the electrodes in the patients headwrap. This helped stabilize the electrodes (see section 3.2.4), but complicated access to the microwires for daily impedance measurements.

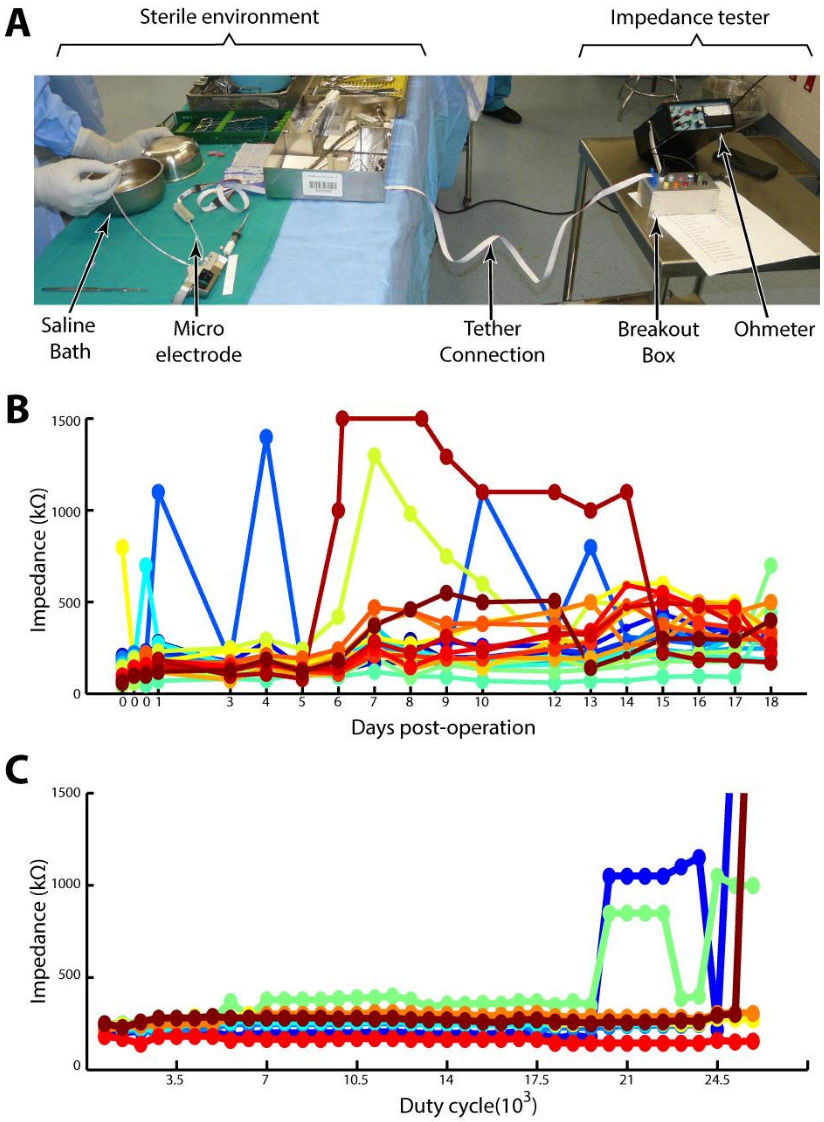

Figure 3. 3 Impedance measurement. A: The set-up to measure impedances in the surgical environment. The left half of the Figure represents the sterile field, the right half the non-sterile area where impedances were obtained by the research assistant. B: Impedances taken every day during one patient's hospital course. Each color represents a different micro-electrode n = 16. Neurons may only be recorded from electrodes with low impedances, thus jumps in impedance correspond to a drop in the associated signal to noise ratio and a loss of all recorded neuron activity C: Impedances taken for 8 micro-electrodes using the fatigue bench-top simulation.

3.2.6 Bench testing

In the results, we document the various "failure modes" of the micro-electrodes. A failure mode is defined as a discrete set of circumstances leading to an irreparable decrease in the signal-to-noise ratio (SNR) of the microwire recording. To more precisely characterize these failure modes, we performed a series of bench tests to reproduce failure in a controlled laboratory setting. The data collected during these bench tests allowed us to formulate more accurate hypotheses regarding the cause of the failure modes and more effectively design workarounds.

Some electrodes experienced a sudden and severe drop in SNR, which we attributed to discrete micro-electrode breaks. To simulate this failure mode, we quantified the absolute tensile strength required to break the IWB. This value served as a loading threshold; forces beyond this threshold would necessarily break the microwires. A benchtop simulation was run on 3 sample IWBs (identical to those used during implantations). It is important to note that the IWB was tested without the BFD to simplify the testing apparatus. It was determined that the silastic material of the BFD is easily deformed and any tensile loading would quickly shift stress to the more rigid platinum wires of the IWB. Axial tensile loading was performed with a Bose Electroforce 3200. Samples were prepared by removing the protective sheath and clamping the IWB into two knurled clamps spaced 10 cm apart. The clamping causes all microwires to short to the reference microelectrode. Microwires were submerged in sterile saline. Starting at 0N, axial tension was increased in increments of 0.5N. After each increment, impedance measurements were made on the reference microwire. As during surgery, typical reference electrode

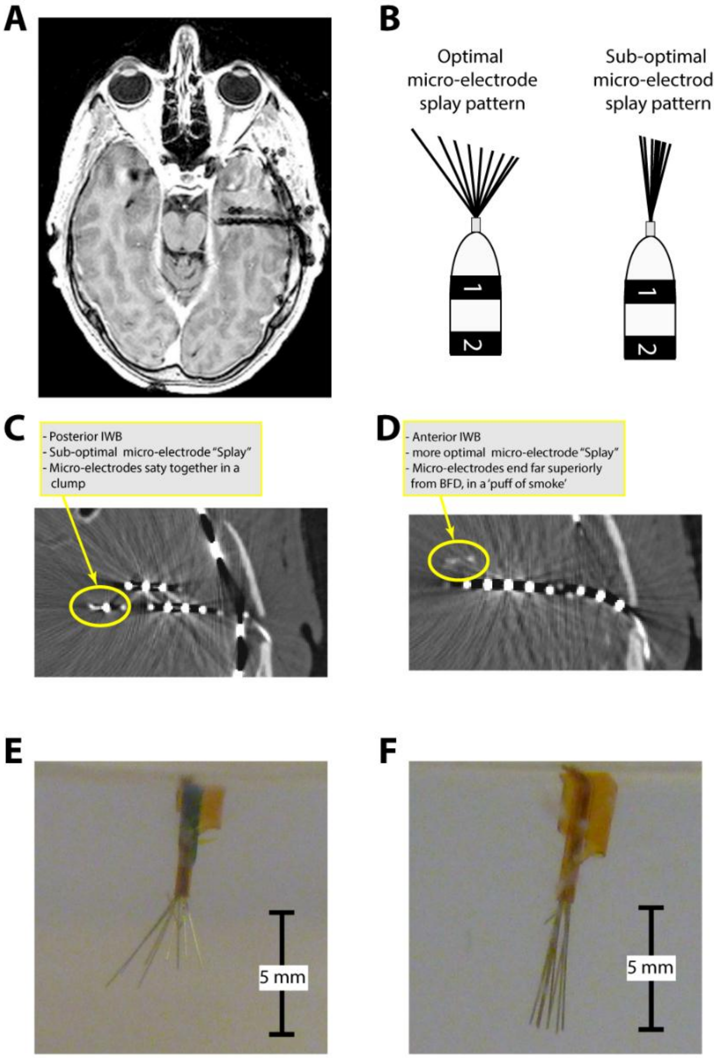

- Posterior IWB
- Sub-optimal micro-electrode "Splay"
- Micro-electrodes saty together in a clump

- Anterior IWB
- more optimal micro-electrode "Splay"
- Micro-electrodes end far superiorly from BFD, in a 'puff of smoke'

Figure 3. 4 Micro-electrode splay in-vivo and ex-vivo. A: Post-operative axial MRI of depth electrodes shown in Figure 3.2. B: Cartoon example of optimal and sub-optimal micro-electrode splay patterns and staggered microwire lengths. C, D: Thin sliced post-operative CT's of the posterior (C) and the anterior (D) depth electrodes. E, F: Benchtop tests of microwire splay patterns using pre-implantation induction of micro-electrode splay (E) and simply implanting the naïve micro-electrode (F).

impedances were between 5 and 10 kOhm. Failure was identified by a relative increase in impedance and a corresponding jump in the generated stress-strain curve.

Other microelectrodes exhibited a gradual and steady degradation of SNR over time, which we attributed to cyclic tensile loading at sub-threshold loading values. To simulate this, a benchtop apparatus was developed to mimic the inner wire bundle configuration during implantation. A single metal plate lined with a 2mm foam rubber pad created a flexion point to act as a stress concentrator. The wire bundle was then deflected to 80 degrees from the horizontal and a 3N impulse was applied every 2 seconds for 50,000

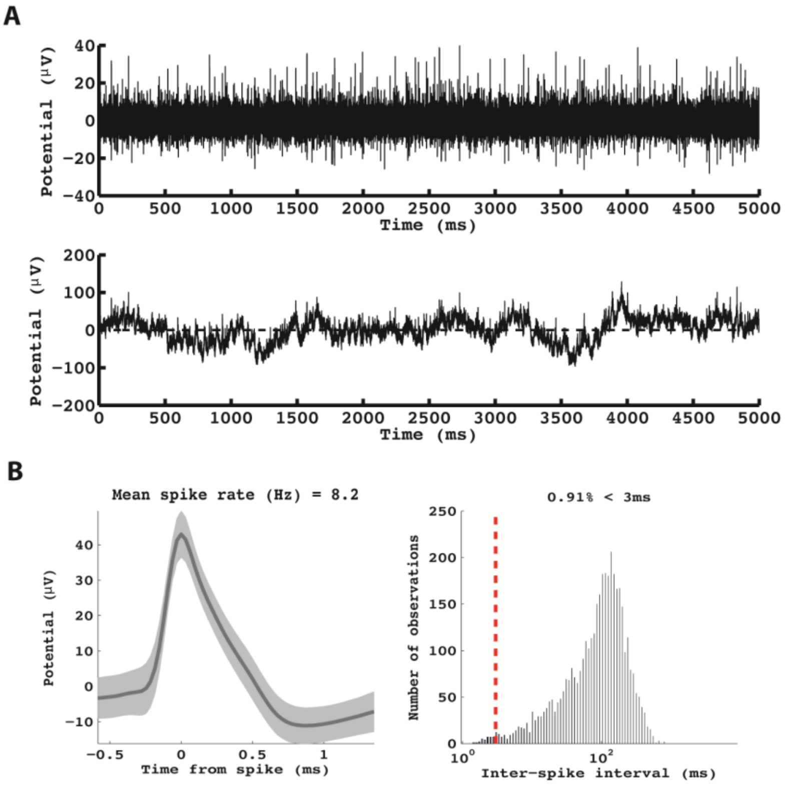

Figure 3. 5 Example of neuronal data obtained from the patient in Figures 3.2 and 3.4. This unit was recorded from the most anterior electrode. A: The raw (bottom panel) and pass-band filtered (300-9000 Hz, top-panel) raw voltage traces are shown for this microwire. B: The average waveform (left panel) and the distribution of inter-spike intervals (right panel) are shown. Putative interneurons and pyramidal cells were segregated in the methods described in Section 4.2.3 and their respective activity during seizure propagation is investigated in Section 4.3

loading cycles. Impedances were recorded periodically to see if cyclic sub-threshold loading at a stress concentrator could break microwires. Two IWBs were tested in this configuration and compared to in-vivo impedance measurements. Unit yield was dependent on the degree of microwire splay in neural tissue (see Figure 3.4b). To actually visualize splay, a benchtop agar model was used. To mimic brain tissue, a clear agar gel was cast in a square Plexiglass chamber. Using published values of Young's modulus and the Poisson ratio of brain tissue[61], a reduced modulus was calculated and compared to published agar concentration-reduced modulus curves[62]. It was determined that a 0.4% agar solution approximates the elasticity of brain tissue. Once solidified, a polyimide tube with the same inner diameter as the lumen of the clinical depth electrodes was inserted into the gel. Two inner wire bundles, one mechanically deformed to encourage splay, and the other as delivered by the manufacturer, were prepared. Inner wire bundles were threaded into the polyimide tube and the protective sheath withdrawn. Inner wire bundles were advanced so that 5mm of microwire extended beyond the polyimide tube (this approximates the amount of microwire that engages tissue in-vivo). High resolution photos were taken to document splay and the electrode was withdrawn. The process was repeated 5 times for each electrode.

3.2.7 Unit identification & analysis

SUA/MUA was manually confirmed using Offline Sorter (Plexon, Dalas TX) following established techniques[63]. In brief, raw data was high pass filtered at 396 Hz, and a threshold was set at 4.5 standard deviations about the mean amplitude. 4 msec waveforms were captured about each threshold crossing and candidate waveforms were plotted in 3 dimensional principal component space. SUA/MUA was identified by a spatial clustering in principal component space. A noise cluster was identified and excluded from further analysis. SUA was identified when isolated clusters contained fewer than 0.5% of spikes within 1 msec of one another and an autocorrelogram that showed evidence of the refractory period. MUA was identified as isolated clusters where between 0.5% and 3% of spikes occurred within 1 msec of one another.

When comparing yields, it is important to note that many published human single neuron studies record activity over the course of several sessions spread out over the course of the patient's stay. With these discrete recording events, it is not possible to definitively track neurons seen on one day to the next. As a result neurons recorded during different recording sessions are treated independently. To avoid bias, we took random 2.5 hour recordings from each day of the patient's stay and have reported the recording with the largest number of identified single units and report yield from this recording alone

3.3. Results

3.3.1 Single- and multi-unit neuronal recordings

Using the protocol described in the methods section, we recorded extracellular SUA/MUA from 11 patients implanted between November 2011 and February 2013. Over thirty-two random 2.5 hour recording sessions within these 11 patients, 125 single units and 39 multi-units were successfully identified An example of unit activity recorded from the patient presented in Figures 3.2 and 3.4 is provided in Figure 3.5. For the 11 patients presented, four had two depth electrodes, three had three depth electrodes and four had four depth electrodes. Single neurons were recorded as far as 2 weeks post implantation but on average recordings persisted for 7 +/- 3 days with over 50% of recordings limited by the clinical decision to proceed with resection. On average, each BFD-IWB (8 microwires) recorded a maximum of 2.1+/-0.9 single neurons. Before failure modes were identified and workaround protocols were developed, the average single neuron yield per depth electrode was 1.4+/- 0.5 (n = 3) single neurons per depth. After recordings were optimized to avoid the identified failure modes, the yield nearly doubled to 2.7+/-0.8 (n=3) single neurons per depth electrode. All patients had at least one multi/single unit during the last recording prior to deplantation.

3.3.2 Failure modes: overview

The primary goal of this technical report is to document the technical challenges encountered during the implantation and recording of extracellular neuronal signals, and also methods to overcome these challenges. In particular, whereas the methods used to record extracellular neuronal data using microwires are, in principle, similar to those used to record routine intracranial EEG, certain failure modes warrant description to mitigate their deleterious effects and allow reliable recordings of firing rate data. For some of these failure modes, we were able to change our protocol and improve recordings, resulting in high-amplitude units for the entire duration of a patient's hospital stay (~2 weeks). In the following sections, each observed failure mode is described and fully characterized, including the hypothesized mechanism underlying the failure mode, any bench tests used to confirm the proposed mechanisms, the adopted workarounds, and the data to support their efficacy.

3.3.2.1 Failure Mode #1: Sudden loss of single neuron activity

The most common failure mode was that micro-electrodes periodically exhibited a sudden and complete loss of single neuron activity. By frequently measuring impedances throughout the patient's hospital stay, we were able to determine that this failure mode most often occurred during periods when the electrodes were physically manipulated (e.g.: surgical tunneling procedure, initial hook-up, headwrap changes, unhooking for imaging, etc). Discrete breaks in micro-electrodes were detected as sudden jumps in impedance (see Figure 3.3b).

We hypothesized that this failure mode was caused by breaks induced by excessive tensile loads placed on the microwires, as in the case of overly aggressive digital manipulation. Indeed, the 40 micron platinum wires that comprise the IWB are inherently fragile. The alloy used has an ultimate tensile strength (UTS) of between 400 and 700 MPa, meaning that each un-insulated microwire breaks at a tension load of ~0.90 N. However, the number of electrodes in the wire bundle and the Teflon insulation imparts some added tensile strength, making it necessary to empirically derive the UTS of the micro-electrodes. To do that, we conducted bench tests (see section 3.2.6 Bench testing) that demonstrated broken wires at an applied force of 13+/-0.5N. To put this in perspective, the reported maximum flexion force of an adult human finger is ~120N[64]. While the silastic tube of the BFD augments the yield stress of the fully assembled electrode, its greater elasticity quickly transfers the majority of applied axial tension to the more rigid IWB. It is therefore no wonder that rigorous or inattentive digital manipulation of the micro-electrodes was a common failure mode.

Three methods were implemented to overcome this failure mode. First, a custom tunneling needle (LBPN: see 3.2.3 Implantation procedure) was designed to reduce electrode manipulation during tunneling, which we isolated as a step that was very prone to electrode breaks. The LBPN worked by minimizing strain on the electrodes as they passed subcutaneously. Second, we used customized electrodes that were 2 inches longer than the standard design (current length: 570 mm). The elongated electrodes allowed technicians excess slack when connecting electrode tails to the recording system, which minimized tensile force when hooking/unhooking the electrodes in the EMU. Third, and most importantly, the clinicians made sure that the entire clinical and research team understood the importance of minimizing excessive tensile force when physically manipulating the micro-electrodes for any reason.

It should also be noted that a new generation of BFD-IWB hybrid electrodes are available that addresses sudden microwire breakages due to tensile loading, specifically at the junction between the platinum microwire and the clinical connection site. The design tested in this study has a structural weak point (lower UTS) where platinum wires are soldered to their clinical contact pads (the component that is clamped onto by the custom Cabrio connector). The new design structurally reinforces this junction with epoxy, thereby reducing the likelihood of failure.

3.3.2.2 Failure Mode #2: Gradual loss of single neuron activity

A second common failure mode was a gradual decrease in SNR from micro-electrodes over time, leading to total loss of signal (presumed electrode break) or a loss of all unit activity from the electrodes. We hypothesized that this progressive electrode failure reflected microwires that were broken through cyclic *sub-threshold* (<13 N; see section

3.3.2.1 loading at a point where the microwire was weakened by electrode geometry (stress concentrator).

To test this hypothesis, we designed a cyclic fatigue model (see section 3.2.6 Bench testing) and used the model to simulate cyclical sub-threshold tensile loading (Figure 3.3c). Confirming our hypothesis, both bench tested and in-vivo impedances demonstrated similar patterns (compare Figures 3.3b and 3.3c). Impedances start between 50 and 500 kΩ and slowly drift upward by 10-100 kΩ followed by sudden jumps to the MΩ range indicating a break in the microwire. Over time, broken wire termini occasionally come back into contact with each other causing sudden and transient drops in impedance back to the 50-500 kΩ range. The similarity in patterns between benchtop and in-vivo measurements supports our sub-threshold cyclic fatigue failure explanation for progressive electrode failure within the headwrap.

To minimize the degree of progressive electrode failure, we attempted to remove points where cyclic fatigue failure could occur. A gentle curve (as opposed to a sharp bend) was formed as the electrode left the burr hole. The electrode was fixed *flush* (specifically not within the burr hole) to the skull in this position using a small surgical plate while not pinching the electrode. Similarly after the electrode tail exited the skin, the headstage was manually oriented to reduce the need for sharp bends. A tight outer headwrap ensured that the headstage and electrode tail maintained their relative positions during the recording as any shifts within the headwrap would introduce sharp bends.

3.3.2.3 Failure Mode #3: Electrode position and microwire splay

As single neurons are only captured within 250 microns of a microwire[28], placement of microwires in low-density cellular areas will result in poor neuron yield. Indeed, some microwires did not record any units despite a technically successful implant (no failure modes observed). We hypothesized that such microwires were not located near enough to active cells. Without intra-operative recording techniques and/or micro-drive technology, such outcomes are, in our estimation, unavoidable.

A more remediable failure mode, however, was the lack of a good "splay pattern" of microwires in neural tissue. In this context, splay pattern refers to the position of the microwires within an IWB with respect to each other (see Figure 3.4b for an illustration). Ever since the BFD-IWB design was first formalized, the splay pattern of the microwires was recognized as an important determinant of unit yield. Indeed, Babb et al. noted that "*the less traumatic "spray" insertion results in successful unit recordings on* more *micro-electrodes and for longer periods than when the wires remain in a bundle*"[60]. We also observed that fewer units were recorded when electrodes stayed clumped together "in a bundle," in neural tissue (Figure 3.4c) versus when they splayed out relative to each other (Figure 3.4d). In Figures 3.4c/d, we identified the splay pattern using high-resolution post-op CT's (<0.9 mm thick slices). In these scans, when microwires successfully splayed into neural tissue they appeared to terminate in a "puff-of-smoke" (Figure 3.4c), while an unsuccessful splay terminated in a narrow radiopaque bundle (Figure 3.4b). Out of 33 BFD implanted during this study, ~76% demonstrated successful splay upon review of post-operative CT. Recordings from depth electrodes demonstrating microwire splay showed significantly more neurons (2.0+/-1.6 neurons n=76) than those that did not (0.9+/-1.1 n = 23) (p = 0.014).

In order to increase the percentage of microwires that engaged neural tissue with the appropriate splay pattern, prior to implantation and during the final cut, the neurosurgeon physically deformed each wire to the desired splayed configuration and re-sheathed the end to thread the IWB into the lumen of the BFD. The goal here was to impart some degree of memory to the wires that would encourage splay as the inner wire bundle was advanced into tissue. Each wire was cut independently. Prior to implementing this technique approximately 29% of implanted IWB would fail to splay. After implementation, only 17% of implanted IWB fail to splay.

Postoperative CT provides only limited insight into how individual microwires of the IWB behave as they engage the tissue. We therefore implemented bench testing using an agar brain analog to investigate whether pre-deforming the micro-electrodes increases the likelihood of achieving the desired splay pattern. Specifically, using an agar model for neural tissue (see section 3.2.6 Bench testing), we performed a mock implant using two IWBs: one mechanically deformed to encourage splay (as was done in the surgical setting), and the other as delivered by the manufacturer (the naïve electrode). While there was some degree of electrode splay from the naive electrode (1.2+/-0.4mm; Figure 3.4f), the electrode that was pre-deformed showed a considerable increase in the width of splay (4.0+/-1.2mm; Figure 3.4e).

3.3.2.4 Failure Mode #4: Motion artifact

Motion artifact can be an ambiguous term. Physiologic motion artifact refers to myogenic potentials contaminating EEG data, however this type of motion artifact is more problematic for scalp EEG. For intracranial and single neuron recordings, electronic motion artifact is the major concern. When connecting intracranial electrodes to a recording system, multiple coupling connectors are required to complete the circuit. As the patient moves, these coupling connectors can shift causing slight changes in impedance which are reflected in the recording as low frequency oscillations or intermittent voltage transients. In addition, in the case of unshielded cables, as conductors move through external magnetic fields (often generated by hospital equipment), transient currents may be generated that can contaminate recordings.

In our present recordings, motion artifact contaminations were avoided through several approaches. First, only shielded cables were used between the electrode tail and the recording system. Second, all electrical coupling connections were secured to minimize motion of the micro-electrodes relative to the headstage. Connections between the electrode tail, the Cabrio connector, and the Neuralynx headstage were stabilized with parafilm, and then securely wrapped in the patient’s headwrap. All connections outside the headwrap were modified to include a latching mechanism and were attached to the patient’s junction box with velcro. Lastly enough cable was used that the patient was never restricted in his/her movement and no tension was put on the wire or the couplers. Extra care was taken to make sure that connections would not break during seizures.

However, for safety, a single breakpoint was set up at the headstage to prevent patients pulling out electrodes by tugging on their wire bundle.

3.3.2.5 Failure Mode #5: Power line noise & ground loops

Power line contamination typically refers to 50 or 60 Hz electromagnetic interference that originates from power lines or other external voltage sources[65]. The generated electric field can induce capacitively coupled currents in unshielded conductors which manifests as a superimposed alternating voltage on recordings. In an in-patient diagnostic setting, both hospital equipment and personal electronic devices can act as electromagnetic radiators and the patient, electrodes, and connecting cables can act as antennas. In general the easiest solution is to remove the source of the electromagnetic interference. In cases where this is not possible, the recording can be protected by shielding the recording cables and equipment. Shielding creates a faraday cage around the recording wires and hardware and prevents external electromagnetic interference. Shielded cables contain a conductive layer surrounding signal carrying wires. This conductive layer is connected to ground at one end of the cable, creating the faraday cage. It should be noted that connecting the shield to ground on both ends of the cable can introduce ground loops (see below). For equipment that doesn't have shielding, a grounded conductive cloth or aluminum foil can be used to the same effect.

Ground loops refer to situations where the electrical grounds of supposedly isolated devices are not at the same potential. The potential difference between circuits can generate a current that contaminates both devices. In the case of human recordings, different electrical outlets in the patient room may have slightly different ground potentials. Thus, connecting a clinical recording system and a research recording system to different outlets with different grounds may create a ground loop. The easiest way to compensate for ground loops is to ensure that equipment ground is short circuited across all devices.

To address power line noise and ground loops, custom shielded tethers and couplers were designed in conjunction with the manufacturer (Neuralynx, Bozemann MT). Both the research recording system and the clinical recording system were plugged into the same outlet to share electrical ground. The research system patient ground and the clinical system patient ground were also short circuited using a touchproof jumper cable. When necessary, a conductive silver cloth was wrapped around the headstage and grounded, which extended the faraday cage up to the patients headwrap. Proper patient grounding not only ensures that no ground loops occur, but also significantly improves the signal to noise ratio.

Lastly, the patient ground refers to a non-current carrying ground wire that is often times connected to the skin above the mastoid process. The human body tends to act as an antenna picking up electromagnetic contamination across the frequency spectrum. By recording the potential seen by the body as a whole it can be subtracted out of neural recordings, resulting in improved signal to noise ratio (common mode rejection). In this case the noise common to both the patient ground and the clinical recording can be rejected leaving only neural signal. Manifestations of poor common mode rejection due to poor grounding include increased power line contamination, and an increase in the noise floor, particularly above 1000 Hz.

3.3.3 Additional considerations

In addition to the failure modes, there were a number of additional considerations. These issues were not severe enough to induce a failure mode per se, but needed to be addressed before neuronal data could be recorded in the clinical setting.

3.3.3.1 Additional considerations #1: Referencing schemes

Most modern recording systems allow for some flexibility in choosing a reference electrode. One option is to choose the reference to be a low-impedance contact in the vicinity of the microwire. Examples of such references include, the dedicated (stripped) microwire reference provided on the IWB by the manufacturer, the most distal macro-electrode contact on the BFD, or a macro contact that is found to be the subdural space based on post-operative imaging. For our recordings, All of these contacts performed equally well as low impedance (<10 kΩ) reference lines. The advantage of using a low-impedance reference was that it was guaranteed to be quiet with respect to unit activity: any unit observed could be localized to the microwire and not the reference line. However, the disadvantage was that using low-impedance contacts caused the SNR to increase. The suspected mechanism of this increase in SNR was that the low-impedance reference acts as more of a high pass filter than its microwire counterpart, and as a result the output of the differential amplifier has a poorer signal to noise ratio at higher frequencies. To combat this problem, we often recorded unit activity using another microwire as a reference, which had a similar impedance profile as the recording electrode. Because the reference microwire is in brain tissue and not CSF, single neuron contamination of the reference wire can artificially inflate the number of neurons detected. It is imperative to review all offline analysis for time locked inverted action potentials to ensure that the reference wire is single neuron free. Single neuron contamination being avoided, the microwire that most improved the signal to noise ratio was routinely chosen as reference.

3.3.3.2 Additional considerations #2: Input impedance on recording amplifier

Perhaps the most limiting factor to unit recording in the clinical setting is the cost needed to purchase an amplifier with appropriate input impedance to record from microwires. A high input impedance on the recording amplifier is needed to avoid impedance mismatch between the electrode and the amplifier. Impedance mismatch refers to signal distortion as a result of connecting a high impedance circuit (IWB) to a low impedance circuit (the differential input of a standard clinical amplifier and analog-digital-converter). The difference in impedance can cause signal reflections, where certain frequency components of the signal are reflected back to the brain instead of transmitted to the recording system. Modern single neuron recording systems avoid this through the use of a voltage buffering headstage. These headstages are designed to have an internal impedance (1-10GΩ) that is several orders of magnitude higher than the source impedance (100k-1MΩ). Standard clinical recording systems are meant to record from scalp or intracranial electrodes (1-10Ω) and have correspondingly lower internal impedances. Thus high impedance microwires recorded on standard EEG systems will likely produce distorted signals[66].

3.3.3.3 Additional considerations #3: alternative electrodes

Lastly, this study has focused exclusively on the use of the Behnke-Fried type of combined macro-micro electrode for single/multi-unit recordings from mesial temporal structures. It should be noted, however, that alternative devices are commercially available and FDA approved for recording in human patients. Hybrid depth electrodes[67,68] have been designed where micro platinum contacts are interspersed along the shaft of traditional depth electrode in between existing macro contacts. Such devices share many of the same potential failure modes that have been discussed with the obvious exception of electrode splay. It is often the case that macro electrode contacts on traditional depth electrodes end up in white matter tracts. In the case of micro electrode contacts, such positioning fails to yield any usable single or multiunit activity, thus these devices require advanced design planning prior to implantation to ensure that microelectrodes are targeted to grey matter regions and not white matter tracts.

3.4. Discussion

3.4.1 Systematic review is critical to chronic recording

Out of all of the optimizations and techniques that have been detailed thus far, the single most important to the success of a chronic recording protocol is a detailed and systematic review of each patient prior to the next. Failures can be classified and potential failure modes can be assessed and confirmed with methodical testing. Once a failure mode is identified, potential solutions can be implemented and revised. Daily tracking of impedance measurements and review of the recorded data will help to isolate when recordings fail in an effort to find a corresponding event or noise source that might explain the failure. Review of video and nursing staff notes will help to track down outlier events that might corrupt the data, and dissection of deplanted electrodes can provide further insight into what elements of the recording setup are causing problems. Each component should be tested individually if possible, especially connectors and cables which are prone to mechanical failure, and signal generators and oscilloscopes should be used to test all other electrical equipment when electrodes are not available.

3.4.2 Necessary infrastructure

A majority of clinical sites that support in-patient diagnostic monitoring already have most of the infrastructure in place to support chronic single neuron recordings. Recording systems and electrodes are commercially available and FDA approved; surgical techniques are not prohibitively difficult; and single neuron recordings work in parallel to existing clinical recordings and do not preclude the ability to collect data to make clinical decisions for epilepsy. Other than minor financial concerns, the only remaining barrier is a matter of implementation. A dedicated research staff member must monitor and troubleshoot recordings and communicate findings with surgical and nursing staff. Nursing staff and technicians must be instructed on the proper handling of new equipment, especially the headstage preamplifier (as it has no counterpart in standard intracranial recordings) and the microwire electrodes (as they are more fragile and break under considerably lower tensile load than traditional clinical electrodes.) Lastly, several ancillary issues may need to be addressed. Synchronizing clinical and single neuron recordings (usually by means of jittered sync pulse) creates a richer dataset for analysis. Data storage must be arranged in advance, as a single patient with only 32 microwires may generate as much as a terabyte of information over the course of their stay. Managing and analyzing that volume of data is challenge in itself. Automatic clustering algorithms like KlustaKwik (http://klustakwik.sourceforge.net) and Wave_clus[69] can identify potential single neuron activity, but should always be verified manually. Motion artifact, noise contamination and even the presence of action potentials on the reference can ruin a dataset and so recordings must be continuously screened for such.

3.4.3 Clinical relevance

Lastly, while we have stressed the importance of single neuron data sets in research settings, the clinical significance of single neuron recordings is not to be overlooked. Characterizing the behavior of neuronal subpopulations may allow insight into personalized treatment; and computational power and availability are quickly making this type of characterization achievable in therapeutically relevant timescales. In the coming decades, the diagnostic power of single neuron recordings will continue to grow, and we can accelerate this growth by adopting chronic single neuron recordings as standard practice for all intracranial diagnostic patients.

3.5 Conclusion

In conclusion, while single neuron recordings in human subjects have been around for the past five decades, only recently has the technology become readily available to roll out chronic single neuron recordings as standard protocol. The methods presented here can improve the yield and longevity of such recordings allowing more in depth studies of seizure generation and seizure propagation in epileptic patients, such as those discussed in the following chapters.

CHAPTER 4: Increased neuronal synchrony prepares mesial temporal networks for recruitment into seizures of neocortical origin

4.1 Introduction

Understanding the mechanisms that allow seizures to propagate to brain regions and subsume normally functioning neural networks is an area of intense study. Of particular interest is propagation beyond the neocortex to deeper brain regions. Cerebral blood flow studies suggest that such deeper structures like the amygdala, basal ganglia, thalamus and brainstem are activated during seizure generalization[70–73] and may be, in part, responsible for the clinical manifestations of seizure[74,75]. In addition to several direct routes, animal studies suggest that propagation of ictal activity to these structures may occur via mesial temporal lobe (MTL) structures like hippocampus and entorhinal cortex[75]. Yet, despite the potentially important role of MTL structures, recruitment of MTL networks into propagating ictal activity at the neuron level has been largely unexplored. In order to investigate MTL structures as a therapeutic target for modifying the clinical presentation of generalizing seizures, an understanding of the neuronal dynamics that allow their recruitment into seizure is critical.

The conventional understanding of epilepsy involves localized network hyper excitability that originates in a distinct focus and propagates along anatomically defined pathways. Indeed, several studies have investigated regional synchrony during the propagation of seizure events by measuring directed coherence of local field potentials (LFPs), providing a means of tracing ictal activity back to a presumptive focus[76–78]. However, while these studies provide insight into which downstream locations may receive ictal “information” during seizure propagation, they do not address the underlying mechanisms that permit ictal activity to spread. This is especially true for MTL networks. For neocortical circuits, it has been demonstrated that recruitment of *adjacent* networks may be the result of a failure of protective downstream inhibition to veto barrages of excitatory synaptic activity from an upstream ictal network[79–83]. Extending this pattern to mesial temporal networks, the inhibitory subpopulation and factors that modulate its activity, may be of particular interest in understanding seizure propagation to MTL networks. In animal models, changes in the oscillatory state of mesial temporal networks are known to modulate local inhibition[84–86], and such changes have been observed prior to spontaneous seizures in animal models[87,88]. In particular, recent work from our own lab indicates that interneuron coherence with local theta oscillations precedes recruitment of MTL in the pilocarpine rat model of epilepsy[8]. Thus, we hypothesize that seizure propagation to MTL networks involves three components, 1) regional synchrony between the presumptive seizure focus and MTL (hippocampus, entorhinal cortex, etc.), 2) synchrony between MTL inhibitory interneurons and their local field potential (LFP), and 3) interneuron firing rate changes in the time leading up to seizure. To avoid confounding seizure generation with seizure propagation, our investigation was limited to seizures with neocortical focus that secondarily generalize to MTL. By simultaneously investigating regional synchrony across the brain and interneuron-field synchrony within the MTL we can observe the frequency and time course for which seizure "information" is transmitted across the brain and the downstream inhibitory interneuron population is modulated. By studying the overlap between these events, the likely mechanisms underlying failure in local inhibition prior to seizure propagation to the MTL can be better understood.

4.2 Methods

4.2.1 Overview

Between November of 2011 and May of 2013, seven patients undergoing diagnostic intracranial EEG (iEEG) studies for surgical resection of epileptogenic regions of the brain were implanted with modified Benkhe-Fried depth electrodes (Ad-Tech, Racine WI) comprised of a platinum microwire bundle threaded through the hollowed out lumen of a standard clinical depth electrode. Implantation was performed by a board certified neurosurgeon using established techniques from the literature[11,89]. Between 1 and 4 depth electrodes were placed (determined by clinical necessity) in each patient equating to between 8 and 32 microwires implanted into mesial temporal lobe (MTL) structures (Hippocampus, Entorhinal Cortex, Perirhinal Cortex, Amygdala) per patient. Electrode locations were verified by co-registered post-operative CT and pre-operative MRI[90] as well as post-operative MRI (Figure 4.1a). After recovery, patients were transferred to a long term monitoring unit where they were tapered off anti-epileptic medication and neural activity was continuously recorded.

4.2.2 Recording/data collection

Neural activity was recorded (24/7) in parallel with the clinical intracranial electroencephalogram (iEEG) recordings using a wideband (0.8Hz to 5.5kHz) unity-gain headstage preamplifier (Neuralynx, Bozeman, MT). The signal was sampled by a DigitaLynx high-speed data-acquisition system (Neuralynx, Bozeman, MT) at 32kHz per channel providing adequate resolution for action-potential waveform discrimination. For the duration of the patient's diagnostic stay, neuronal activity was continuously recorded and time synchronized to clinical recordings.

Seizure events were identified and documented by trained technicians and clinicians in the EEG Monitoring Unit at Thomas Jefferson University Hospital. For each seizure event, seizure activity was characterized as either remaining focal or generalizing to multiple brain structures. For this study, only seizures that originated in the neocortex and subsequently generalized to MTL structures were considered. A board certified electroencephalographer who was not involved in further data analysis reviewed each seizure and determined the time of earliest seizure associated change in iEEG activity at the presumptive neocortical focus (global electrographic seizure onset) as well as the time of earliest seizure associated change in the local field potential (LFP) of microwires in the MTL (MTL electrographic seizure onset).

For further analysis, neuronal activity starting 2 hours prior to global electrographic seizure onset and ending 30 minutes after seizure termination was isolated. In addition, several randomly selected 2-hour representative samples of interictal data were also isolated that was least 12 hours before and 12 hours after a seizure. Although neural signals were recorded continuously, extracellular action potential waveforms were prone to variation over time, making tracking neurons over the entire patient's stay prohibitively difficult. As such, neurons isolated from each 2 or 2.5 hour sample of data were considered independent from those identified in any other sample. For simplicity these isolated samples are henceforth referred to as independent "recordings."

4.2.3 Unit discrimination and classification

Single neurons were identified using a manual cluster-cutting technique as described in the literature[91,92]. In brief, recorded raw signals were first high-pass filtered at 296 Hz using zero-phase finite impulse response (FIR) filter to preserve waveform shape. To identify candidate waveforms that could be single-neuron action potentials, an amplitude threshold was applied, usually -5 times the standard deviation of the signal. Waveforms that exceeded this threshold were collected and aligned. To discriminate single neurons, the first 3 principal components of the waveforms were obtained and the projection of each waveform on these component axes were used as features to cluster the data manually with Offline Sorter (Plexon, Dallas TX). (Figure 4.1d) To prevent the influence of waveform contamination during the large amplitude rhythmic LFP spiking of seizure, clustering was *only* done on waveforms prior to the clinician-determined electrographic onset of rhythmic LFP spiking. These waveforms were found to be stable over the course of the recording up to ~10 seconds after clinician-determined seizure onset. Clustered units were considered true single units if A) less than 0.5% of identified waveforms occur at inter-spike intervals that violate the refractory period (<1msec) and B) if the autocorrelogram showed the characteristic central trough associated with a refractory period.

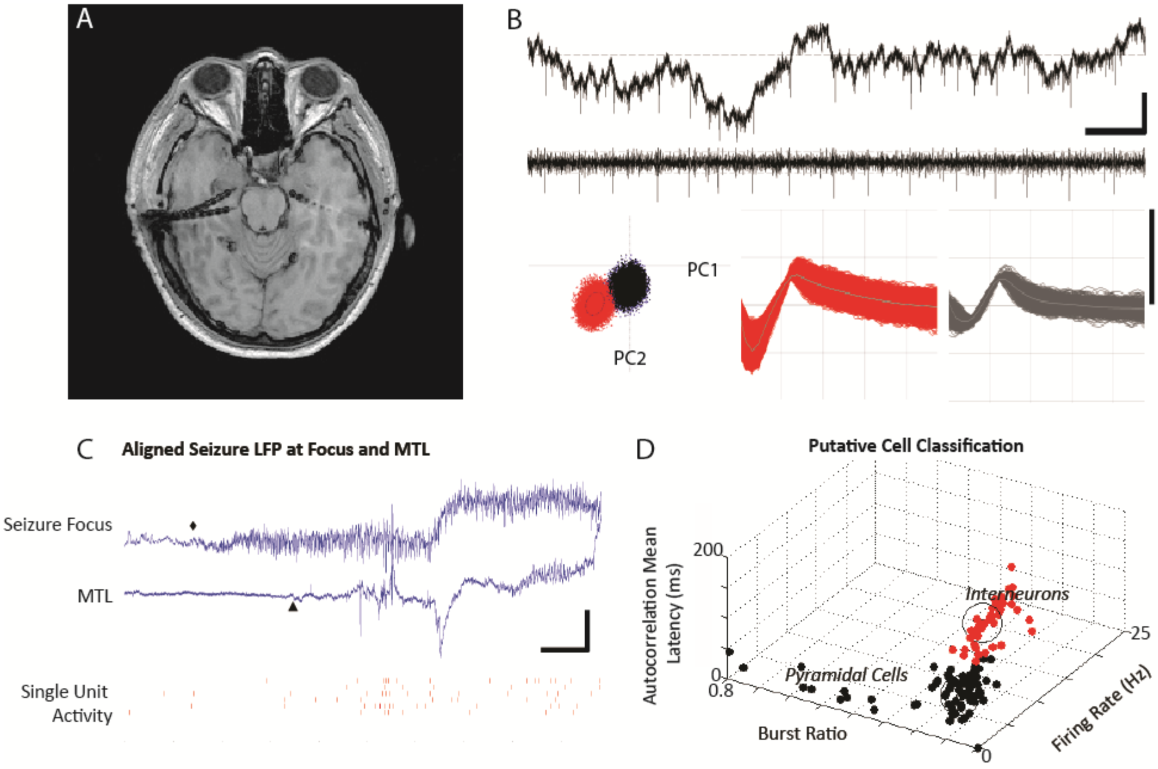

Figure 4. 1 A) Post-operative MRI identifying 3 depth electrodes placed bilaterally in mesial temporal lobe. B) Top, raw and high-pass filtered recordings showing clear single neuron activity. Bottom, two example single units in principal component space with their associated mean waveform shape (width = 1 msec). Vertical scale bar represents 250 microvolts, horizontal scale bar represents 1 second. C) Example of simultaneous recordings at the seizure focus and in the MTL. Diamond and triangle represent clinician determined seizure onsets in each location. Underlying unit activity in the MTL increases after seizure spreads to MTL, making the electrographic onset of seizure in the MTL a good landmark for aligning seizure events across patients. D) K-means clustering of recorded neurons shows a natural separation between putative pyramidal cells and putative interneurons.

Peri-ictal firing rate heterogeneity has been well documented in human epileptic patients[93–95], and may, in part, be attributed to recording site variability. Because all of our recordings were in the MTL and a majority occurred in hippocampal structures, single neurons could be characterized as either putative pyramidal cell or interneuron on the basis of firing rate, autocorrelation morphology and waveform peak-trough ratio as described in the literature[96], using a custom Matlab k-means clustering algorithm (Figure 4.1c). For this data set, the majority of recordings were hippocampal which simplified the putative classification. Because waveform contamination interferes with single unit discrimination during the ictal period, multiunits were identified during the ictal period by band pass filtering between 400Hz and 3000Hz and using a 3 sigma threshold. Valid neural activity was distinguished from filtering artifacts and noise as described by Weiss et al.[97] In brief, raw data was downsampled to 6.5kHz and the morlet wavelet transform was computed. Noise and filtering artifact demonstrate a "tapered cone" morphology on the wavelet scalogram whereas physiologic neural activity demonstrate discrete "islands" of increased high frequency power.

4.2.4 Ictal periods: multiunit rhythmicity

MTL networks were considered recruited into a generalizing seizure if they demonstrated rhythmic multiunit firing that contributes to rhythmic LFP spiking during seizure. Rhythmic firing was determined by plotting the inter-spike interval histogram in 10 millisecond bins in a window of +/- 1 second and identifying peaks in addition to the central peak that exceed a threshold of 3 times the expected value as determined by average firing rate. A multiunit was considered rhythmic if it contained one or more of these significant peaks. A seizure was considered to recruit an MTL network if one or more multiunits were recruited during a given seizure.

4.2.5 Baseline & interictal periods

For all of the variables described above, comparisons were made between a pre-ictal window of interest and a baseline period occurring between 1 hour and 30 minutes prior to seizure onset. Single neurons could be tracked during this entire period and, therefore, neurons could be normalized to their average firing rate before averaging activity across all neurons for all seizures. To validate the selection of the baseline period and ensure activity during this period was not influenced by early, unidentified seizure activity, population averaged data during baseline periods and interictal periods were compared with respect to the following 3 variables: 1) normalized firing rate, 2) unit-field coherence 3) directional field-field coherence. To assess differences in firing rate between interictal and baseline periods, a resampling technique was employed.

Differences in the population average normalized firing rate were assessed by shuffling the firing rate histogram of *individual* neurons and determining the 95% confidence interval of the number of significant bins (μ +/- 3σ) per hour in the resulting *population average* normalized firing rate histogram. This process was repeated for both baseline and interictal periods 100,000 times. For both directed field-field coherence and unit-field coherence differences between interictal and baseline periods were assessed in the same fashion. The coherence spectrograms of *individual* neurons were shuffled in time (not frequency) and a resultant shuffled population average spectrogram was created for baseline data and interictal data. These shuffled population averages were compared using a series of non-parametric Mann Whitney U-tests per frequency band. A false detection rate of 0.1% was used to determine significance for a given series of U-tests. This process was repeated 100,000 times and the fraction of repetitions where the U-test was significant was determined for each frequency band. If this fraction was greater than 0.05 baseline and interictal periods were considered to be different from each other at that frequency band.

4.2.6 Directed field-field coherence

To correlate patterns of single neuron activity in the MTL with the activity at the presumptive seizure focus directed field-field coherence was calculated between the presumptive focus and the MTL using established methods[98,99]. In brief, raw clinical iEEG data was down-sampled from 1kHz to 250Hz. One clinical iEEG channel at the presumptive seizure focus and a second in proximity to microwire recordings in MTL was selected (Figure 4.1c). In the case of multiple depth electrodes, one clinical MTL iEEG channel was selected to represent the local field of each microwire bundle and directed field-field coherences were calculated independently for every focus-MTL iEEG pair. The deterministic linear trend and temporal mean were then removed to satisfy stationarity requirements for the subsequent analysis. The directed transfer function (DTF)[98] is a measure based on the concept of Granger causality and was chosen as the variable to describe directed field-field interactions. The DTF was calculated using the eConnectome toolbox for MATLAB[100] for 10 second bins with 9 seconds of overlap in both directions and a fixed autoregressive model order of 125. The DTF was calculated for 24 logarithmically spaced frequency bands from 1 to 100 Hz as above.

A 20 second window prior to MTL electrographic seizure onset was chosen as a pre-ictal window of interest based on interneuron firing rate changes (see 4.2.7 Analysis of population firing-rate changes). To determine whether the field-field coherence in the pre-ictal window of interest significantly differed from baseline periods, time-frequency bins in this window for each band were compared to an equivalent set of time-frequency bins in the baseline period using a non-parametric Mann-Whitney U test. This process was repeated 100,000 times and if the fraction of non-significant U-tests was less than 0.05, the pre-ictal window was considered significantly different in that frequency band.

4.2.7 Analysis of population firing-rate changes

To identify patterns in population activity for pyramidal cells and interneurons, peri-event time histograms (PETHs) were created by aligning all seizures to a common reference point[101,102]. From the data, a common pattern of neuronal activity occurred in conjunction with the MTL electrographic seizure onset making this a reasonable alignment point across seizures. (Figure 4.1b) Each neuron's firing rate was then normalized to its average firing rate during the baseline period (1 hour to 30 minutes prior to seizure) to identify influences of seizure propagation within the 30 minutes prior to seizure onset on neuronal activity. The normalized firing rate was binned in 2 second intervals. For interneurons and pyramidal cells separately, these binned histograms were then averaged over all cells and all seizures. Activity from the baseline period was used to establish significance thresholds for changes around onset (e.g. mean +/- 3 standard deviations from baseline firing rate). By averaging across neurons and across seizures when aligned to MTL electrographic seizure onset, the neuronal activity was time-locked to the MTL seizure onset and common firing-rate changes of the different cell populations become evident. A pre-ictal window of interest showing significant change in population activity was identified and further analyzed for changes in unit-filed and field-field coherence.

4.2.8 Unit-field coherence

To further characterize putative inhibitory and excitatory populations during the pre-ictal window of interest (20 seconds before seizure onset in the MTL, see above) population average unit-field coherence was assessed for changes from baseline. Unit-field coherence was calculated using a bias corrected approach to account for sparse firing of some neurons[9]. In brief, recorded raw signal was low-pass filtered at 600 Hz offline. Filtered data was binned in 10 second intervals with 9 seconds of overlap and in 24 logarithmically spaced, non-overlapping frequency bins between 1 and 100 Hz. Unit-field coherence was calculated by first creating a spike triggered average (STA) by averaging windows of LFP around each action potential and then calculating the ratio of the average power spectrum of these segments to the power of the spike triggered average[103]. Statistically significant changes in coherence from baseline were identified in the same fashion as in field-field coherence.

4.3 Results

4.3.1 Overview

Neuronal activity recorded around the time of seizures and an equivalent number of interictal periods were analyzed (Table 1). For each patient (n=7), single neuron activity was recorded from 1 to 4 MTL regions depending upon the number of clinical depth electrodes utilized. (e.g. right anterior hippocampus, left posterior hippocampus, etc.) For each seizure (n=11), data were analyzed only from regions where ictal activity propagated, as determined by a board certified electroencephalographer. In total, 125 single neurons were recorded, 91 of which were classifiable as either putative interneuron (n=36) or putative pyramidal cells (n=55) based on firing rate, burst-ratio and autocorrelation morphology (see section 4.2.3 Unit discrimination and classification). The remaining cells that could not be completely classified by these parameters were excluded from analysis. Prior to MTL electrographic seizure onset, directed field-field coherence showed an increase in information flow from the neocortical seizure focus to MTL at frequencies below 16 Hz. Moreover, putative interneurons showed a decrease in firing rate that was accompanied by an increase in coherence of the interneuron activity with the local LFP at frequencies similar to that of the directed coherence from the neocortical focus. These data suggest that information flow from the cortical seizure focus may prepare MTL networks for recruitment into generalizing seizures.

4.3.2 Assessing recruitment of MTL into seizure after seizure onset

It is possible for seizure activity to pass through the MTL, modulating the local field, without recruiting the local neuronal populations[97]. Therefore, only seizures that recruited MTL neuronal activity into ictal activity were analyzed. To test recruitment of

Table 4.1 Breakdown of the seven patients involved in this study by age and gender. A majority of patients exhibited onset zones in the temporal lobe and a seizure etiology involving secondary generalization. Of patients who were surgical candidates, all showed reduction in seizure frequency and severity corresponding to Engel class 1 (free of disabling seizures). Acronyms: RST (Right subtemporal), RAT (Right anterior temporal), LAT (Left anterior temporal), LOF (Left orbitofrontal)

Patient	Age	Gender	Focus	# of analyzed seizures	# of brain regions per recording	Seizure Type	Outcome Class (Engel)
1	48	F	RST	1	1	2nd gen	no surgery
2	52	F	RAT	1	1	CPS	1
3	18	M	RAT	2	3	2nd gen	1
4	45	F	LAT	2	3	2nd gen	1
5	22	M	RAT	2	4	2nd gen	no surgery
6	47	M	LOF	1	1	2nd gen	no surgery
7	56	M	RAT	2	1	2nd gen	no outcome data

MTL, the presence of rhythmic multiunit activity at frequencies comparable to those of ictal spiking of the local field potential was used to observe participation of the local MTL networks into the propagating seizure. Multiunits were chosen over single units as ictal spiking has been demonstrated to corrupt waveform morphology and confound single neuron template sorting. In the 11 seizures analyzed, 41 channels of multiunit activity were recorded. Multiunit activity recorded during all of the 11 seizures that were analyzed demonstrated rhythmic firing behavior. This was observed in 22 out of 24 MTL regions that exhibited ictal activity. Rhythmic multiunit behavior progressed in a series of stages (Figure 4.2a&b). At seizure onset (i) multiunit activity is sparse or inhomogeneous, but as rhythmic ictal spiking develops in amplitude (i/ii), multiunit discharges occur in bursts corresponding with the dominant ictal frequency. As rhythmic LFP discharges become more complex (ii/iii/iv) and involve multiple frequency components, multiunit rhythmicity becomes more pronounced with different multiunits rhythmically bursting in conjunction with various components of the rhythmic ictal LFP oscillation. Across all seizures studied, neurons within the MTL were found to participate in seizure activity.

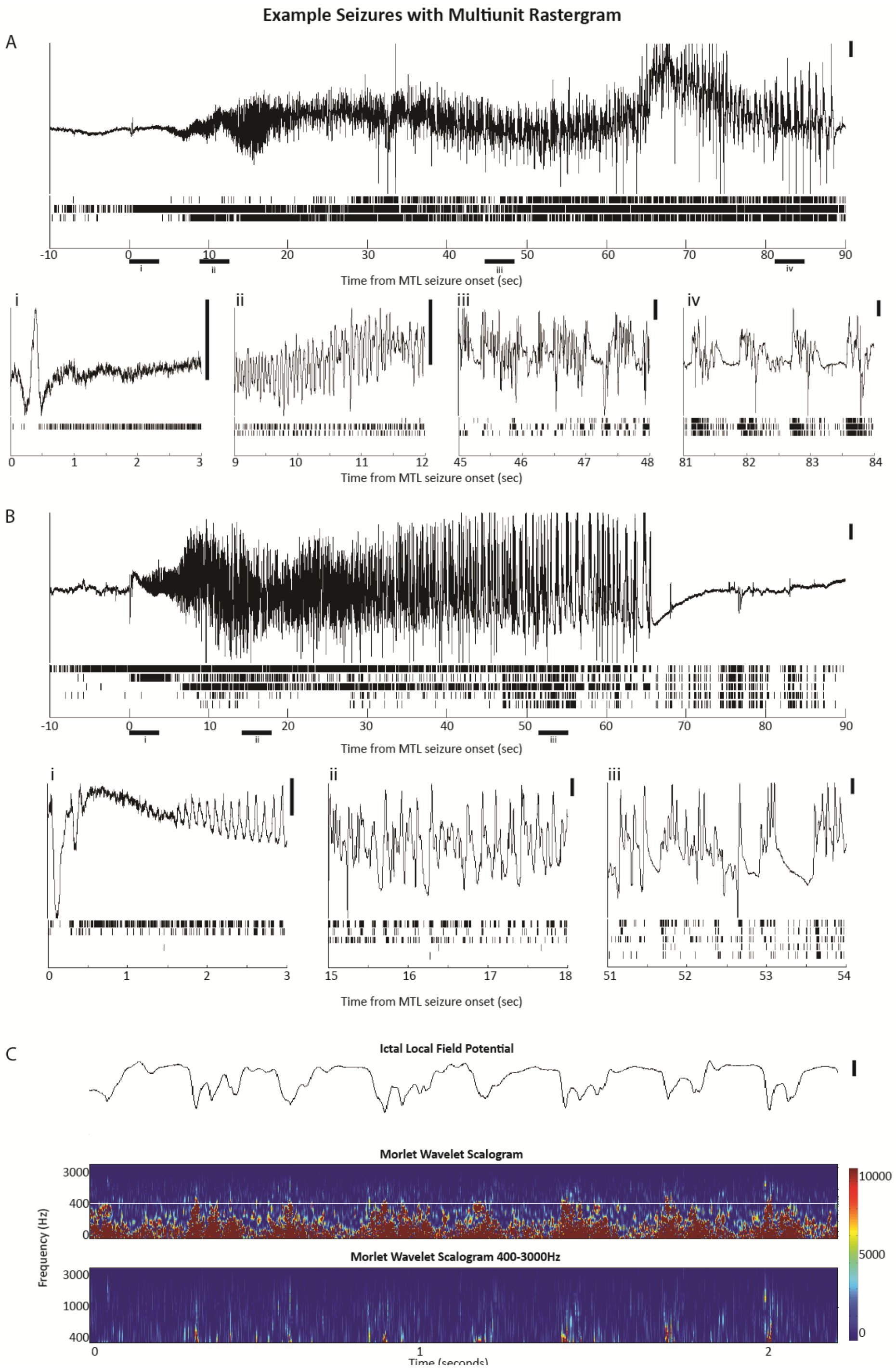

Figure 4. 2 Exemplars that demonstrate recruitment of the multiunit population in the population of seizures analyzed. A/B) Example local field potentials of seizure event with multiunit rastergram. Vertical scale bar represents 1mV. Lettered subplots show expanded 3 second windows of activity corresponding to horizontal bars. Both seizure events exhibit an increase in rhythmic ictal spiking and concomitant rhythmic multiunit activity as the seizure event progresses. C) (TOP) Two second window of large amplitude ictal spiking. (MID) Accompanying wavelet power scalogram (0-3kHz) and (BOT) expanded view of high frequency wavelet power above 400Hz. Distinct islands of increased high frequency power are observable consistent with multiunit activity rather than the stereotypic tapered cone pattern seen with filtering artifact.

4.3.3 Neural activity during baseline periods do not differ from that of interictal periods

For each seizure recording, a 30 minute baseline period starting 1 hour prior to seizure established thresholds for significant changes in unit activity. To ensure that baseline periods were truly representative of interictal data for firing rate, unit-field and field-field coherence, interictal and baseline distributions were compared using a shuffling procedure (see 4.2 Methods). For average normalized firing rate, a distribution of the number of significant firing rate changes across 10,000 population average firing rate histograms with shuffled data during baseline and interictal periods was created. For both pyramidal cells and interneurons, distributions were found to be normal and the 95% confidence intervals for baseline and interictal periods completely overlapped (Baseline Interneurons: 0-16 bins/hr; Interictal Interneurons: 3.5-9.5 bins/hr; Baseline Pyramidal Cells: 16-36 bins/hr; Interictal Pyramidal Cells: 23.1-32.5 bins/hr) indicating no difference in the likelihood of finding significant changes in interneuron or pyramidal cell firing between baseline and interictal periods. For directed field-field coherence in both directions (cortex -> MTL & MTL-> Cortex), no frequency bands were found to significantly differ between baseline and interictal periods. For interneuron-field coherence, baseline and interictal coherence distributions differed from 3-4Hz and above 37Hz ($p<0.0004$). For pyramidal cell-field coherence baseline and interictal coherence distributions differ above 5Hz ($p<0.002$). In the ensuing analysis, no pre-ictal patterns were found to occur in these frequency ranges for each respective population. As such, for frequencies of interest, baseline and interictal periods are effectively indistinguishable from one another.

4.3.4 Directed field-field coherence shows cortical influence on MTL prior to seizure onset

To assess the influence of neural activity in the neocortical seizure focus on the neuronal populations of the MTL, directed coherence analysis was performed on iEEG data from 40 pairs of clinical electrodes from the MTL and presumptive focus during 11 seizures across 7 patients. Average directional coherence across all electrode pairs in all seizures showed an increase in information flow from the presumptive focus to MTL immediately prior to MTL electrographic seizure onset at frequencies below 16 Hz ($p < 0.00001$ for 1-2Hz, 3-6Hz and 7.5-16Hz, Figure 4.3). On a per-electrode pair basis, 65% of electrode pairs participated in this pre-ictal increase in average directional coherence. Even when restricting the analysis to only those electrode pairs with simultaneously recorded interneurons, the percentage of pairs participating in the trends seen in average directional coherence remains at ~65%.

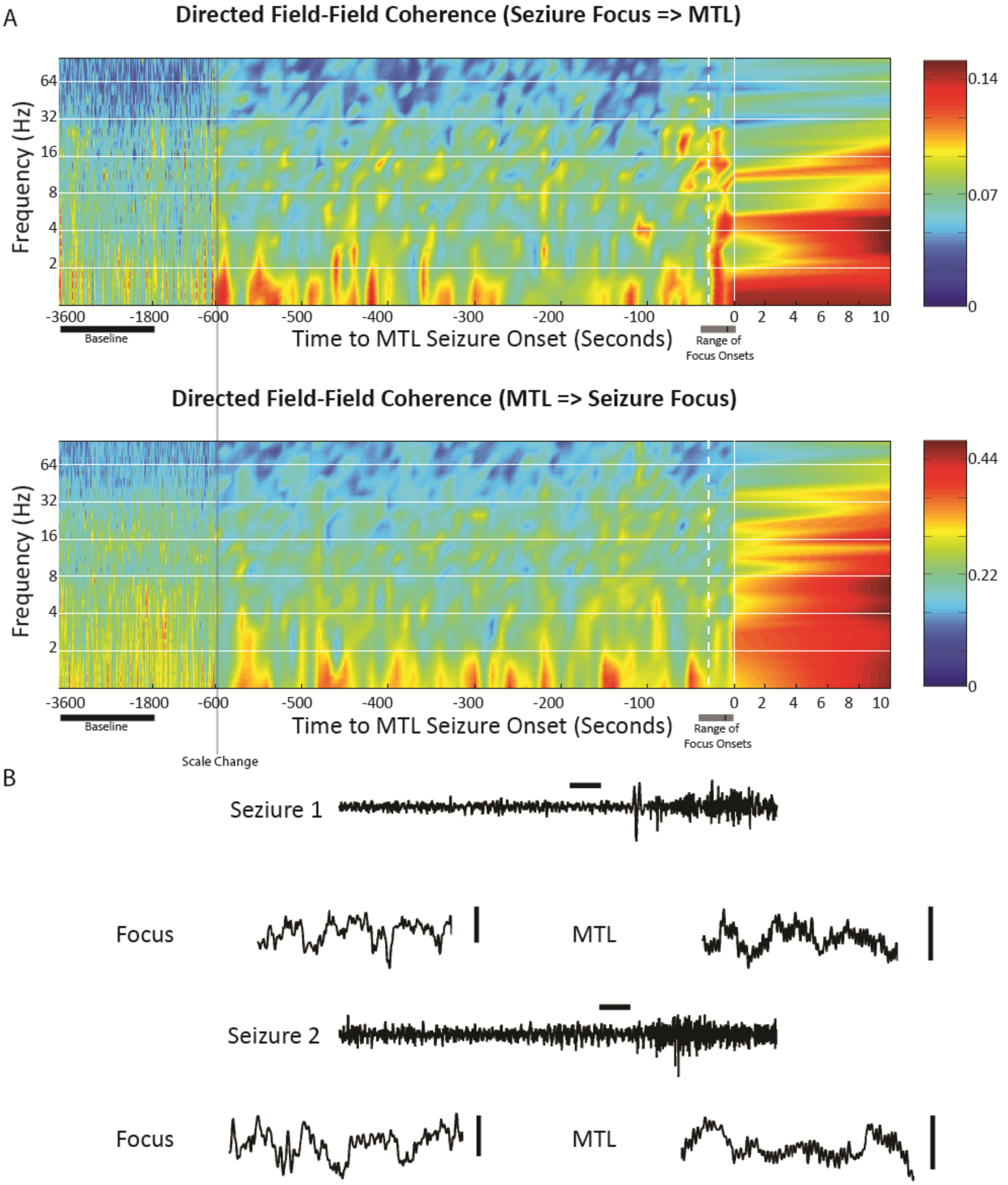

Figure 4. 3 Population average field-field coherence show unidirectional information flow. A) Directed field-field coherence spectrograms show an increase in information flow from seizure focus to downstream MTL structures in the 20 seconds prior to electrographic seizure onset in the MTL. At this same time, no significant reverse information flow was observed suggesting that seizure propagation form the neocortex is associated with a unidirectional flow of ictal information. B) Examples of simultaneous local field potential recordings in the seizure focus (Left) and the MTL (Right) that share dominant oscillation frequencies. Vertical scale bars represent 1mV while horizontal scale bars represent 1 second and correspond to the temporal window of the expanded insert.

4.3.5 Decreased interneuron but not pyramidal cell activity precedes seizure in MTL

An averaged normalized firing rate histogram across all seizures for all patients was used to identify pre-ictal windows of interest containing changes in neuronal activity. For the putative interneurons, average neuronal firing rate begins to decrease approximately 100 seconds prior to MTL electrographic seizure onset. Some putative interneurons demonstrate an almost complete cessation of firing activity in the seconds leading up to electrographic seizure onset in the neocortex. To quantify the effect, changes in average neuronal firing rate greater than 3 standard deviations from the mean firing rate were identified as significant. Average firing rates of putative interneurons fell below the 3 standard deviation level in a single window starting approximately 20 seconds prior to MTL electrographic seizure onset (Figure 4.4a). This decrease was found for 91% of interneurons in all seizures with recorded interneurons (6 seizures across 5 patients). This window corresponds with the period of time when the seizure started at its neocortical focus and was in the process of spreading to adjacent brain structures as assessed by neocortex to MTL field-field coherence defined above.

In contrast, putative pyramidal cells did not change their firing rate prior to seizure onset in MTL. The only significant change in pyramidal cell firing rate occurred after MTL electrographic seizure onset (Figure 4.5a) when pyramidal cells increased their firing during the development of rhythmic ictal oscillations. These results are consistent with our earlier work in the pilocarpine rat model of epilepsy[8] that showed changes in

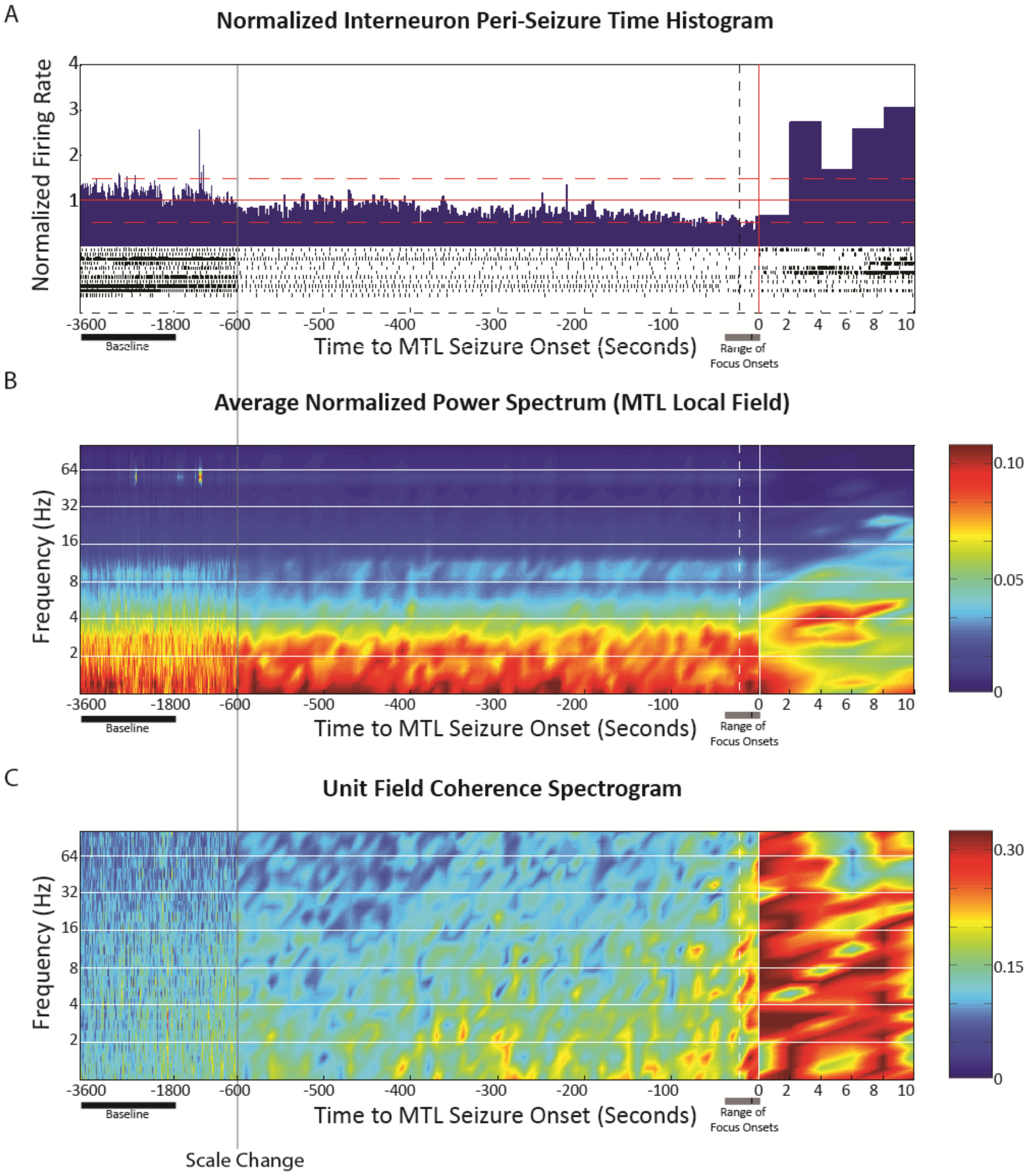

Figure 4. 4 Population average of interneuron firing rate and unit-field coherence shows changes in activity prior to arrival of ictal activity in MTL. A: Peri-seizure time histogram of interneuron activity aligned to seizure onset in the MTL (solid white line) and averaged over all seizures across all patients. A time scale change occurs at 10 minutes prior to seizure. Solid red indicates mean firing rate for a 30 minute baseline period occurring 1 hour prior to electrographic seizure onset in the MTL. Dashed red lines indicate +/- 3 standard deviations from baseline firing activity. Dashed white line is a 20 second pre-ictal window of interest where interneuron firing rate significantly compared to baseline activity. There appears to be a trend towards decreasing interneuron activity in the ~2 minutes prior to seizure that may be associated with aberrant pre-ictal patterns in LFP (spike wave complexes, & slow oscillations) that were observed in a small fraction of seizures, however such patterns were also frequently observed during interictal periods and thus could not be classified as ictal patterns. 20 seconds prior to seizure onset in MTL the drop in firing

rate exceeded 3 standard deviations of baseline activity with 91% of interneurons participating. Below the histogram, black lines indicate a decimated rastergram of example neurons showing reduced firing rate prior to seizure. B: Average normalized power spectrum shows no pre-ictal changes, and a shift towards ictal frequencies after seizure onset. C: Averaged interneuron-field coherence shows a significant elevation in coherence in the 20 seconds prior to seizure onset in MTL. This activity occurs predominantly below 11 Hz and coincides with the window of time where seizure activity has started in the neocortex but not yet reached the MTL.

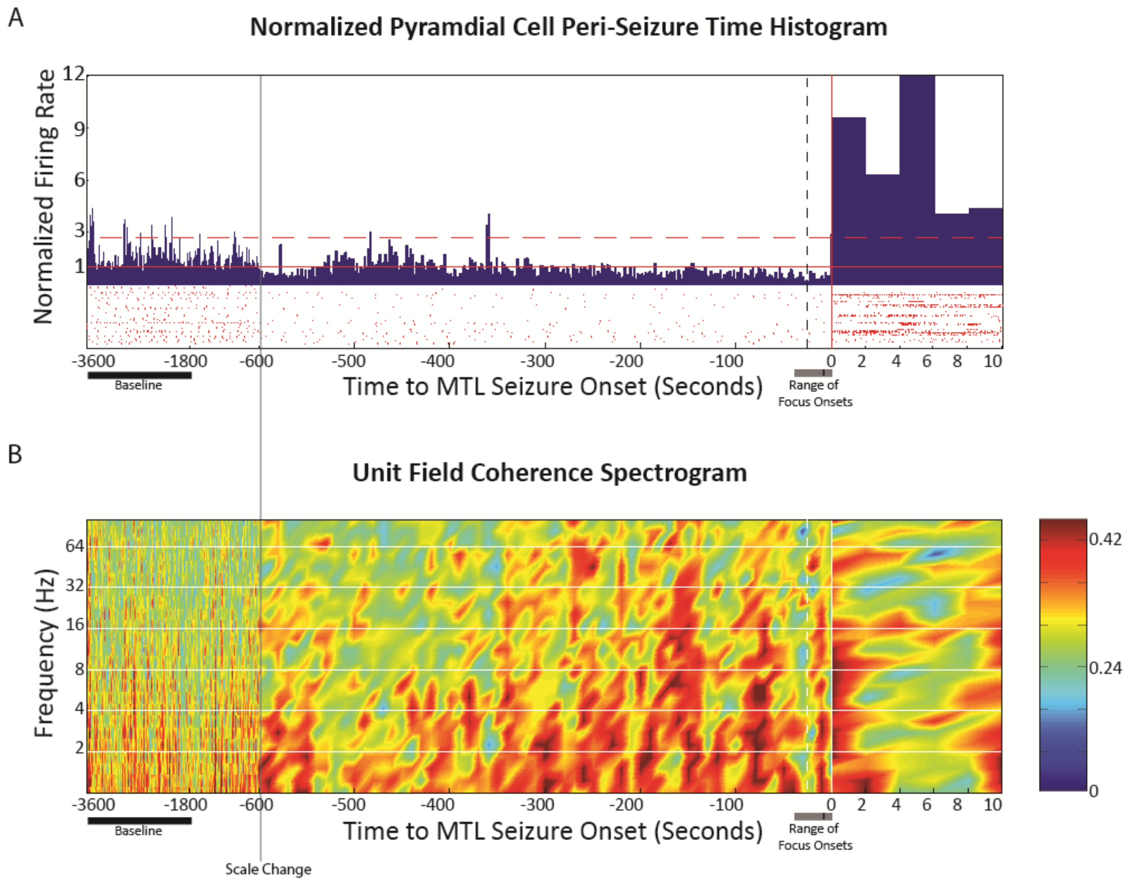

Figure 4. 5 Population average of pyramidal cell firing rate and unit-filed coherence show no changes over time leading up to seizure. A: Peri-seizure time histogram of pyramidal cell activity aligned to seizure onset in the MTL (solid white line) and averaged over all seizures across all patients. Solid red indicates mean firing rate for a 30 minute baseline period occurring 1 hour prior to electrographic seizure onset in the MTL. Dashed red lines indicate +/- 3 standard deviations from baseline firing activity. Dashed white line is a 20 second pre-ictal window of interest where interneuron firing rate significantly compared to baseline activity. Below the histogram, red lines indicate a decimated rastergram of several individual neurons. No significant changes in firing rate occur in the 5 minutes prior to seizure onset in MTL. B: Unlike interneuron-field coherence, averaged pyramidal cell-field coherence shows no significant change in coherence in the 20 seconds prior to seizure onset in MTL as compared to baseline.

interneuron activity prior to seizure initiation in the CA3 hippocampus but no change in pyramidal cell activity.

4.3.6 Modulation of interneurons at frequencies consistent with neocortex to MTL field-field coherence

To identify possible sources that could be responsible for modulating interneuron activity during this pre-ictal window of interest, subsequent analysis characterized the unit-field coherence of 20 seconds prior to MTL electrographic seizure onset. To give context to the unit-field coherence and ensure that interpretations were physiologically relevant, an average fractional power spectrum was made to identify the dominant ongoing oscillations during this pre-ictal window (Figure 4.4b). As expected, the majority of the power in LFP signal was accounted for by oscillations between 1 and 8 Hz with lower frequencies being more prominent. Visual inspection of the raw data suggested that oscillations within this frequency range occurred in 2-3 second bursts.

During the 20 second pre-ictal window, significant increases in interneuron-field coherence (Figure 4.4c) but not pyramidal cell-field coherence (Figure 4.5b) occurred at frequencies similar to that of neocortex to MTL directed field-field coherence ($p< 0.0004$ for 1-3Hz, 4-11Hz). At the individual interneuron level, 58% of interneurons originating from 5 out of the 6 seizures with interneurons across 4 out of 5 patients show increases in interneuron-field coherence that participate in the population average. Individual neurons did not, however, show a uniform increase in coherence across these three frequency ranges, rather, each neuron was associated with 1 or 2 specific frequency bands with increased interneuron-field coherence.

4.4 Discussion

4.4.1 Regional synchrony entrains inhibition in MTL

This study presents evidence of a pattern of directed-field and unit-field coherence with a corresponding failure in local inhibition that precedes the propagation of ictal activity from a neocortical focus to the structures of the mesial temporal lobe. During the pre-ictal period, the distinct and overlapping frequencies of regional and interneuron-field coherence along with the notable lack of pyramidal cell-field coherence suggests that the presumptive seizure focus in the neocortex may selectively modulate downstream inhibitory subpopulations in the MTL, either directly or through intermediate networks. Moreover, the overlapping behavior of the interneuron population (i.e. simultaneous increases in interneuron-field coherence and decreases in firing rate) suggests that changes in regional synchrony may be responsible for attenuating interneuron firing activity, effectively shutting down local MTL interneuron populations prior to MTL recruitment.

Unlike simple field-field coherence measures, the directed field-field coherence measure allows for the assignment of a source and sink for information flow[98]. While this technique is particularly useful in identifying potential foci of epileptiform activity[76–78,104,105], it also provides insight into the specific frequencies that mediate ictal “information” transmission throughout the brain. Here we describe a series of frequency bands (delta-alpha) that show an increase in information flow in the seconds before MTL electrographic seizure onset as seizures propagate from neocortex. While the MTL and neocortex have a well described history of mutually modulating oscillatory activity in the context of memory formation and recall[106,107], in this instance, the observed modulation is specifically associated with the propagation of seizure. More importantly, the frequencies that demonstrate directed information flow from seizure focus to MTL coincide with frequencies of interneuron-field coherence in the MTL. That the local inhibitory population becomes coherent with local field potentials (LFP) at these same frequencies is reflective of the underlying synaptic activity that is driving the MTL, the LFP being a summation of inhibitory and excitatory post-synaptic potentials that are being input to the MTL network. Thus coherence to particular frequency components of the LFP suggests that the local MTL network is responsive to information from the upstream neocortical networks that are themselves oscillating at these frequencies. The observed overlap in frequencies of elevated directed-field coherence and interneuron-local field coherence during seizure propagation may then be interpreted as an entrainment of MTL inhibitory network activity by the seizure focus.

Pre-ictal increases in interneuron-field coherence, particularly to theta oscillations, have been described before in animal models of spontaneous seizure[8,87]. Indeed, the ability of local field oscillations to selectively modulate inhibitory activity has been well documented, especially in the MTL[84,86,108–110], and it is possible that similar mechanisms are at play in the context of seizure propagation. In this case, the seizure focus or upstream networks recruited into seizure may act in a similar fashion to the rodent medial septum for theta rhythms, as an extrinsic generator of oscillations that selectively entrain MTL interneuron subpopulations[111].

4.4.2 Inhibition fails prior to propagation of seizures to MTL

In the neocortex, seizure propagation to adjacent cortex has been proposed to be the result of a failure of surround inhibition to restrain the spread of ongoing seizure activity [79,80]. In this model, an ictal core is identified as consisting of a population of neurons firing rhythmically with the large amplitude LFP oscillations characteristic of ictal spiking. Surrounding this core, adjacent neuronal populations receive excitatory synaptic barrages that created rhythmic oscillations of the LFP; however local protective inhibition prevent these populations from firing synchronously with their oscillating LFP and, thus, the seizure fails to spread. However, if this protective inhibition fails, the rhythmic excitatory barrages entrain adjacent neuronal populations and the seizure propagated to the adjacent cortex. Thus, in the neocortex, seizures are surrounded by an ictal "penumbra" that demonstrates rhythmic LFP activity without underlying rhythmic multiunit activity [112] and represents a wave front for seizure propagation.

In this study, propagation of ictal activity to MTL shares several features with the local propagation of seizures within the neocortex. First, the observed increases in directed coherence, (after seizures start in the neocortex but before the MTL is recruited), may be a representation of similar barrages of synaptic activity through polysynaptic circuits from the neocortex to MTL. Second, the inhibitory subpopulation of the MTL demonstrates a failure in local inhibition that becomes more pronounced concomitant with the increase in directed field-field coherence (excitatory barrages) and unit-field coherence but precedes the arrival of ictal activity. Finally, the failure of local inhibition in MTL was followed by an increase in rhythmic LFP spiking with concomitant rhythmic multiunit discharges after ictal activity propagated to MTL, demonstrating that the seizure was manifest in the neuronal network. Therefore, like neocortical seizure propagation, seizure propagation to MTL may also be a result of a failure of inhibitory veto.

Using unit-field coherence, we showed that interneurons, but not pyramidal cells, exhibit increased coherence with the local MTL field preceding the arrival of ictal activity. This result suggests that the synaptic barrages from the cortex are likely to be part of a selective, feed-forward inhibitory network. However, unlike the existing neocortical seizure propagation model would suggest, prior to failure of inhibition, the interneuron population in MTL did not show any transient increase in inhibitory activity that would reflect the initial response to excitatory synaptic barrages from the seizure focus. Given the limitations of recording in the MTL of epileptic patients, it is possible that such activity may have been present in an adjacent unrecorded population. Alternatively, this may reflect potentially important differences between neocortical and MTL anatomical structure and the impact of epilepsy on those structures, e.g. synaptic remodeling or altered local inhibition[113]. For example, it is well described that neocortical seizures often spread through established circuits and enter the MTL via the mossy fiber system of the dentate gyrus[114]. In the healthy system, these mossy fibers synapse onto both inhibitory and excitatory cells in downstream networks transmitting information from the neocortex to the MTL.[115] Thus in the context of receiving excitatory synaptic barrages from the neocortex, MTL pyramidal cells receive both feed forward excitation via mossy fibers and feed forward inhibition via mossy fibers synapsing onto perisomatic interneurons that maintain a balance of controlled activity within the MTL. A hallmark of seizure mediated reorganization in MTL is novel sprouting of mossy fibers from dentate gyrus to downstream hippocampal networks. Simultaneously these downstream networks exhibit a selective loss of interneurons and a reorganization of the surviving population to form new synaptic patterns onto both pyramidal cells and other surviving interneurons[116]. However, due to aberrant rewiring of surviving MTL interneurons, local inhibitory populations of the MTL have the potential to become partially auto-inhibitory[117]. Thus, excessive drive from mossy fibers that entrain interneuron activity to the local field potential could slowly reduce the capacity for MTL inhibition allowing excitatory drive to dominate and seizures to propagate. This interpretation explains the observed decrease in interneuron activity without corresponding increase in pyramidal cell activity prior to propagation of seizure to MTL. Simultaneous recordings of larger numbers of interneurons are needed to fully explore the inhibitory response of the MTL and determine whether a transient increase in protective inhibition may be observed or if this pattern of decreasing activity is unique to the MTL.

In conclusion, this study identifies a number of events that immediately precede seizure propagation to the MTL. At seizures’ onset, increased information from the seizure focus to downstream structures is conveyed at frequencies below 16Hz which is consistent with frequencies at which downstream local inhibitory populations become increasingly coherent. Concomitant with this change in coherence is significant a decrease in firing activity of inhibitory cells while excitatory cells show neither change in unit-field coherence or firing rate behavior. This pattern is consistent with those seen in proposed models of seizure spread within the neocortex and suggests that failure of inhibitory veto may be a robust mechanism for seizure propagation across many brain structures. Thus, future therapeutic interventions may take advantage of these population specific changes in firing rate, unit-field synchrony and field-field synchrony to deliver specifically timed therapies that can prolong protective inhibition and restrict seizure spread, and the associated clinical manifestations.

CHAPTER 5: Extra-focal changes in inhibitory firing and coherence precede the earliest electrographic onset of generalizing seizures

5.1 Introduction

The previous chapter identified changed in firing patterns and low frequency unit-field coherence specific to interneurons during their recruitment into a propagating seizure. Presumably, such changes reflect and possibly facilitate the transition of a local network into a seizing state. By extension, they may also be reflective of the initial generation of seizure activity as well. Interestingly, numerous single neuron studies in epileptic patients have failed to demonstrate any such pattern prior to the first electrographic manifestation of seizure. Indeed, the activity of individual neurons in the minutes leading up to spontaneous seizures in humans has generally been described as heterogeneous. These studies have identified populations of neurons that either increase firing, decrease firing or remain unchanged during the transition to seizure[45,93,95,118], however, the underlying cause for this heterogeneity is unclear.

Of the potential causes for pre-ictal neuronal heterogeneity, the most obvious contributor is the lumping together of activity from both excitatory and inhibitory cells. Several studies suggest that inhibitory populations, in particular, change their activity during the transition to large amplitude ictal spiking. Thus isolation of such populations may draw usable information from otherwise heterogeneous patterns. Unfortunately, when studying spontaneous seizures in epileptic patients, researchers have been limited to making extracellular recordings, due to the technical and ethical complexity of intracellular recordings or other advanced electrochemical techniques to identify the presence of specific neurotransmitters in-situ. As a result, our ability to classify neurons as excitatory or inhibitory has been severely limited. Only in the last 2 decades have studies involving simultaneous intracellular and extracellular recordings provided guidelines for neuron classification *in humans*, and even this is limited to neurons recorded from mesial temporal structures[96]. Moreover, recent studies have suggested that even if neurons can be classified as inhibitory or excitatory, they may not act with their archetypic behavior. For example, in neonatal rat seizure models of focal epilepsy, conversion of traditionally inhibitory neurons to a depolarizing (rather than hyperpoloarizing) state[119–121] has been observed during ictogenesis. Thus within the focus, identifying cells by patterns in their extracellular recordings alone may not be sufficient to group cells that are actively inhibiting or exciting the system.

Lastly, a large contributor to pre-ictal neuronal heterogeneity is an inherent variability between the focus of ictal activity and the location of single neuron recordings across seizures. Traditionally, studies have mitigated the effects of this variability by limiting their analyses to seizures that originate at the site of recordings (neocortical or mesial temporal)[45,93,118], however this only increases the potential for pathologic alterations to corrupt our already limited ability to separate inhibitory from excitatory cells.

In an effort to tease out information regarding inhibition from the overall neuronal heterogeneity, this study uses the same population of seizures as the previous chapter (those that originate in neocortical networks and propagates to single neuron recording sites located in the mesial temporal lobe (MTL).) For this choice of seizures, the MTL facilitates separation of inhibitory and excitatory subpopulations while also having fewer confounding by pathologic changes that affect neurons within the seizure focus. Having thus reduced potential sources that may contribute to heterogeneity in single neuron activity, the resulting inhibitory subpopulation that was identified consistently provided information about impending seizure. Notably, for most of these seizures, inhibitory interneuron activity changed prior to electrographic onset of the seizure at the neocortical focus, indicating the presence of decentralized changes in network activity downstream from the seizure focus.

5.2 Methods

5.2.1 Overview

As described in our previous work[11], high speed recordings were performed in the mesial temporal lobe (MTL) of 7 patients undergoing diagnostic in-patient monitoring for surgical resection of epileptic brain tissue. For each patient, between 1 and 4 depth electrodes, each with an 8-wire, platinum microwire bundle, were implanted using a frameless stereotactic technique. For each depth electrode, a single microwire, not containing any single/multiunit activity, was selected as the local field potential (LFP). For the remaining wires, single neurons were extracted and clustered in principal component space using standard techniques[122] with offline sorter (Plexon, Dallas TX). Single units were defined as those clusters containing at least 1000 action potentials/hour, with amplitude greater than 5 standard deviations from the mean, and fewer than 0.5% of detected action potentials occurred within 1 millisecond of one another. Each microwire recorded between 0 and 3 distinct single unit clusters. Multiunits were defined as clusters containing at least 1000 action potentials/hour, an amplitude greater than 4.5 standard deviations from the mean and fewer than 3% of detected action potentials occurred within 1 millisecond of one another. No more than 1 multiunit was identified for each microwire. As a consequence, multiunit activity can generally be considered an aggregate of all single neuron activity recorded on a given channel.

A total of 10 seizures with neocortical foci, and ictal activity that spread to recording sites in the MTL, were captured (2 hour segments terminating in seizure). For implementation with our automated detection algorithm, each depth electrode was treated as an independent channel, resulting in a total of 19 channels of seizure data. For the purposes of assessing false detection rate, a corresponding 2 hour interictal recording (at least 12 hours from the nearest seizure) was analyzed for each channel of seizure data.

5.2.2 Variable extraction

Five variables were extracted from each channel of data in 1 second intervals: 1) LFP peak-to-peak amplitude, 2) Multiunit firing rate, 3) Multiunit-field coherence, 4) Interneuron firing rate, and 5) Interneuron-field coherence, the interneuron specific variables only being extracted for the subset of channels (7/19) that contained recorded interneurons. Firing rates were calculated by binning action potential timestamps in 1 second bins.

c

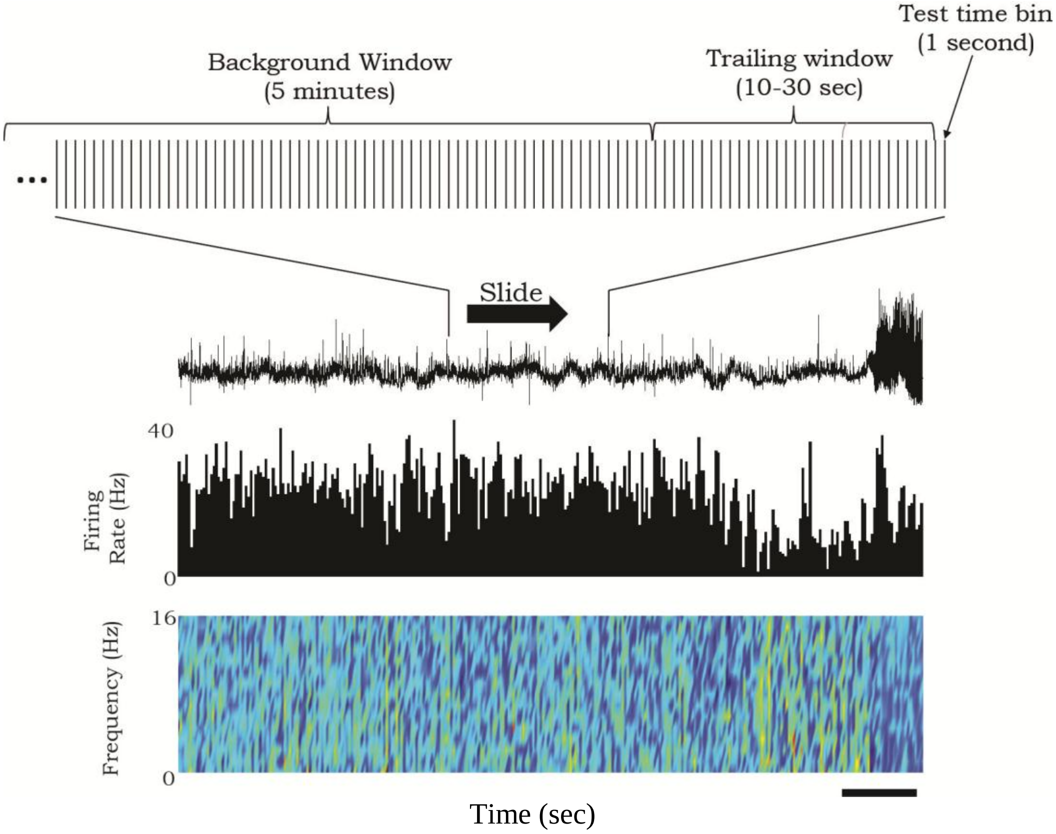

Figure 5. 1 Schematic representation of algorithm. TOP: 1 second sub-divisions breaking up a 5 minute background, 10-30 second trailing window and 1 second detection window and their corresponding position in an ongoing pre-ictal LFP . MID: Example of simultaneous single neuron firing rate broken up in 1 second bins. BOT: Example of simultaneous unit-field coherence spectrogram from 0-16 Hz broken up into 1 second time bins. The background window is used to establish the variance of a given variable to establish a detection threshold. The trailing window reduces false detection rate by setting a requirement for a sufficient number of simultaneous supra-threshold values before returning a positive detection. Scale bar is 30 seconds, and is shared across panels.

As described in previous work, unit-field coherences were calculated using in-house algorithms[9] in 10 second windows with 9 seconds of overlap creating a 1 second resolution to match firing rate. Unit-field coherence, at each time point, was calculated for 12 logarithmically spaced frequency bands between 1 and 16Hz and summed to create a single coherence value for each 1 second interval.

5.2.3 Algorithm design

A threshold based detection algorithm was used to detect seizures. For each variable, the value of the threshold was determined by calculating the standard deviation of a 5 minute sliding background window and applying a static multiplier. The value of this multiplier was varied between -5 and 5 to create pseudo-receiver operator characteristic curves. To reduce the effects of spurious threshold crossings on the false detection rate, the algorithm returned a positive seizure detection only if the value of the variable exceeded threshold in the current time bin, and in at least X% of a trailing window of time bins. The width of this trailing window was set to 10 seconds for local field variables and 30 seconds for single/multiunit variables. The value of X for each variable was determined from interictal recordings by setting a threshold of +/- 3 standard deviations from the mean and optimizing X to obtain a false detection rate of less than 1 detection per hour. To avoid contaminating the threshold, if the algorithm returned a positive seizure detection, the background window was frozen in place for the duration of that detection and an additional 5 minutes plus the trailing window width (Figure 5.1). In accordance with the average seizure duration of ~1 minute, after a positive detection, all subsequent positive detections that occurred within 1 minute were merged into a single detection. Detections persisting longer than 1 minute were treated as multiple detections.

5.2.4 Determining true and false positives & assessing performance

A board certified electroencephalographer was used to determine a set of gold standard seizure onsets and offsets for the dataset. These times were determined at the neocortical seizure focus and not in the MTL where unit recordings and LFPs were obtained. True positives were defined as any positives detections that overlap a window of +/- 60 seconds around seizure onset. This window was chosen to accommodate any variables that changed prior to the electrographic onset of seizure. For each variable, a pseudo-ROC curve was created by varying the threshold and plotting sensitivity (# of seizures detected/ total number of seizures) versus false detection rate averaged over all seizures. A normalized area-under-the-curve (AUC) was calculated. The maximum sensitivity and the minimum FDR required to achieve that sensitivity was determined. For true positives, a detection latency was calculated as the difference between the start time of the merged true positive detection and the clinician defined onset of electrographic seizure at the seizure focus. The median and interquartile range for these latencies was reported.

5.2.5 Statistical comparisons

For channels where seizure activity spread to the MTL recording site, only a subset (7/19) had simultaneous interneuron recordings. To validate that this subset was representative of the whole, planned comparisons (Mann-Whitney U) of detection latency and false detection rate were performed for LFP amplitude, multiunit firing rate, and multiunit coherence. Having established that the subset did not differ from the whole, one-way Kruskal-Wallis tests with Mann-Whitney post-hoc on the 7 seizures with interneuron activity were performed for false detection rate and detection latency to identify differences in algorithm performance when using LFP amplitude, multiunit firing rate, multiunit coherence, interneuron firing rate and interneuron coherence. For all planned comparisons a Bonferroni correction for multiple comparisons was employed.

5.3 Results

5.3.1 Overview

To ensure that algorithm performance across different variables was compared on an equal footing, pseudo-ROC curves (sensitivity vs. false detection rate) were created by varying the threshold as described in the methods above. (Figure 5.2a) Sensitivities and false detection rates are reported for the threshold value that yielded the lowest false detection rate at the maximum observed sensitivity. As expected, LFP amplitude outperformed all other variables with 100% sensitivity and a median false detection rate of 1.1 detection per hour, which is comparable with published reports[123]. Interneuron firing rate and interneuron field coherence also showed a 100% sensitivity but with an increased median FDR of 3.1 and 4.5 respectively. Interestingly, neither multiunit firing rate nor multiunit-field coherence were able to reach 100% sensitivity, and were accompanied by false detection rates of between 31 and 55 detections/hour.

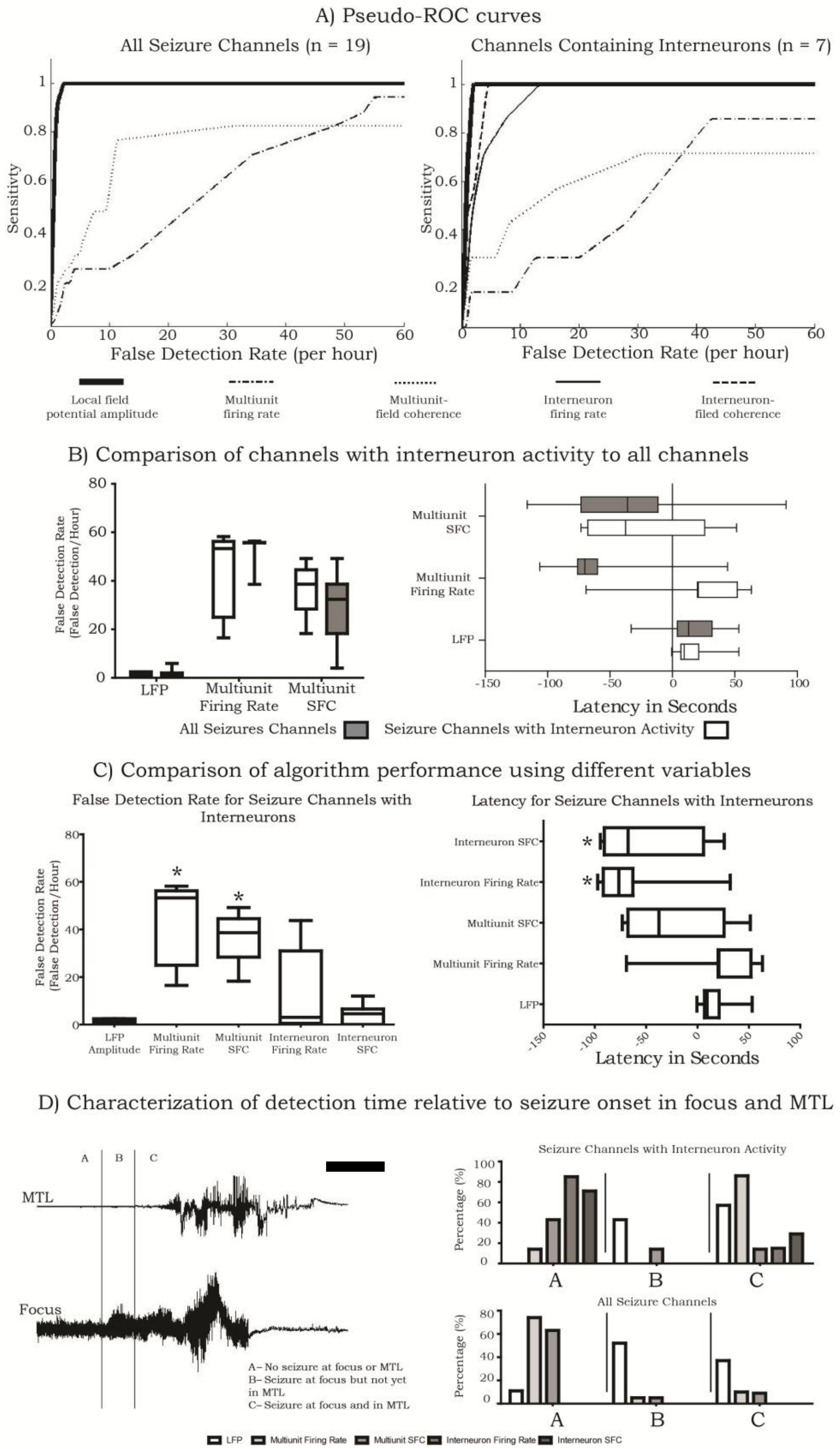

Figure 5. 2 Caption next page

Figure 5. 2 Relative improvement of sensitivity false detection rate and detection latency using interneuron specific variables. A) Sensitivity vs. false detection rate plots for each of the 5 variables. RIGHT, using only seizures containing interneuron data; LEFT, using all seizures. B) Comparison of the subset of seizures containing interneurons and the parent set of all seizures shows no significant difference in FDR or detection latency across the 3 variables. Note that multiunit firing rate is skewed in opposite directions, and though this difference not significant, additional n is required to verify if the subset of seizures containing interneurons does acting differently than the parent set in terms of detection latency. C) For seizures containing interneurons, a comparison of FDR (LEFT) and latency (RIGHT) across all 5 variables. Significant increase in FDR are seen for multiunit variables while significant decreases in latency are seen for interneuron variables. D) A breakdown of when detections occur relative to the seizure onsets at the focus and MTL. Scale bar represents 5 seconds and vertical scale has been normalized to peak amplitude for display purposes.. LFP variables tend to detect seizure after seizures spread to MTL while interneuron measures tend to detect seizures before they start at the focus.

5.3.2 Channels with interneurons do not differ from those without interneurons

Due to the lower amplitude of interneurons in the MTL, detecting their activity using extracellular recordings is more difficult and as a result, such recordings are biased towards capturing pyramidal cells. Consequently, we observe an approximate 4:1 ratio in the number of recorded pyramidal cells compared to the number of interneurons, and over half of our recordings did not have interneuron recordings at all. To ensure that channels containing interneuron activity were truly representative of all seizure channels, algorithm performance, using LFP amplitude, multiunit firing rate and multiunit-filed coherence were compared between the subset of seizure channels containing interneuron activity and the larger parent set. For each of these variables, false detection rate and detection latency were compared and no significant differences were found for any of the variables ($p > 0.2$), suggesting that while the number of channels containing interneuron are limited in this study, their findings should generalize to the larger population of seizures that propagate to the mesial temporal lobe. (Figure 5.2b)

5.3.3 Interneurons outperform multiunits in latency to detection and false detection rate

Omnibus results were significant for Kruskal-Wallis comparisons of latency ($p < 0.015$) and false detection rate ($p < 0.0005$) indicating that for the subset of seizures with interneuron recordings, algorithm performance significantly differed between variables. (Figure 2c Left) Post-hoc Mann-Whitney U tests show a significant decrease in the detection latency when using either interneuron firing rate or interneuron-field coherence when compared to using LFP amplitude, or multiunit firing rate, but not when using multiunit field coherence ($p < 0.025$). (Figure 5.2c Left) False detection rates when using either interneuron firing rate or interneuron-field coherence did not significantly differ when compared to using LFP amplitude ($p > 0.2$). However, using either multiunit firing rate or multiunit-field coherence resulted in a significant increase in false detection rates ($p < 0.03$) (Figure 5.2c Right).

5.3.4 Local field variables change after seizure spread while interneuron variables change prior to focal seizure onset

Despite recordings occurring downstream of the neocortical seizure focus, interneuron based variables (firing rate and interneuron-field coherence) showed an median detection latency of 68 seconds prior to focal electrographic onset of seizure compared to 9 seconds after focal electrographic seizure onset when using LFP amplitude. To account for variability in propagation time across seizures for each variable, each detection was characterized as occurring either A) prior to electrographic seizure onset at the focus, B) after electrographic onset at the seizure focus, but prior to electrographic onset in the MTL, or C) after electrographic onset in the MTL. For LFP amplitude, most detection occurs during propagation or after ictal activity has spread to the MTL, whereas for interneuron variables, detections have mostly occurred prior to electrographic onset of seizure. Multiunit variables are of little interest given their high false detection rate and lower sensitivity. (Figure 5.2d)

4 Discussion

5.4.1 Overview

This presented data demonstrates that while heterogeneity in neuronal activity limits its usefulness in determining earliest seizure onset, isolation of the inhibitory subpopulation improves specificity, sensitivity and detection latency. Moreover, in most cases, this isolated subpopulation was found to change activity prior to the first electrographic manifestation of seizure despite not being located in the seizure focus, reinforcing the concept that seizures start prior to the first electrographic manifestation and not may be reflected outside the seizure onset zone.

5.4.2 Local field potentials versus unit activity

Local field potentials have long been the basis for seizure detection algorithms, however, successful detection relies on gross changes in the LFP such as amplitude, or dominant frequency. These changes reflect the aggregate activity of large populations of single neurons that are progressively recruited as seizures develop and propagate. As a result, changes in the local field potential are both sensitive and specific to seizure, with typical reported false detection rates at or below 1 per hour[123]. The tradeoff is the amount of time required to recruit sufficient populations of neurons to elicit changes in the local field, which corresponds to a more prolonged latency to detection, usually on the order of seconds as is the case with the presented dataset.

In contrast, at the level of the single neuron, fluctuations in background activity are more common, making the separation of background and seizure periods more difficult. In the case of aggregate neuron activity (multiunit activity), the presented data suggest that information that is sensitive to seizure onset is lost in background fluctuations, resulting in high false detection rates and a maximum sensitivity below 100%. This is in agreement with other studies that have observed pre-ictal neuronal heterogeneity in epileptic patients[94]. Previous work has suggested that changes specific to the inhibitory population occur during the transition to seizure. Interneuron coherence to theta oscillations have been shown to increase prior to spontaneous seizure in rats[8], and reduced interneuron firing rates have been reported prior to ictal spiking[6–8], thus the inhibitory interneuron subpopulation is an ideal target for isolation. By isolating subpopulations of inhibitory neurons from the aggregate multiunit activity, background activity becomes more consistent, resulting in fewer false detections and making it easier to find changes in activity that are specific to seizure. In this study, a decrease in interneuron firing rate and an increase in interneuron-field coherence were often associated with the seizure event, however, outside the MTL, other patterns in activity may be present.

5.4.3 Downstream interneuron activity changes prior to electrographic seizure onset at the focus.

While the isolation of the inhibitory subpopulation dramatically improved algorithm performance compared to aggregate multiunit activity, (higher sensitivity and order of magnitude reduction in FDR), using the local field potential, the algorithm still showed a median false detection rate that was over 4 times lower than when using interneuron specific variables (e.g. firing rate & interneuron-field coherence). While this difference was not statistically significant, we may still improve upon the FDR by adding additional simultaneous interneurons recordings. In terms of latency, interneuron specific variables showed a significant reduction in the latency to detection, in most cases identifying a seizure event over a minute prior to first electrographic change in the LFP. This is particularly noteworthy, as the interneurons that were being recorded were in the MTL rather than in the neocortical seizure focus. This downstream change in interneuron activity could reflect either the participation of extra-focal networks in seizure generation, or more likely, downstream representations of ictogenic changes in the focus that occur prior to changes in the LFP. It has been suggested that seizures may initiate through the cumulative activity of numerous pathologically interconnected clusters of neurons[124], and calcium imaging studies have observed populations of neurons with behavior similar to this in the animal models[125]. Thus prior to the electrographic onset of seizure at the focus, such clusters may be activating, but not yet engendering a change in the LFP at the seizure focus. As a result of repeated propagation to MTL during previous seizures, these clusters likely have established pathways to create downstream effects in MTL, such as the observed change in interneuron activity. Further studies are needed, specifically of seizures that do not propagate to MTL to see if similar changes in interneuron activity are present when there are no established propagation pathways between the focus and MTL.

In conclusion, this study has demonstrated that it is possible to tease usable information about seizure onset out of heterogeneous neuronal activity if specific subpopulations can be isolated. In the MTL, the inhibitory interneuron population lends itself to this type of isolation and has previously been identified as participating in the transition to seizure, making it an ideal candidate. By using the firing rate and unit-field coherence of MTL interneurons, we were reliably able to detect seizures with no significant increase in FDR, and a statistically significant decrease in the latency to detection (compared to traditional

LFP based detection). The latencies were so improved that in a majority of cases, changes in interneuron firing rate and unit-field coherence preceded the first electrographic manifestation of seizure in the seizure focus.

Chapter 6: General Discussion

6.1 Review of findings

The body of work presented here has attempted to address the gap in our understanding of seizure propagation in human epileptic networks, specifically those of the mesial temporal lobe (MTL). While studies in both the MTL and the neocortex have suggested a failure of protective inhibition followed by synchronous recruitment of underlying neuronal activity to ictal oscillations[79], these findings have yet to be demonstrated in the epileptic patient. The closest evidence of such comes from the observation of a transition in neuronal activity from an asynchronous state to one that is synchronous to ictal oscillations during the electrographic development of seizure[112]. Even with this observation, no failure in inhibition has been demonstrated, likely due to the technical difficulty of performing such a separation using only extracellular recordings. By studying propagation of seizure in MTL networks, we take advantage of previous work that has characterized the inhibitory and excitatory subpopulations as well as the relationship between MTL neurons and local their local field potential.

After segregating inhibitory and excitatory activity in MTL prior to seizure propagation, only the inhibitory subpopulation showed a consistent pre-ictal change in activity. Specifically, the firing rate of interneurons dropped significantly during seizure propagation. Assuming that the interneuron population has not become depolarizing, the drop in firing rate suggest an attenuation of local protective inhibition prior to seizure, similar to what is suggested by Trevelyan et al. in his earlier work in brain slices (chapter

4). These MTL networks also show synchronous firing to ongoing ictal oscillations after the seizure has propagated, indicating that they are indeed participating in the seizure propagation and are not simply part of the so-called “ictal penumbra” This is the first demonstration of such a failure in inhibition prior to seizure propagation in-vivo in epileptic patients.

Moreover, the observed drop in interneuron firing also complements animal work in the MTL, studying the transition to ictal spiking. Numerous studies in brain slices, ex-vivo brain preparations and in-vivo animal models observe a change in dynamics of the interneuron population[6–8] where interneurons stop firing, and pyramidal cells start firing while large amplitude ictal spiking develops. An important difference between this animal work and the present findings is that in the animal, interneuron firing was shown to transiently increase before dropping in favor of pyramidal cell firing and ictal spiking, whereas in the present work inhibitory firing stays constantly high in the background and drops immediately prior to seizure spread. This is likely due to the different time windows that are being analyzed relative to the electrographic onset of seizure in the MTL. While the present work is focused on early phases of seizure propagation, (i.e. prior to the electrographic spread of seizure to MTL), the animal work has focused later on during the transition to ictal spiking. The failure of inhibition that we observed during early propagation may lead to changes similar to those described by animal studies later on during the development of ictal spiking. This is supported by increases in interneuron firing rate immediately after the electrographic onset of seizure in the MTL, however the lack of simultaneously recorded interneurons and pyramidal cells within close spatial proximity limits the ability of this study to draw conclusive parallels to animal work. It is likely that changes in unit-field coherence mediate the transition of interneuron activity from a depressed to an elevated state during the transition to ictal spiking as previously described by Grasse et al, and supported by increases in low frequency unit-field coherence described previously in the present work. The exact mechanism for this transition is still unknown, however studies suggest that the participation of interneuron networks in the generation of low voltage fast oscillations prior to the generation of large amplitude ictal spiking may play a role[126].

Because we are particularly interested in finding evidence for a failure of inhibition, it is particularly interesting that, in MTL, inhibitory subpopulations are known to both modulate and be modulated by specific frequencies of local oscillations. GABAergic input from medial septum has been implicated in inducing hippocampal interneurons to generate theta rhythms[108,127], while theta rhythms, in turn, have been observed to modulate the activity of specific interneuron classes in MTL[86]. Interneuron coherence to theta oscillations has even been demonstrated to occur in bursts prior to spontaneous seizures in animal models of epilepsy[8]. We also observe similar changes in coherence that are specific to the inhibitory population. Prior work during spontaneous seizure in the rat show an increasing frequency of bursts of theta band interneuron-field coherence lasting 2-4 seconds at a time. In the present work in humans, interneurons showed bursts of coherence to various frequencies below 12Hz (including theta frequencies) in similar 1-2 second bursts. The concentration of these bursts were highest in the seconds prior to seizure arrival in MTL when ictal activity is in the process of spreading and when the interneuron firing rate was dropping significantly below baseline averages. These frequencies, theta in particular, have been observed modulating interneuron activity during spatial navigation and memory formation[128–130], so it is possible that similar mechanism are at play in this pre-ictal window of seizure propagation. The specific consequences of this phenomenon for epileptogenesis are still unknown. While studies have associated theta oscillations with an anti-epileptic effect[131], animal studies have also shown that there is a pathologic theta oscillation (and "twice-theta" oscillation ~10-16Hz) mediated by specific neurons in multiple MTL structures that reliably precedes ictal activity[87,132]. The change in low-frequency coherence that was observed prior to seizure in patients, support this alternate interpretation of the role of theta oscillations, or low frequency oscillations in general) and may change our future implementation of disruptive low frequency electrical stimulation to abort seizure.

In the window of seizure propagation, increases in directed coherence from the seizure focus to the MTL coincide with changes in interneuron firing rate and unit-field coherence. This agrees with traditional coherence studies that show a desynchronization in local fields prior to seizure that is reflective of seizure activity being present in one field but not yet in the other[133]. Directed coherence analyses can go one step farther and attribute this apparent desycnhronization across fields to the active transmission of information from the seizure focus to the MTL. This increase in information flow occurs at frequencies that overlap with those of increased interneuron coherence and may correspond to the barrages of synaptic activity that have been described during neocortical seizure propagation[79]. It is unclear whether this increase in information flow from seizure focus to MTL directly effects local oscillations and in turn modulates interneuron activity, or if the modulation of interneuron activity allows this ictal information to more easily recruit the MTL into seizure, though the overlap in frequency bands suggests the former.

From this limited extracellular data set, the similarities that are observed between our data and that reported in both the human neocortex and the rodent MTL, supports a mechanism for seizure propagation whereby local oscillations modulate the local inhibitory population and reduce the magnitude of protective inhibition, allowing barrages of excitatory synaptic activity to affect downstream networks in the MTL and recruit them into seizure. This suggest that by interrupting the transmission of excitatory barrages or by bolstering the local inhibition we may be able to limit seizure propagation to MTL networks. Electrical stimulation may provide a means for doing just this, by hyperpolarizing local networks to reduce the influence of excitatory ictal synaptic barrages or interrupting low frequency oscillations and resultant interneuron modulation.

Lastly, while interneuron firing and coherence changed significantly during seizure propagation, there appeared to be a trend towards changing activity that started minutes prior. This is particularly notable, as these changes started prior to the electrographic onset of seizure at the seizure focus, and the measures were reliable across different seizures and different patients. Electrographic seizure onset is a common clinical definition for seizure onset, but the true onset of seizure activity likely starts well prior. The PIN cluster hypothesis[125] suggests that seizures start as small pathologically interconnected clusters of neurons that become hypersynchronous. As multiple hypersynchronous clusters within the seizure focus coalesce, seizure activity becomes visible on EEG. This hypothesis is supported by studies that have described cortical micro-domains that exhibit transient microseizures[134] well before gross ictal spiking on

EEG. Since the seizure populations that this report studies all generalize to the MTL, there are established pathways for ictal activity from these cortical microdomains to be conveyed to the MTL where we may observe the effects in the form of changes in interneuron firing rate and unit-field coherence. To validate this hypothesis, follow-up studies are needed with a population of seizures that do not generalize to MTL to see if MTL interneuron activity still changes prior to electrographic onset of seizure at the focus when there is no spread. At the very least, the data presented reinforces the concept of seizures initiating prior to electrographic onset. More importantly, the ability to detect seizures, prior to electrographic onset, when recording outside the seizure focus, may be a powerful tool for standardizing implantable devices for seizure detection or intervention. By always recording from a centralized location of seizure spread, interventional devices can be more robust to patients with multiple seizure foci, or otherwise inaccessible seizure foci.

6.2 Clinical implications and future directions

The work presented in this thesis has both clinical and research applications and additional projects are needed to fully realize the implications of this work. The following section will discuss these applications and how they may be expanded upon in future studies.

6.2.1 Poloxamer coated electrodes

The evidence presented shows clear improvements to the short term performance of neural recordings performed with Poloxamer coated electrodes. This is particularly important as the FDA has recognized the use of Poloxamer in pharmacotherapeutic applications and for tissue repair outside the CNS. While additional validation is required before applications within the CNS can be fully implemented, the major issue of biocompatibility and long term safety have been partially dressed through these alternate uses for Poloxamer. While there is no specific pathology associated with the use of Poloxamer in this manner, there is a marketable potential for its use in reduction of acute cellular damage during implantation of both macro and micro electrodes. For the former, the administration of Poloxamer during stereotactic implantation may reduce pain and swelling associated with the acute immune response to macro-electrode implantation. For the latter, while not clinically relevant, single neuron recordings should show significant improvements in yield.

Follow-up studies are needed to determine appropriate dosing and delivery methods. The current work used a so-called “dip-coating” which limits the amount of Poloxamer that may be delivered to tissue during implantation. Additional preparations such as direct administration to the craniotomy during implantation or deposition of lyophilized compound on the electrode surface, should be explored to assess the effect of Poloxamer loading on the duration of neuroprotective effects. In addition, long term biocompatibility studies are needed to fully characterize the neural tissue response to the long term presence of Poloxamer, and the clearance rate of Poloxamer from the local microenvironment.

6.2.2 Single neuron dynamics in seizure propagation

The presented work has provided a small window of insight into the behavior of interneurons during the recruitment of MTL (mesial temporal lobe) networks into seizure, and in doing so has invited further questions regarding our understanding of seizure propagation. Seizure propagation was accompanied by changes in regional coherence across the brain and in local interneuron coherence within the MTL and drops in firing rate. It is unknown, however, if such patterns are true outside the MTL as well or if there are variations in this pattern of activity within the MTL. In addition the specific interplay between the drop in interneuron firing rate and the activity of neighboring pyramidal cells is not known. The presented work shows only changes in interneuron firing prior to seizure propagation, and no such changes in pyramidal populations. However, this may be a result of the spatially sparse recordings that were made. Many interneurons were not recorded from the same local population as pyramidal cells so a direct relationship between the activities of both is difficult to identify. Improved recording density from these MTL structures can allow recording of interneurons and pyramidal cells in close proximity to see if the local excitatory population is truly disengaged from the network, or if local inhibition can still modulate their activity. Additionally, improved post-implant imaging may provide a better idea of specific structures that are being recorded from to reduce variability from different networks and subfields within the MTL. Future studies should incorporate these improvements to better localize the regions where interneuron coherence changes during seizure propagation.

The observed change in interneuron firing rate that occurs during seizure propagation is inferred to be the result of extrinsic influences from the seizure focus that then allows for propagation. However, it is equally possible that such changes are a periodically occurring phenomenon that predispose the whole brain to hyperexcitability. Seizure generation many simply be a manifestation of such a global change in inhibitory tone acting on a pathological network in the seizure focus. To further explore this alternative interpretation, simultaneous single neuron activity must be recorded from the seizure focus as well as the MTL. This may be achieved in future studies through the use of silicon multi-electrode arrays like those used in the work of Truccolo and Schevon. While these arrays have an increased recording density, cortical networks do not benefit from the simple differentiation of putative interneurons and pyramidal cells based on extracellular recording parameters. Studies using these arrays will have to rely on cross-correlation analysis to identify putative inhibitory and excitatory cells.

Lastly, a more thorough investigation of the differences between generalizing and non-generalizing seizure is needed. The current work is limited to generalizing seizure, and preliminary data on non-generalizing seizures shows no similar trends in interneuron activity. It may be the case that without predetermined synaptic pathways mediating propagation, changes in interneuron behavior are not observable. Such a finding would suggest that non-generalizing seizures are the result of differences in seizure generation at the focus rather than differences in the response of the MTL.

6.2.3 Early detection of seizure

Changes in interneuron firing and coherence in the MTL were demonstrated prior to the electrographic onset of seizure at the seizure focus. It was hypothesized that such activity was the downstream correlate of changes in the focus that occur prior to electrographic onset of seizure at the focus. This hypothesis may be verified by simultaneously recording single neuron activity from the focus as described in the previous session. Regardless, the changes in interneuron firing and coherence in the MTL prior to generalizing seizures can be used to reliably detect seizure activity prior to electrographic onset (at the focus). Additional seizure data is required for prospective validation of these results. If consistent with future data, the detection latency using interneuron specific variables (firing rate and unit-field coherence) is enough to allow for clinical intervention or activation of a feedback alarm to the patient. Clinical intervention may be in the form of direct localized electrical stimulation (analogous to the existing Neuropace RNS) or a more delocalized activation of the brain (transcranial direct stimulation or transcranial magnetic stimulation). Additionally, pharmacologic agents may be directly transfused into the brain using microdialysis devices or a simple feedback alarm may be delivered to warn the patient of impending seizure so safety measures can be taken to reduce injury during seizure. Follow-up studies are needed to identify which, if any, of these neuro-modulatory approaches best reduces seizure frequency.

The isolation of inhibitory cells from the aggregate neuronal activity was found to make a significant difference in overall performance, and may explain why, until now, researchers have shied away from the use of single neuron activity in detecting seizures. Future studies should benefit from putative cell type classification before looking for pre-ictal changes in activity. Future investigations should also asses the performance of this algorithm for non-generalizing seizures as well, as well as implement more advanced machine learning techniques like support vector machines and artificial neural networks to see if latency and false detection rate can be further optimized. These approaches require a much larger n that can be separated into a training and testing set that is mutually exclusive.

6.3 Conclusion

In conclusion, this thesis presents data that improves our understanding of how seizures propagate, the role of interneurons in this propagation, and approaches to use this newfound understanding of interneuron activity to improve the ability to detect seizures in human epileptic patients. It is the hope of this project that future work will continue to expand upon this understanding with the goal of restricting seizure propagation and potentially even seizure generation.

LIST OF REFERENCES

LIST OF REFERENCES

1. CDC. *Targeting Epilepsy: Improving the lives of people with one of the nation's most common neurological conditions*. (2011).

2. Lowenstein, D. H. in *Harrison's Princ. Intern. Med.* (McGraw Hill, 2012).

3. Cherlow, D. G., Dymond, A. M., Crandall, P. H. & Walter, R. D. Evoked response and after-discharge thresholds to electrical stimulation in temporal lobe epileptics. *Arch. Neurol.* **34,** 527 (1977).

4. Wilson, C. L. *et al.* Paired pulse suppression and facilitation in human epileptogenic hippocampal formation. *Epilepsy Res.* **31,** 211–30 (1998).

5. Isokawa-Akesson, M., Wilson, C. L. & Babb, T. L. Inhibition in synchronously firing human hippocampal neurons. *Epilepsy Res.* **3,** 236–47 (1989).

6. Ziburkus, J., Cressman, J. R., Barreto, E. & Schiff, S. J. Interneuron and pyramidal cell interplay during in vitro seizure-like events. *J. Neurophysiol.* **95,** 3948–54 (2006).

7. Gnatkovsky, V., Librizzi, L., Trombin, F. & de Curtis, M. Fast activity at seizure onset is mediated by inhibitory circuits in the entorhinal cortex in vitro. *Ann. Neurol.* **64,** 674–86 (2008).

8. Grasse, D. W., Karunakaran, S. & Moxon, K. a. Neuronal synchrony and the transition to spontaneous seizures. *Exp. Neurol.* **248,** 72–84 (2013).

9. Grasse, D. W. & Moxon, K. a. Correcting the bias of spike field coherence estimators due to a finite number of spikes. *J. Neurophysiol.* **104,** 548–58 (2010).

10. Misra, A. *et al.* Preventing neuronal damage and inflammation in vivo during cortical microelectrode implantation through the use of Poloxamer P-188. *J. Neural Eng.* **10,** 016011 (2013).

11. Misra, a *et al.* Methods for implantation of micro-wire bundles and optimization of single/multi-unit recordings from human mesial temporal lobe. *J. Neural Eng.* **11,** 026013 (2014).

12. Szarowski, D. H. *et al.* Brain responses to micro-machined silicon devices. *Brain Res.* **983,** 23–35 (2003).

13. Vetter, R. J., Williams, J. C., Hetke, J. F., Nunamaker, E. a & Kipke, D. R. Chronic neural recording using silicon-substrate microelectrode arrays implanted in cerebral cortex. *IEEE Trans. Biomed. Eng.* **51,** 896–904 (2004).

14. Biran, R., Martin, D. C. & Tresco, P. a. Neuronal cell loss accompanies the brain tissue response to chronically implanted silicon microelectrode arrays. *Exp. Neurol.* **195,** 115–26 (2005).

15. McConnell, G. C. *et al.* Implanted neural electrodes cause chronic, local inflammation that is correlated with local neurodegeneration. *J. Neural Eng.* **6,** 056003 (2009).

16. Winslow, B. D., Christensen, M. B., Yang, W.-K., Solzbacher, F. & Tresco, P. a. A comparison of the tissue response to chronically implanted Parylene-C-coated and uncoated planar silicon microelectrode arrays in rat cortex. *Biomaterials* **31,** 9163–72 (2010).

17. Zhong, Y. & Bellamkonda, R. V. Biomaterials for the central nervous system. *J. R. Soc. Interface* **5,** 957–75 (2008).

18. Moxon, K. a, Leiser, S. C., Gerhardt, G. a, Barbee, K. & Chapin, J. K. Ceramic-based multisite electrode arrays for chronic single-neuron recording. *IEEE Trans. Biomed. Eng.* **51,** 647–56 (2004).

19. He, L., Lin, D., Wang, Y., Xiao, Y. & Che, J. Electroactive SWNT/PEGDA hybrid hydrogel coating for bio-electrode interface. *Colloids Surf. B. Biointerfaces* **87,** 273–9 (2011).

20. Spataro, L. *et al.* Dexamethasone treatment reduces astroglia responses to inserted neuroprosthetic devices in rat neocortex. *Exp. Neurol.* **194,** 289–300 (2005).

21. Zhong, Y. & Bellamkonda, R. V. Dexamethasone-coated neural probes elicit attenuated inflammatory response and neuronal loss compared to uncoated neural probes. *Brain Res.* **1148,** 15–27 (2007).

22. Grand, L. *et al.* Short and long term biocompatibility of NeuroProbes silicon probes. *J. Neurosci. Methods* **189,** 216–29 (2010).

23. Grill, W. M., Norman, S. E. & Bellamkonda, R. V. Implanted neural interfaces: biochallenges and engineered solutions. *Annu. Rev. Biomed. Eng.* **11,** 1–24 (2009).

24. Serbest, G., Horwitz, J. & Barbee, K. The effect of poloxamer-188 on neuronal cell recovery from mechanical injury. *J. Neurotrauma* **22,** 119–32 (2005).

25. Serbest, G., Horwitz, J., Jost, M. & Barbee, K. Mechanisms of cell death and neuroprotection by poloxamer 188 after mechanical trauma. *FASEB J.* **20,** 308–10 (2006).

26. Moxon, K. a, Hallman, S., Aslani, A., Kalkhoran, N. & Lelkes, P. Bioactive properties of nanostructured porous silicon for enhancing electrode to neuron interfaces. *J. Biomater. Sci. Polym. Ed.* **18,** 1263–1281 (2007).

27. Nissanov, J., Bertrand, L. & Tretiak, O. Cryosectioning distortion reduction using tape support. *Microsc. Res. Tech.* **53,** 239–40 (2001).

28. Buzsáki, G. Large-scale recording of neuronal ensembles. *Nat. Neurosci.* **7,** 446–51 (2004).

29. West, M. J. in *Do seizures damage brain* (Thomas Sutula, A. P.) **135,** 43–51 (Elsevier, 2002).

30. He, W., McConnell, G. C. & Bellamkonda, R. V. Nanoscale laminin coating modulates cortical scarring response around implanted silicon microelectrode arrays. *J. Neural Eng.* **3,** 316–26 (2006).

31. Polikov, V. S., Tresco, P. a & Reichert, W. M. Response of brain tissue to chronically implanted neural electrodes. *J. Neurosci. Methods* **148,** 1–18 (2005).

32. Kim, Y.-T., Hitchcock, R. W., Bridge, M. J. & Tresco, P. a. Chronic response of adult rat brain tissue to implants anchored to the skull. *Biomaterials* **25,** 2229–2237 (2004).

33. Bjornsson, C. S. *et al.* Effects of insertion conditions on tissue strain and vascular damage during neuroprosthetic device insertion. *J. Neural Eng.* **3,** 196–207 (2006).

34. Fawcett, J. W. & Asher, R. a. The glial scar and central nervous system repair. *Brain Res. Bull.* **49,** 377–91 (1999).

35. Kreutzberg, G. W. Microglia: a sensor for pathological events in the CNS. *Trends Neurosci.* **19,** 312–8 (1996).

36. Goss, J. R. *et al.* Astrocytes are the major source of nerve growth factor upregulation following traumatic brain injury in the rat. *Exp. Neurol.* **149,** 301–9 (1998).

37. Azemi, E., Lagenaur, C. F. & Cui, X. T. The surface immobilization of the neural adhesion molecule L1 on neural probes and its effect on neuronal density and gliosis at the probe/tissue interface. *Biomaterials* **32,** 681–92 (2011).

38. Zhou, Q. *et al.* Biocompatibility of implantable electrodes coated with PVA films in the brain of rats: a histological evaluation. *J. Wuhan Univ. Technol. Sci. Ed.* **24,** 393–396 (2009).

39. Hannig, J. Poloxamine 1107 sealing of radiopermeabilized erythrocyte membranes. *Int. J. Radiat. Biol.* **75,** 379–385 (1999).

40. Murphy, A. D. *et al.* Poloxamer 188 protects against ischemia-reperfusion injury in a murine hind-limb model. *Plast. Reconstr. Surg.* **125,** 1651–60 (2010).

41. Rieke, F., Warland, D., de Ruyter van Steveninck, R. & Bialek, W. *Spikes: exploring the neural code.* (MIT, 1997).

42. Hebb, D. O. *Organization of Behavior*. (New York: Wiley, 1949).

43. Buzsáki, G. Neural syntax: cell assemblies, synapsembles, and readers. *Neuron* **68,** 362–85 (2010).

44. Maynard, E., Nordhausen, C. & Normann, R. The Utah intracortical electrode array: a recording structure for potential brain-computer interfaces. *... Clin. Neurophysiol.* **102,** 228–239 (1997).

45. Babb, T. L., Wilson, C. L. & Isokawa-Akesson, M. Firing patterns of human limbic neurons during stereoencephalography (SEEG) and clinical temporal lobe seizures. *Electroencephalogr. Clin. Neurophysiol.* **66,** 467–82 (1987).

46. Babb, T. L. & Crandall, P. H. Epileptogenesis of human limbic neurons in psychomotor epileptics. *Electroencephalogr. Clin. Neurophysiol.* **40,** 225–43 (1976).

47. Verzeano, M. & Crandall, P. H. Neuronal activity of the amygdala in patients with psychomotor epilepsy. *Neuropsychologia* **9,** 331–344 (1971).

48. Dichter, M., Herman, C. & Selzer, M. Extracellular unit analysis of the hippocampal penicillin focus. *Electroencephalogr. Clin. Neurophysiol.* **34,** 619–29 (1973).

49. Bragin, A., Engel, J. J., Wilson, C. L., Fried, I. & Buzsáki, G. High-frequency oscillations in human brain. *Hippocampus* **9,** 137–42 (1999).

50. Kawasaki, H. *et al.* Single-neuron responses to emotional visual stimuli recorded in human ventral prefrontal cortex. *Nat. Neurosci.* **4,** 15–6 (2001).

51. Rutishauser, U., Schuman, E. M. & Mamelak, A. N. Online detection and sorting of extracellularly recorded action potentials in human medial temporal lobe recordings, in vivo. *J. Neurosci. Methods* **154,** 204–24 (2006).

52. Worrell, G. a *et al.* High-frequency oscillations in human temporal lobe: simultaneous microwire and clinical macroelectrode recordings. *Brain* **131,** 928–37 (2008).

53. Alarcón, G. *et al.* In vivo neuronal firing patterns during human epileptiform discharges replicated by electrical stimulation. *Clin. Neurophysiol.* **123,** 1736–44 (2012).

54. Hefft, S. *et al.* Safety of hybrid electrodes for single-neuron recordings in humans. *Neurosurgery* **73,** 78–85; discussion 85 (2013).

55. Kreuz, T., Chicharro, D., Houghton, C., Andrzejak, R. G. & Mormann, F. Monitoring spike train synchrony. *J. Neurophysiol.* **109,** 1457–72 (2013).

56. Moxon, K. a & Nicolelis, M. a L. in *Methods simultaneous neuronal ensemble Rec.* (CRC Press, 1999).

57. Gold, C., Henze, D. A., Koch, C. & Buzsaki, G. On the Origin of the Extracellular Action Potential Waveform: A Modeling Study. *J. Neurophysiol.* **95,** 3113–3128 (2006).

58. Engel, A. K., Moll, C. K. E., Fried, I. & Ojemann, G. A. Invasive recordings from the human brain--clinical insights and beyond. *Nat. Rev. Neurosci.* **6,** 35–47 (2005).

59. Fried, I. *et al.* Cerebral microdialysis combined with single-neuron and electroencephalographic recording in neurosurgical patients. *J. Neurosurg.* **91,** 697–705 (1999).

60. Babb, T. L., Carr, E. & Crandall, P. H. Analysis of extracellular firing patterns of deep temporal lobe structures in man. *Electroencephalogr. Clin. Neurophysiol.* **34,** 247–257 (1973).

61. Soza, G. *et al.* Determination of the elasticity parameters of brain tissue with combined simulation and registration. *Int. J. Med. Robot. Comput. Assist. Surg.* **01,** 87 (2005).

62. Nayar, V. T., Weiland, J. D., Nelson, C. S. & Hodge, a M. Elastic and viscoelastic characterization of agar. *J. Mech. Behav. Biomed. Mater.* **7,** 60–8 (2012).

63. Brown, E. N. E. N., Kass, R. E. & Mitra, P. P. Multiple neural spike train data analysis: state-of-the-art and future challenges. *Nat. Neurosci.* **7,** 456–61 (2004).

64. Hazelton, F. T., Smidt, G. L., Flatt, a E. & Stephens, R. I. The influence of wrist position on the force produced by the finger flexors. *J. Biomech.* **8,** 301–6 (1975).

65. Rangan, C. S., Sarma, G. R. & Mani, V. S. V. in *Instrum. Devices Syst.* 233–261 (Tata McGraw-Hill, 1997).

66. Stacey, W. *et al.* Potential for unreliable interpretation of EEG recorded with microelectrodes. *Epilepsia* **doi: 10.11,** (2013).

67. Howard, M. a *et al.* A hybrid clinical-research depth electrode for acute and chronic in vivo microelectrode recording of human brain neurons. Technical note. *J. Neurosurg.* **84,** 129–32 (1996).

68. Howard, M. a *et al.* A chronic microelectrode investigation of the tonotopic organization of human auditory cortex. *Brain Res.* **724,** 260–4 (1996).

69. Quiroga, R. Q., Nadasdy, Z. & Ben-Shaul, Y. Unsupervised spike detection and sorting with wavelets and superparamagnetic clustering. *Neural Comput.* **16,** 1661–87 (2004).

70. Norden, A. D. & Blumenfeld, H. The role of subcortical structures in human epilepsy. *Epilepsy Behav.* **3,** 219–231 (2002).

71. Faeth, W. H., Walker, a E. & Andy, O. J. The propagation of cortical and subcortical epileptic discharge. *Epilepsia* **3,** 37–48 (1954).

72. Gale, K. Progression and generalization of seizure discharge: anatomical and neurochemical substrates. *Epilepsia* **29,** S15–S34 (1988).

73. Gale, K. Subcortical structures and pathways involved in convulsive seizure generation. *J. Clin. Neurophysiol.* **9,** 264–277 (1992).

74. Englot, D. J. *et al.* Remote effects of focal hippocampal seizures on the rat neocortex. *J. Neurosci.* **28,** 9066–81 (2008).

75. Englot, D. J. *et al.* Cortical deactivation induced by subcortical network dysfunction in limbic seizures. *J. Neurosci.* **29,** 13006–18 (2009).

76. Wilke, C., van Drongelen, W., Kohrman, M. & He, B. Neocortical seizure foci localization by means of a directed transfer function method. *Epilepsia* **51,** 564–72 (2010).

77. Wilke, C., van Drongelen, W., Kohrman, M. & He, B. Identification of epileptogenic foci from causal analysis of ECoG interictal spike activity. *Clin. Neurophysiol.* **120,** 1449–56 (2009).

78. Wilke, C., Worrell, G. a & He, B. Graph analysis of epileptogenic networks in human partial epilepsy. *Epilepsia* **52,** 84–93 (2011).

79. Trevelyan, A. J., Sussillo, D., Watson, B. O. & Yuste, R. Modular propagation of epileptiform activity: evidence for an inhibitory veto in neocortex. *J. Neurosci.* **26,** 12447–55 (2006).

80. Cammarota, M., Losi, G., Chiavegato, A., Zonta, M. & Carmignoto, G. Fast Spiking Interneuron Control of Seizure Propagation in a Cortical Slice Model of Focal Epilepsy. *J. Physiol.* **00,** 1–16 (2013).

81. Dichter, M. & Spencer, W. A. A. Penicillin-induced interictal discharges from the cat hippocampus. II. Mechanisms underlying origin and restriction. *J. Neurophysiol.* **32,** 663 (1969).

82. Schwartz, T. H. & Bonhoeffer, T. In vivo optical mapping of epileptic foci and surround inhibition in ferret cerebral cortex. *Nat. Med.* **7,** 1063–7 (2001).

83. Timofeev, I. & Steriade, M. Neocortical seizures: initiation, development and cessation. *Neuroscience* **123,** 299–336 (2004).

84. Montgomery, S. M., Sirota, A. & Buzsáki, G. Theta and gamma coordination of hippocampal networks during waking and rapid eye movement sleep. *J. Neurosci.* **28,** 6731–41 (2008).

85. Czurkó, A., Huxter, J., Li, Y., Hangya, B. & Muller, R. U. Theta phase classification of interneurons in the hippocampal formation of freely moving rats. *J. Neurosci.* **31,** 2938–47 (2011).

86. Klausberger, T. *et al.* Brain-state-and cell-type-specific firing of hippocampal interneurons in vivo. *Nature* **421,** 844–848 (2003).

87. Kitchigina, V. F. & Butuzova, M. V. Theta activity of septal neurons during different epileptic phases: the same frequency but different significance? *Exp. Neurol.* **216,** 449–58 (2009).

88. Colom, L. V. Septal networks: relevance to theta rhythm, epilepsy and Alzheimer’s disease. *J. Neurochem.* **96,** 609–23 (2006).

89. Thorp, C. K. & Steinmetz, P. N. Interference and noise in human intracranial microwire recordings. *IEEE Trans. Biomed. Eng.* **56,** 30–6 (2009).

90. Dykstra, A. R. *et al.* Individualized localization and cortical surface-based registration of intracranial electrodes. *Neuroimage* **59,** 3563–70 (2012).

91. Chapin, J. K. K., Moxon, K., Markowitz, R. S. S. & Nicolelis, M. a. Real-time control of a robot arm using simultaneously recorded neurons in the motor cortex. *Nat. Neurosci.* **2,** 664–70 (1999).

92. Henze, D. A. a *et al.* Intracellular features predicted by extracellular recordings in the hippocampus in vivo. *J. Neurophysiol.* **84,** 390 (2000).

93. Bower, M. R. & Buckmaster, P. S. Changes in granule cell firing rates precede locally recorded spontaneous seizures by minutes in an animal model of temporal lobe epilepsy. *J. Neurophysiol.* **99,** 2431–42 (2008).

94. Bower, M. R., Stead, M., Meyer, F. B., Marsh, W. R. & Worrell, G. a. Spatiotemporal neuronal correlates of seizure generation in focal epilepsy. *Epilepsia* **53,** 807–16 (2012).

95. Truccolo, W. *et al.* Single-neuron dynamics in human focal epilepsy. *Nat. Neurosci.* **14,** 635–41 (2011).

96. Viskontas, I. V, Ekstrom, A. D., Wilson, C. L. & Fried, I. Characterizing interneuron and pyramidal cells in the human medial temporal lobe in vivo using extracellular recordings. *Hippocampus* **17,** 49–57 (2007).

97. Weiss, S. a *et al.* Ictal high frequency oscillations distinguish two types of seizure territories in humans. *Brain* (2013). doi:10.1093/brain/awt276

98. Franaszczuk, P. J., Bergey, G. K. & Kamiński, M. J. Analysis of mesial temporal seizure onset and propagation using the directed transfer function method. *Electroencephalogr. Clin. Neurophysiol.* **91,** 413–27 (1994).

99. Kaminski, M. & Blinowska, K. A new method of the description of the information flow in the brain structures. *Biol. Cybern.* **210,** 203–210 (1991).

100. He, B. *et al.* eConnectome: A MATLAB toolbox for mapping and imaging of brain functional connectivity. *J. Neurosci. Methods* **195,** 261–9 (2011).

101. Foffani, G. & Moxon, K. a. PSTH-based classification of sensory stimuli using ensembles of single neurons. *J. Neurosci. Methods* **135,** 107–20 (2004).

102. Foffani, G., Tutunculer, B. & Moxon, K. Role of spike timing in the forelimb somatosensory cortex of the rat. *J. Neurosci.* **24,** 7266–71 (2004).

103. Fries, P., Womelsdorf, T., Oostenveld, R. & Desimone, R. The effects of visual stimulation and selective visual attention on rhythmic neuronal synchronization in macaque area V4. *J. Neurosci.* **28,** 4823–35 (2008).

104. Cadotte, A. J. *et al.* Granger causality relationships between local field potentials in an animal model of temporal lobe epilepsy. *J. Neurosci. Methods* **189,** 121–9 (2010).

105. Zhang, L. *et al.* Hippocampal theta-driving cells revealed by Granger causality. *Hippocampus* **22,** 1781–93 (2012).

106. Brockmann, M. D., Pöschel, B., Cichon, N. & Hanganu-Opatz, I. L. Coupled oscillations mediate directed interactions between prefrontal cortex and hippocampus of the neonatal rat. *Neuron* **71,** 332–47 (2011).

107. Sirota, A. *et al.* Entrainment of neocortical neurons and gamma oscillations by the hippocampal theta rhythm. *Neuron* **60,** 683–97 (2008).

108. Stewart, M. & Fox, S. E. Do septal neurons pace the hippocampal theta rhythm? *Trends Neurosci.* **13,** 163–8 (1990).

109. Chapman, C. a & Lacaille, J. C. Cholinergic induction of theta-frequency oscillations in hippocampal inhibitory interneurons and pacing of pyramidal cell firing. *J. Neurosci.* **19,** 8637–45 (1999).

110. Ewell, L. A. & Jones, M. V. Frequency-tuned distribution of inhibition in the dentate gyrus. *J. Neurosci.* **30,** 12597–607 (2010).

111. Tukker, J. J., Fuentealba, P., Hartwich, K., Somogyi, P. & Klausberger, T. Cell type-specific tuning of hippocampal interneuron firing during gamma oscillations in vivo. *J. Neurosci.* **27,** 8184–9 (2007).

112. Schevon, C. A. *et al.* Evidence of an inhibitory restraint of seizure activity in humans. *Nat. Commun.* **3,** 1060 (2012).

113. Parent, J. & Lowenstein, D. Mossy fiber reorganization in the epileptic hippocampus. *Curr. Opin. Neurol.* (1997). at <http://journals.lww.com/co-neurology/Abstract/1997/04000/Mossy_fiber_reorganization_in_the_epileptic.6.aspx>

114. Milton, J. G., Chkhenkeli, S. A. & Towle, V. L. in *Handb. brain Connect.* 477–503 (Springer, 2007).

115. Kotti, T., Riekkinen, P. J. & Miettinen, R. Characterization of target cells for aberrant mossy fiber collaterals in the dentate gyrus of epileptic rat. *Exp. Neurol.* **146,** 323–30 (1997).

116. De Lanerolle, N. C., Kim, J. H., Robbins, R. J. & Spencer, D. D. Hippocampal interneuron loss and plasticity in human temporal lobe epilepsy. *Brain Res.* **495,** 387–95 (1989).

117. Dugladze, T. *et al.* GABA(B) autoreceptor-mediated cell type-specific reduction of inhibition in epileptic mice. *Proc. Natl. Acad. Sci. U. S. A.* **110,** 15073–8 (2013).

118. Keller, C. J. *et al.* Heterogeneous neuronal firing patterns during interictal epileptiform discharges in the human cortex. *Brain* **133,** 1668–81 (2010).

119. Staley, K. J., Soldo, B. L. & Proctor, W. R. Ionic Mechanisms of Neuronal Excitation by Inhibitory GABA-A Receptors. *Science (80-.).* **269,** 977–981 (1995).

120. Lamsa, K. *et al.* Ionic Mechanisms of Spontaneous GABAergic Events in Rat Hippocampal Slices Exposed to 4-Aminopyridine Ionic Mechanisms of Spontaneous GABAergic Events in Rat Hippocampal Slices Exposed to 4-Aminopyridine. 2582–2591 (1997).

121. Kaila, K., Lamsa, K., Smirnov, S., Taira, T. & Voipio, J. Long-lasting GABA-mediated depolarization evoked by high-frequency stimulation in pyramidal neurons of rat hippocampal slice is attributable to a network-driven, bicarbonate-dependent K+ transient. *J. Neurosci.* **17,** 7662–72 (1997).

122. Lewicki, M. S. A review of methods for spike sorting: the detection and classification of neural action potentials. *Network* **9,** R53–78 (1998).

123. Sackellares, J. C., Shiau, D.-S., Halford, J. J., LaRoche, S. M. & Kelly, K. M. Quantitative EEG analysis for automated detection of nonconvulsive seizures in intensive care units. *Epilepsy Behav.* **22 Suppl 1,** S69–73 (2011).

124. Bragin, a, Wilson, C. L. & Engel, J. J. Chronic epileptogenesis requires development of a network of pathologically interconnected neuron clusters: a hypothesis. *Epilepsia* **41 Suppl 6,** S144–52 (2000).

125. Feldt Muldoon, S., Soltesz, I. & Cossart, R. Spatially clustered neuronal assemblies comprise the microstructure of synchrony in chronically epileptic networks. *Proc. Natl. Acad. Sci. U. S. A.* **110,** 3567–72 (2013).

126. De Curtis, M. & Gnatkovsky, V. Reevaluating the mechanisms of focal ictogenesis: The role of low-voltage fast activity. *Epilepsia* **50,** 2514–25 (2009).

127. Hangya, B., Borhegyi, Z., Szilágyi, N., Freund, T. F. & Varga, V. GABAergic neurons of the medial septum lead the hippocampal network during theta activity. *J. Neurosci.* **29,** 8094–102 (2009).

128. Mizumori, S. J., Barnes, C. A. & McNaughton, B. L. Behavioral correlates of theta-on and theta-off cells recorded from hippocampal formation of mature young and aged rats. *Exp Brain Res* **80,** 365–373 (1990).

129. Dragoi, G., Carpi, D., Recce, M., Csicsvari, J. & Buzsáki, G. Interactions between hippocampus and medial septum during sharp waves and theta oscillation in the behaving rat. *J. Neurosci.* **19,** 6191–9 (1999).

130. Csicsvari, J., Hirase, H., Czurkó, a, Mamiya, a & Buzsáki, G. Oscillatory coupling of hippocampal pyramidal cells and interneurons in the behaving Rat. *J. Neurosci.* **19,** 274–87 (1999).

131. Miller, J. W., Turner, G. M. & Gray, B. C. Anticonvulsant effects of the experimental induction of hippocampal theta activity. *Epilepsy Res.* **18,** 195–204 (1994).

132. Kispersky, T., White, J. a & Rotstein, H. G. The mechanism of abrupt transition between theta and hyper-excitable spiking activity in medial entorhinal cortex layer II stellate cells. *PLoS One* **5,** e13697 (2010).

133. Jiruska, P. *et al.* Synchronization and desynchronization in epilepsy: controversies and hypotheses. *J. Physiol.* **4,** 787–97 (2013).

134. Schevon, C. A. *et al.* Microphysiology of epileptiform activity in human neocortex. *J. Clin. Neurophysiol.* **25,** 321–30 (2008).